MONTHLY NOTICES

OF THE

ROYAL ASTRONOMICAL SOCIETY

Volume 118 No. 6 1958

Published and Sold by the

ROYAL ASTRONOMICAL SOCIETY
BURLINGTON HOUSE
LONDON, W.1

Price £1 0s. 0d.; in U.S.A. $3

Annual Subscription for volume of six numbers: £5 5s. 0d. ; in U.S.A. $16

The Geophysical Journal

OF THE

ROYAL ASTRONOMICAL SOCIETY

Editors

A. H. Cook
M.A., Ph.D., F.R.A.S., F.G.S.
National Physical Laboratory
Teddington

T. F. Gaskell
M.A., Ph.D., F.R.A.S.
British Petroleum Company
London

Price £1 per number; in U.S.A. \$3. *Annual Subscription £3; in U.S.A.* \$9

Volume 1 No. 4 1958

CONTENTS

This number also contains a note on progress in Geophysics entitled " Geophysical studies in polar regions : the Antarctic ice sheet " by G. de Q. Robin ; a letter to the Editors by W. D. Parkinson and J. Cleary on " The eccentric geomagnetic dipole " ; a Report on the 83rd Colloquium of the French National Centre of Scientific Research (Topography and Ecology of Oceanic Deeps) held at Nice, 1958 May 5–14; and reviews of recent geophysical publications. An Index to Vol. 1, which is completed by the present issue, is also included.

Orders should be addressed to:

The Assistant Secretary
Royal Astronomical Society, Burlington House, London, W.1.

MONTHLY NOTICES

OF THE

ROYAL ASTRONOMICAL SOCIETY

Vol. 118 No. 6

MEETING OF 1958 OCTOBER 10

Dr W. H. Steavenson, President, in the Chair

The election by the Council of the following Fellows was duly confirmed:—

John Evan Baldwin, Cavendish Laboratory, Cambridge (proposed by F. Graham Smith); and

Norman Arthur Routledge, Department of Geodesy and Geophysics, Cambridge (proposed by M. N. Hill).

The election by the Council of the following Junior Member was duly confirmed:—

James Martin Hall, 70 Bishop's Road, London, S.W.6 (proposed by J. M. Bruckshaw).

One hundred and forty-five presents were announced as having been received since the last meeting, including:—

G. de Vaucouleurs, *L'exploration des galaxies voisines* (presented by the author); and

J. W. Dungey, *Cosmic electrodynamics* (presented by the author).

MEETING OF 1958 NOVEMBER 14

Dr W. H. Steavenson, President, in the Chair

The election by the Council of the following Fellows was duly confirmed:—

Frederick Donald Abbott, Dept. of Astronomy, The University, St. Andrews, Scotland (proposed by E. Finlay Freundlich);

Reginald Edds, 10 Orme Court, London, W.2 (proposed by H. C. King);

Harold Hicks, 34 Kingsley Road, Plymouth, Devon (proposed by E. A. Beet);

Joachim Christoffel Cornelius van Loggerenberg, 3b Abraham Grayling Street, Wilgehof, Bloemfontein, S. Africa (proposed by A. D. Thackeray);

Cecil Newman-Sanders, The Little House, Hatch End, Middlesex (proposed by H. C. King);

Derek William Sida, Dept. of Mathematics, The University, Leeds (proposed by T. G. Cowling);

Julius Dirk Willem Staal, Quarterdeck, Two-mile-Ash, Horsham, Sussex (proposed by H. C. King); and

Bengt Strömgren, Institute for Advanced Study, Princeton, New Jersey, U.S.A. (proposed by H. Bondi).

The election by the Council of the following Junior Members was duly confirmed:—

Dennis Keith Richards, 9 High Holborn, Sedgley, Worcs. (proposed by H. E. Howle); and

Robert Reginald Shobbrook, 75 Romway Road, Leicester (proposed by E. Finlay Freundlich).

Eighty-five presents were announced as having been received since the last meeting, including:—

R. S. Ball, *The story of the heavens* (presented by Col. J. A. Watson);

J. C. Begg, *Essays on thoughts and worlds* (presented by the author); and

International Astronomical Union and International Union of Theoretical and Applied Mechanics, *Proceedings of third symposium on cosmical gas dynamics* (presented by the I.A.U. and the I.U.T.A.M.).

MEETING OF 1958 DECEMBER 12

Dr W. H. Steavenson, President, in the Chair

The President announced the death of Dr John Jackson, a former President of the Society, and paid a tribute to his memory, the Fellows standing.

The election by the Council of the following Fellows was duly confirmed:—

Geoffrey Basil Anderton, 10 Taybank Road, Westering, Port Elizabeth, S. Africa (proposed by H. Welsh);

Arnold Noel Argue, The Observatories, Madingley Road, Cambridge (proposed by D. E. Blackwell);

Leslie Barraclough, 52 School Street, Low Moor, Bradford (proposed by G. Fielder);

Cecil Maxwell Cade, 42 Latton Green, Commonside Road, Harlow, Essex (proposed by H. Spencer Jones);

Barry Arthur James Clark, 11 Ryan Street, Coburg N. 13, Victoria, Australia (proposed by W. E. L. Clapham);

Brian Clegg, 29 Primley Park Crescent, Leeds 17 (proposed by G. Fielder);

William Davidson, Battersea College of Technology, Battersea Park Road, London, S.W.11 (proposed by W. H. McCrea);

Peter Donnelly, King's Arms Hotel, Wigton, Cumberland (proposed by W. L. Rae);

George Alfred Eveleigh, 5 Hale Road, Walton, Liverpool 4 (proposed by J. R. Platt);

Pierre Gouin, University College Geophysical Observatory, Addis Ababa, Ethiopia (proposed by D. O'Connell);

Ronald Green, 12 Masson Street, Turner, Canberra, Australia (proposed by A. W. Rodgers);

Ernest David Jones, Alba S.A., Caixa Postal 738, Curitiba, Parana, Brazil (proposed by C. A. Ronan);

Peter James Jooste, 58 Strathleven Road, London, S.W.2 (proposed by H. Wildey);

Raymond Leopold Kerdel, St. Peter's Rectory, Broken Hill, N.S.W., Australia (proposed by C. S. Middleton);

Otto Ernst Walter Rudolph Kurth, Dept. of Astronomy, The University, Manchester 13 (proposed by Z. Kopal);

John Wishart Macvey, 15 Adair Avenue, Saltcoats, Scotland (proposed by A. E. Roy);

James Gault Mitchell, c/o Marischal College, Aberdeen, Scotland (proposed by R. V. Jones);

Thomas William Olle, P.O. Box 174, The Hague, Netherlands (proposed by Z. Kopal);

Miroslav Plavec, Astronomical Institute, Czech Academy of Sciences, Ondrejov, Czechoslovakia (proposed by Z. Kopal);

James Dickie Raeside, D.S.I.R., P.O. Box 733, Dunedin, New Zealand (proposed by A.F.A.L. Jones);

Richard Edwin Ridley, 23 Woodlands Avenue, Wolstanton, Newcastle, Staffs (proposed by T. E. Sadler);

Richard Langley Sears, Goethe Link Observatory, Indiana University, Bloomington, Indiana, U.S.A. (proposed by J. B. Irwin);

Uli W. Steinlin, Astronomisch-Meteorologische Anstalt, Universitat Basel, Binningen, Switzerland (proposed by W. P. Bidelman);

Peter Antony Eabry Stewart, 11 Fairhaven Road, Bristol 6 (proposed by A. F. Collins);

John H. Waddell III, Upper Air Research Observatory, Sacramento Peak, Sunspot, New Mexico, U.S.A. (proposed by J. T. Jefferies); and

Arne A. Wyller, Sproul Observatory, Swarthmore College, Pa., U.S.A. (proposed by M. K. Vainu Bappu).

The re-election by the Council of the following Fellows was duly confirmed:—

Colin Kerr Grant, c/o Bank of Adelaide, 11 Leadenhall Street, London, E.C.3 (proposed by T. F. Gaskell);

David George Kendall, Magdalen College, Oxford (proposed by H. H. Plaskett); and

Cecil Francis Retter, 40 Parkhurst Road, Torquay (proposed by T. A. Brown).

THE SCATTERING OF RADIO WAVES IN THE SOLAR CORONA

A. Hewish

(Received 1958 July 29)

Summary

Observations of the radio emission from the Crab nebula during June, when it passes within a small angular distance of the Sun, have shown that the radiation suffers considerable scattering during its passage through the solar corona. In this paper an account is given of measurements carried out each year over the period 1952–1958. The following new results have been obtained:

(i) measurements at a wave-length of 7·9 m have suggested the presence of refraction effects, in addition to scattering, which may provide information about the mean electron density in the corona;

(ii) extension of the measurements to the shorter wave-length of 1·9 m has enabled the large scattering at the distance of closest approach to be determined more accurately;

(iii) a pronounced sunspot-cycle variation has been observed in regions of the corona at a distance of $8R_\odot$; and

(iv) the scattering has been shown to exhibit anisotropy. This result strengthens the earlier conclusion that the scattering is caused by filamentary irregularities aligned in a magnetic field and suggests that the direction of the field is approximately radial at distances of 15–$20R_\odot$.

1. *Introduction.*—The possibility of investigating the solar corona by studying the refraction effects which arise when a radio star is viewed through it was first tested experimentally in 1951 and 1952 (Machin and Smith 1952, Vitkevitch 1958). In these experiments the Crab nebula was observed during June when it passed within $1^\circ{\cdot}5$ of the Sun's southern limb. The measurements were made with phase-switching interferometers aligned on an east–west axis and the recorded amplitude of the radio source decreased gradually as it approached the Sun, the reduction first becoming apparent at an angular distance of about 5°.

The results could not be explained by simple refraction or absorption, but were consistent with a scattering process in which the apparent diameter of the source was increased to such an extent that it became partially resolved by the interferometer (Hewish 1955). The spread of the scattered waves was found to be considerably greater than the angle through which the radiation would be deviated by the radial gradient of electron density and the scattering therefore masks any simple refraction effects.

The scattering was explained by the presence of irregularities in the corona having a scale which could lie in the range 1–10^5 km. It was suggested that the irregular structure was maintained by a general magnetic field in a similar manner to the visible polar plumes (van de Hulst 1950).

In the present paper an account is given of more recent observations which have been made each year since 1953. In addition to confirming the earlier work a number of new results have been obtained (see Summary, (i) to (iv), above).

2. *The observations.*—All observations have been of the Crab nebula during the period June 6–23 when it passes within $4{\cdot}6R_\odot$ of the Sun's southern limb.

Phase-switching interferometers were used at a variety of spacings and wave-lengths in order to study the scattering over as wide a range of angular distances as possible. Observations at long wave-lengths and with large interferometer spacings are necessary to study the small scattering in the outermost corona, while observations at shorter wave-lengths must be used to measure the largest scattering at the distance of closest approach. Interferometers employing a spacing of only a few wave-lengths, for which the scattering is always much smaller than the angular separation of the interference lobes, have also been used to study changes of integrated intensity of the source. While most of the interferometers have been aligned on an east–west axis, measurements were made in 1956 using NS and EW axes and in 1958 using axes in NE, NW and EW directions. Also in 1958 observations were made using a 3 000 ft array which gave a fan beam of width 1° to half power at 7·9 m. Use of the fan beam enabled the scattering to be determined directly from the broadening of the response. The 1958 measurements, which were carried out in conjunction with J. A. Högbom, will be discussed at greater length elsewhere. Some preliminary results are included in the present account as they remove an ambiguity concerning the direction of the scattering anisotropy.

Rejection of radio emission from the Sun itself, which is considerably more intense than that from the Crab nebula except at the longest wave-length used, represents the main experimental difficulty. The use of interferometers greatly reduces the response due to the quiet Sun and the most precise observations were carried out with the large four-aerial interferometer, first at 3·7 m and

Table I

	Wave-length	Interferometer spacing	Aerial system
1952	7·9 m	49 λ EW	150 ft × 16 ft corner reflectors
	3·7 m	105 λ ,,	40 element linear array
1953	7·9 m	49 λ ,,	As in 1952
	,,	8 λ ,,	150 ft × 16 ft corner reflectors
	3·7 m	105 λ ,,	As in 1952
	,,	157 λ ,,	Four-element radio telescope
1954	7·9 m	8 λ ,,	As in 1953
	,,	49 λ ,,	,, ,, ,,
	3·7 m	157 λ ,,	,, ,, ,,
1955	7·9 m	8 λ ,,	As in 1953
	,,	56 λ ,,	Twelve-element Yagi arrays
1956	7·9 m	8 λ ,,	As in 1953
	,,	52 λ NS	100 ft × 30 ft corner reflectors
	,,	56 λ EW	As in 1955
	3·7 m	105 λ ,,	As in 1953
	1·9 m	300 λ ,,	Four-element radio telescope
1957	1·9 m	300 λ ,,	As in 1956
1958	7·9 m	135 λ ,,	Six-element Yagi arrays
	,,	43 λ NW	Yagi array plus 3000 ft array
	,,	52 λ NE	,, ,, ,, ,, ,,
	,,	$\pm\frac{1}{2}°$ fan beam	3000 ft array plus 200 ft × 40 ft corner

later at 1·9 m. This system allowed the solar response, in the absence of sunspots, to be reduced to about 1 per cent of that of the radio source.

Details of the aerial systems used for the different experiments are summarized in Table I, and some typical records are shown in Fig. 1.

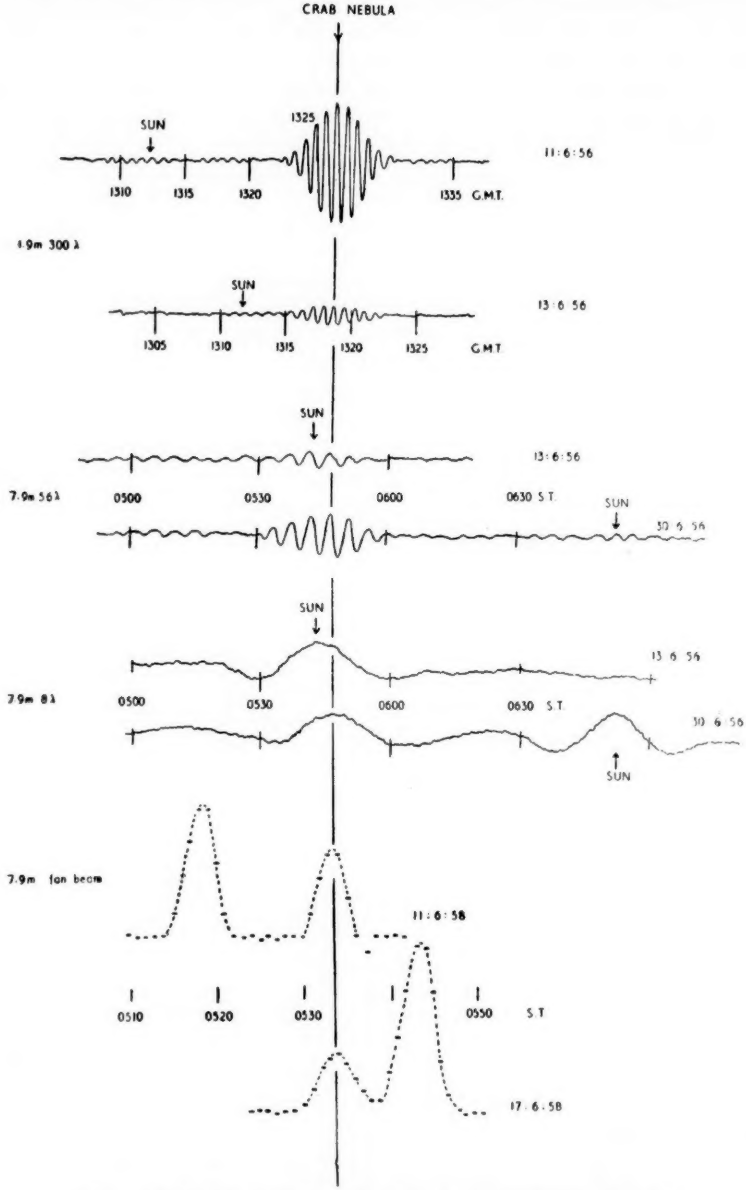

FIG. 1.—*Some typical records obtained with the different systems during the course of the 1956 occultation, and two fan beam records obtained in 1958.*

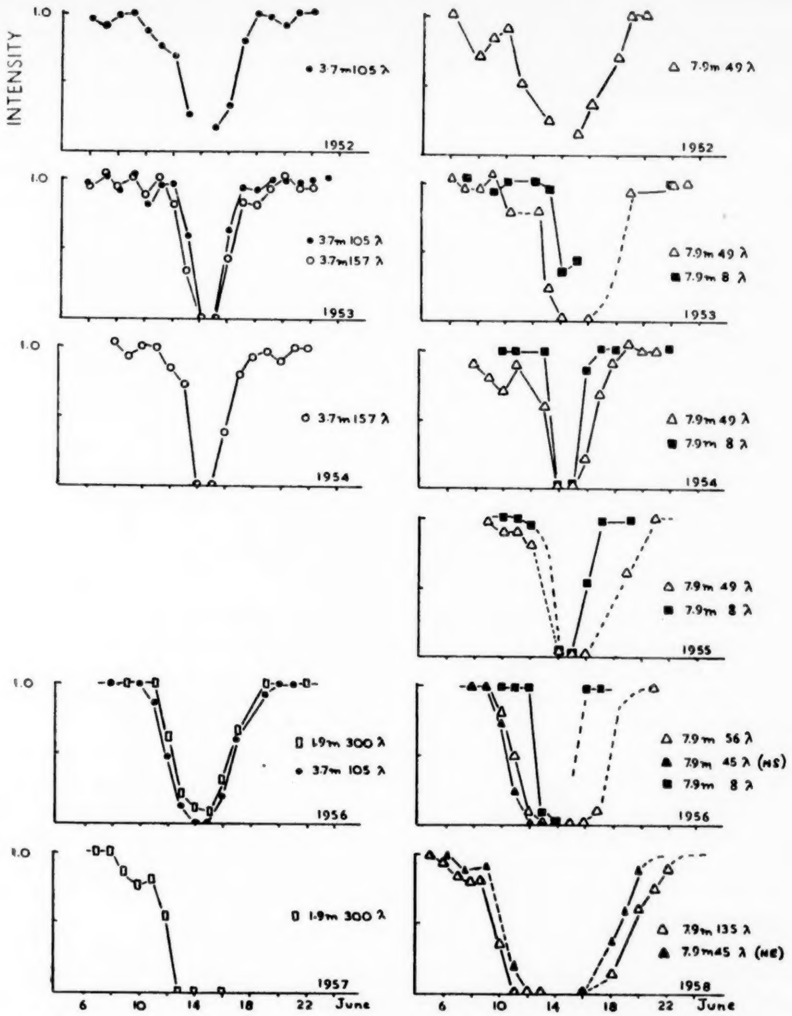

FIG. 2.—*The normalized response of the Crab nebula as observed with interferometers of different spacing and wave-length during the occultations of 1952–1958.*

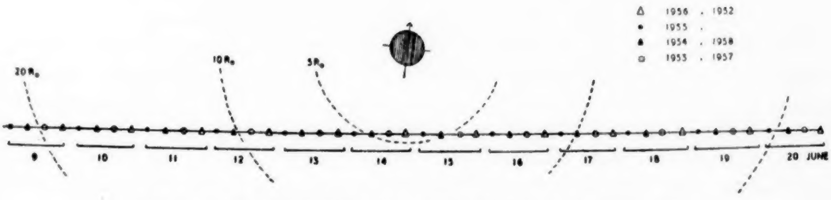

FIG. 3.—*The position of the Crab nebula relative to the Sun at noon.*

The basic results are illustrated in Fig. 2 in which the apparent intensity of the source is plotted as a function of the date of observation. The position of the Crab nebula on the corresponding dates at noon is shown in Fig. 3. The general similarity of the occultation curves from year to year is immediately apparent, although greater reductions were observed towards sunspot maximum. It is also apparent that the reductions increase both with the wave-length, and with the interferometer spacing at a given wave-length. The detailed interpretation of these curves will be considered in the following section.

3. *The interpretation of the observations*

(*a*) *The scattering theory.*—It was shown previously that the results obtained in 1953 were explained by a scattering mechanism in which the integrated intensity of the source was unchanged, but the radiation emerging from the corona could be represented by an angular spectrum of the form $\exp(-\phi^2/\phi^2{}_0)$. The half-width (ϕ_0) of the angular spectrum depends upon the square of the wave-length, the size of the irregularities, and on the deviation of the electron density from its mean value. The present results have entirely confirmed this theory, which is also in agreement with other observations (Vitkevitch 1955, Blum and Boischot 1957). A contrary hypothesis has been suggested by Slee (1956) corresponding to a mechanism previously considered (Hewish 1955, p. 244, Case I) and shown to disagree with the observations. This point has been discussed elsewhere (Hewish 1957).

The amplitude of the record obtained when radiation having an angular spectrum given by $\exp -(\phi^2/\phi^2{}_0)$ is incident upon a phase-switching interferometer of spacing d and wave-length λ is proportional to $\exp -(\pi^2 d^2 \phi^2{}_0/\lambda^2)$. A comparison of the occulted and unocculted responses of the radio source enables ϕ_0 to be determined.

The values of ϕ_0 derived from the different observations are shown in Fig. 4, plotted against angular distance from the Sun. It is interesting to note that in 1956 and 1958 the scattering along an EW line was less than that along NS, NE, and NW lines*. In 1958 the largest scattering at closest approach was determined from the fan beam records and it was interesting to find that the results at greater angular distance agreed well with the interferometric data.

In Fig. 5, values of $\log \phi_0$, obtained simultaneously at the different wave-lengths during 1956, have been plotted against $\log \lambda$. It is seen that the points lie reasonably well on straight lines of slope 2. Such a result, which is not accounted for by Slee's hypothesis, confirms the scattering theory over a 4 : 1 range of wave-length corresponding to a 16 : 1 variation of scattering angle.

(*b*) *Modifications to the simple scattering theory at long wave-lengths.*—The simple scattering theory assumes that the scattered distribution is isotropic. When the scattering is so great that the scattered distribution extends over an appreciable range of radial distance then the shape of the distribution depends upon the radial gradient of scattering. This effect must certainly occur at 7·9 m at the distance of closest approach when the scattered distribution extends over at least two solar diameters. Some computations for this wave-length have been made on the assumption that the scattering is isotropic and follows

* Only the NE scattering has been plotted in Fig. 4. The NW scattering was similar and has been omitted to avoid confusion.

a radial law with spherical symmetry. The degree of scattering was obtained from the 1·9 m observations of 1956, appropriately scaled, since at this short wave-length such effects are believed to be negligible. Brightness contours were computed for the scattered distribution at angular distances of $6R_\odot$ and $12R_\odot$ and are shown in Fig. 6. It is seen that the scattering is only slightly anisotropic at $12R_\odot$ but significantly so at the shorter distance.

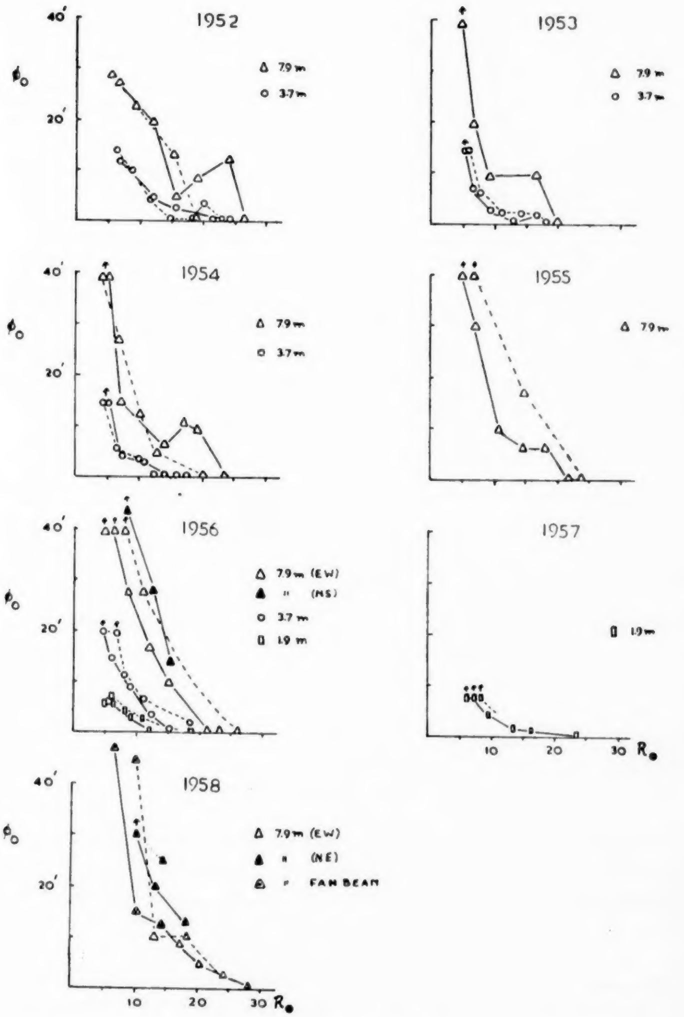

FIG. 4.—*The scattering half-width ϕ_0 measured at different wave-lengths plotted as a function of angular distance from the Sun. The arrows denote lower limit.*

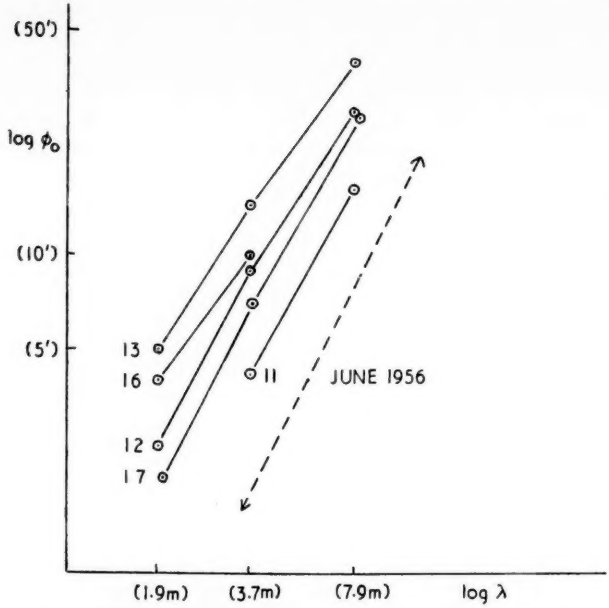

FIG. 5.—*The scattering half-width ϕ_0 measured at three wave-lengths simultaneously during 1956 plotted as a function of the wave-length on a logarithmic scale. The broken line indicates a slope of 2 as predicted by the scattering theory.*

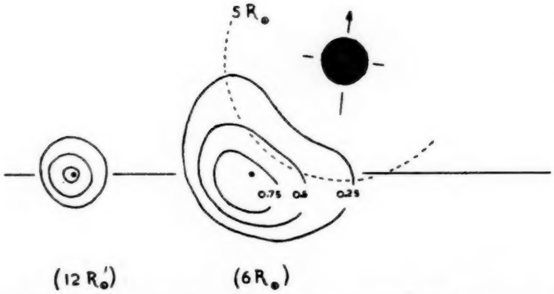

FIG. 6.—*The theoretical scattered distribution at 7·9 m computed for isotropic scattering in a spherically symmetrical corona.*

(*c*) *Evidence for refraction.*—Observations at 7·9 m using an interferometer spacing of 8 λ exhibit marked decreases of integrated intensity when the source lies within an angular distance of $8R_{\odot}$. The relevant observations have been re-plotted in Fig. 7 to demonstrate the effect more clearly. These occultation curves can only be accounted for by a real decrease of integrated intensity since the scattered distribution would otherwise need to subtend an angle greater than 6°; it is known from measurements at the same wave-length at greater angular differences (but still within $\pm 3°$) that the scattering irregularities are not distributed widely enough to produce such an effect.

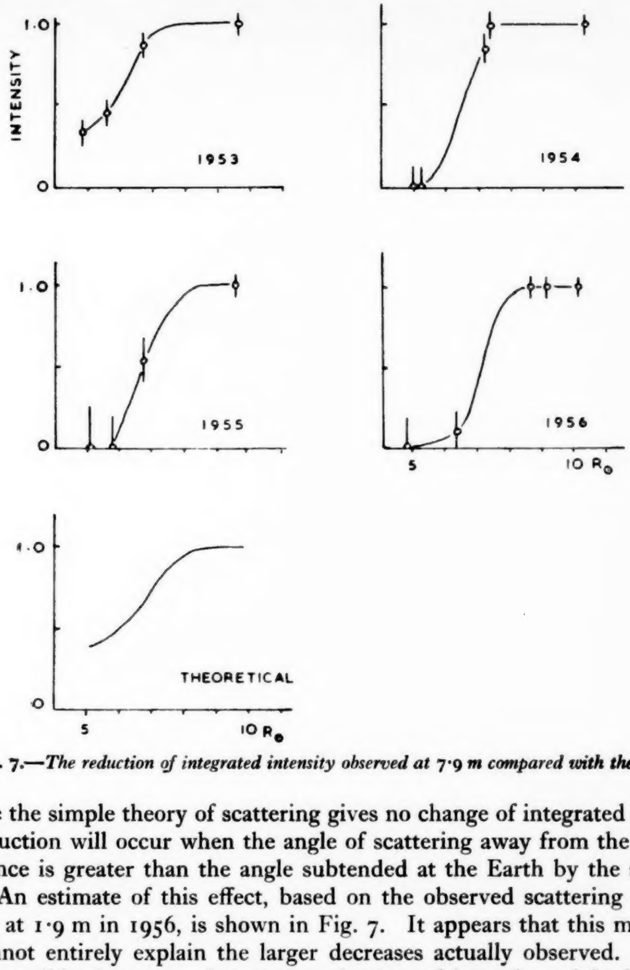

FIG. 7.—*The reduction of integrated intensity observed at 7·9 m compared with theory.*

While the simple theory of scattering gives no change of integrated intensity, some reduction will occur when the angle of scattering away from the direction of incidence is greater than the angle subtended at the Earth by the scattering region. An estimate of this effect, based on the observed scattering at closest approach at 1·9 m in 1956, is shown in Fig. 7. It appears that this mechanism alone cannot entirely explain the larger decreases actually observed.

It is possible, however, that some reduction of intensity might be caused by refraction phenomena arising from the radial gradient of the mean electron density. In the absence of scattering, refraction would cause a divergence of the incident rays away from the Sun's centre, which would give rise to a caustic surface. If the Earth passed through this caustic a complete occultation would occur, preceded by a sharp increase of intensity (Link 1951). Calculations based on the electron densities quoted by Blackwell (1956) show that the Earth would pass through the caustic when the source was at an angular distance of about $7R_\odot$. In fact, as shown in Fig. 8, the observed scattering is appreciably greater than the computed angle of refraction at distances exceeding $5R_\odot$ and so a straightforward occultation of this type is not possible. At smaller angular distances the refraction phenomena may well predominate, however, owing to the steeper radial variation of the refraction angle. Occultation of a portion of the scattered distribution nearest the Sun is then a possibility. The precise

reduction of intensity which might arise cannot be estimated without more knowledge of the form of the scattered distribution close to the Sun, but it seems difficult to account for the reductions shown in Fig. 7 without increasing the refraction angle. A two-fold increase of the mean electron density would make the refraction angle and the scattering angle comparable at about $6R_\odot$ and a sufficiently great reduction might then occur, but this question must remain open in the absence of further data.

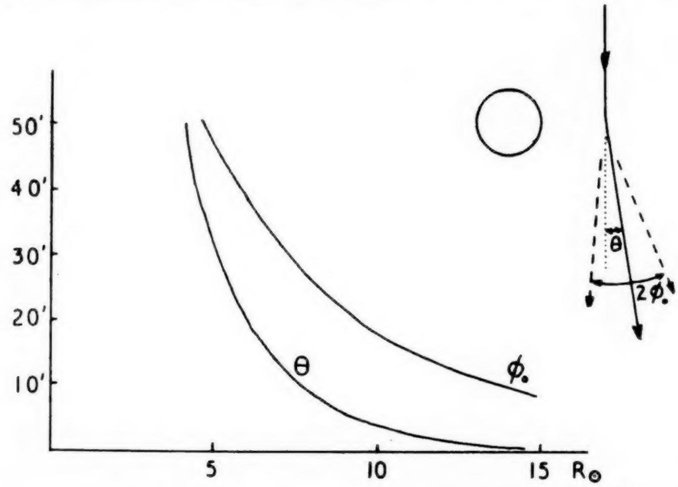

FIG. 8.—*The computed angle of refraction (θ) due to the radial gradient of the mean electron density compared with the measured scattering angle at 7·9 m (1956).*

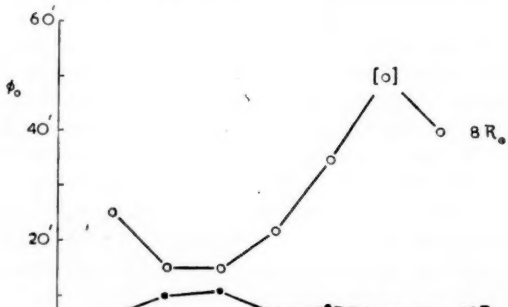

FIG. 9.—*The solar cycle variation of scattering at 7·9 m. The point for 1957 was derived by scaling a measurement at 1·9 m.*

(*d*) *Solar cycle variations.*—In Fig. 9 the scattering at an angular distance of $8R_\odot$ has been plotted as a function of the solar epoch. It is seen that the scattering falls to its least value in 1953–54, the period of sunspot minimum, and increases rapidly to a maximum in 1957–58. At an angular distance of $16R_\odot$ no such variation is apparent and there seems to be no significant change during

the solar cycle. Since at $16R_\odot$ we are concerned with scattering in the equatorial region, and at $8R_\odot$ with regions nearer the pole, these results suggest that the distribution of the scattering irregularities follows the changing form of the visible corona, which tends to become more spherical towards sunspot maximum.

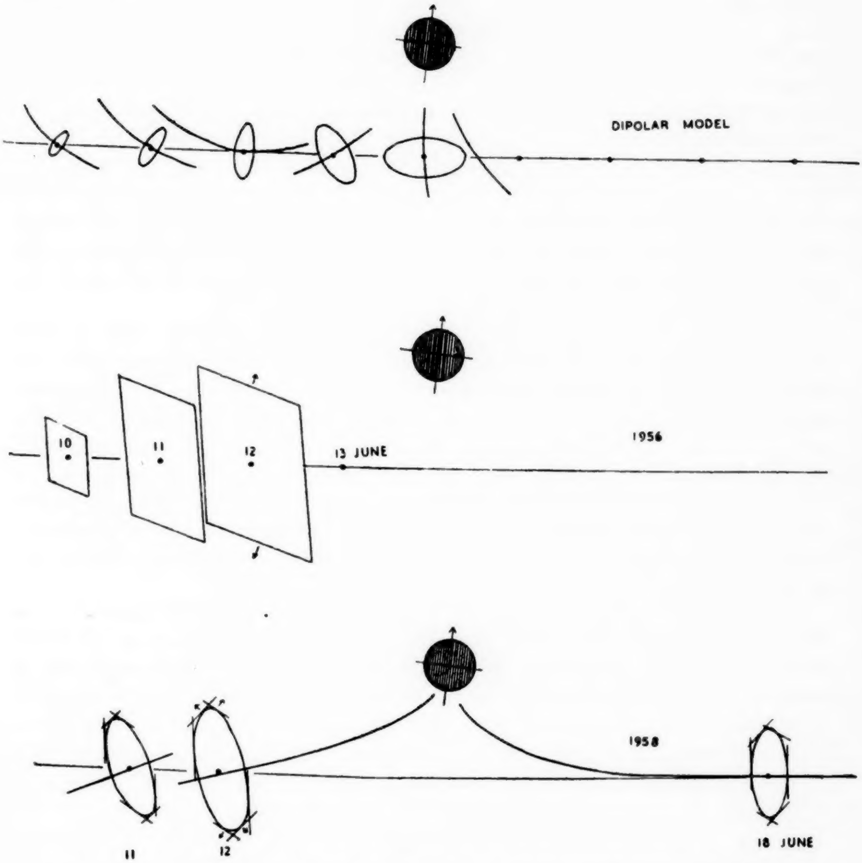

FIG. 10.—*The scattering computed for a dipolar model of the general magnetic field compared with observations carried out in 1956 and 1958 at 7·9 m. The arrows denote lower limits of the observed scattering.*

(*e*) *The scattering anisotropy.*—The observations carried out in 1956 and 1958 (outlined in Section 2), using interferometers aligned in different directions, showed that the scattering was more pronounced in a direction parallel to the solar axis. In 1956 only two axes were used so that the observations could either be interpreted as a scattering of the radiation over an elliptical area, or simply along a line in a direction intermediate between the interferometer axes. This ambiguity was removed in 1958 by the use of three axes and some ellipses defined by the three scattering angles are shown in Fig. 10*. The

* It is likely that the ellipses for other days will be known after a more complete analysis of the 1958 data has been carried out.

results for the two years are seen to be quite compatible since, for 1956, any ellipse which has the observed limits of scattering in the two directions as tangents represents a possible interpretation.

It was shown in Section 3 (*b*) that anisotropy arising from the radial gradient of scattering was small at angular distances exceeding $12R_\odot$ and it follows that the irregularities themselves must scatter anisotropically.

The origin of coronal irregularities whose size is smaller than the mean free path raises difficulties unless it is assumed that they are maintained by a magnetic field (Hewish 1955). If a general magnetic field pervades the outer corona to distances of at least $20R_\odot$, then material will diffuse rapidly along the direction of the field but not across it, and it is reasonable to suppose that this process will produce a filamentary structure similar to the visible polar plumes. Any individual filament will scatter perpendicularly to its axis and it is likely that the integrated scattering along a line of sight will show anisotropy dependent upon the mean direction of the magnetic field. It is shown in the next section that such a model accounts for the observations, provided that the lines of force are more radial than those of a dipole field.

4. *Scattering by irregularities aligned in a magnetic field.*—The present observations are not sufficient to deduce, uniquely, the precise shape and distribution of the scattering irregularities throughout the corona. It is, however, possible to suggest a type of coronal model in reasonable agreement with the data. Such a model must account both for the variation of scattering with angular distance from the Sun and for the shape of the scattered distribution. In computing the scattering the following quantities are relevant: (i) the size and shape of the irregularities; (ii) $\Delta N/N$, the variation of the electron density from its mean value; and (iii) the radial variation and latitude dependence of both (i) and (ii).

In the model adopted it has been assumed (*a*) that the irregularities are aligned by dipole magnetic field in the range 5–$20R_\odot$, (*b*) that the mean equatorial electron density is that given by Blackwell (1956) and that the contours of constant density are ellipses of axial ratio 3 : 1, (*c*) that the value of $\Delta N/N$ is constant and (*d*) that the average size of the irregularities is independent of latitude near the Sun's surface. The regions of higher and lower density thus take the form of slightly conical filaments along the field lines whose area of cross-section is approximately the same at their base.

Since, as we suppose, the irregular structure arises from diffusion along the field of density variations generated at the base of the corona, conditions (*a*) and (*b*) may not be quite independent. The radial variation of density along visible streamers is, however, known to be more rapid than can be accounted for by an outward flow alone (van de Hulst 1950) and it seems not unreasonable to assume that the shape of the filaments is determined by the magnetic field, while their density is controlled by other factors.

To compute the scattering for various lines of sight the model corona was divided into ten concentric shells, the bounding surface between adjacent shells being swept out by the rotation of a particular loop of force about the dipole axis. The scattering was assumed to be constant along each element of a line of sight within a given shell, and its value was estimated from the mean density, cross-sectional area and orientation of the filaments. Finally, the contributions due to each shell were integrated to yield the approximate

elliptical distributions shown in Fig. 10, where the lines of sight correspond to 1956 June 10–14*. Since neither $\Delta N/N$, nor the cross-section of the irregularities, is known absolutely only relative values of the scattering may be derived. Modifications due to the radial gradient of scattering have also been ignored, which implies that the results are not applicable to a wave-length of 7·9 m for angular distances less than about $10R_\odot$ (cf. Section 3 (*b*)). The latter effect will tend to distort the ellipses into a crescent form.

Comparing these theoretical results with the observations of 1956 and 1958, it is seen that the eccentricity of the ellipses agrees reasonably well; their inclination, however, is not in agreement with the expectations of a dipole model. The observations suggest that the field lines extend more or less radially with no tendency to turn into the equatorial plane.

In order to check the radial variation of scattering the relative scattering in an EW direction only has been plotted as a function of radial distance. This curve has been fitted to the experimental results for 1956 as shown in Fig. 11. The experimental curve is a composite one in which observations

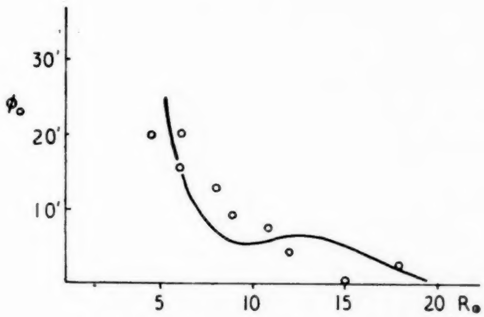

FIG. 11.—*The radial variation of EW scattering observed in* 1956 *compared with that predicted for a dipolar model.*

at all wave-lengths have been scaled to a wave-length of 3·7 m. It is seen that there is fair agreement although there is no evidence for the flattening of the theoretical curve at about $10R_\odot$. This flattening arises from the rotation of the axis of the ellipse and its absence again suggests that the magnetic field does not bend towards the equatorial plane as must a dipole field.

It is concluded that the type of model discussed, with some modification of the magnetic field, gives a fair representation of the observed scattering. It seems likely that more detailed measurements will provide valuable information on the direction of the solar magnetic field at great distances from the Sun.

It should also be noted that the model discussed is one in which material flows outwards from the base of the corona. The alternative possibility, in which the outer corona consists of matter flowing inwards, makes it difficult to account for the present observations.

* For a line of sight crossing the polar axis the projected direction of the filaments is entirely north–south and purely east–west scattering might be expected. This does not occur, owing to the strong isotropic scattering from the particular filaments tangential to the line of sight in front of, and behind, the Sun.

Acknowledgments.—It is a pleasure to express my thanks to Mr M. Ryle for his encouragement and advice throughout this work. I am also indebted to Dr R. G. Conway and Mr J. A. Högbom for their assistance with the observations in 1954 and 1958 respectively.

Cavendish Laboratory,
Cambridge:
1958 *July* 28.

References

K. E. Machin and F. G. Smith 1952, *Nature* (*Lond.*), **170**, 319.
A. Hewish 1955, *Proc. Roy. Soc.* A, **228**, 238.
H. C. van de Hulst 1950, *B.A.N.*, **410**, 135.
V. V. Vitkevitch 1955, *Dokl. Akad. Nauk. U.S.S.R.*, **101**, 429.
— 1958, *Astr. Zh.*, **35**, 52.
E. J. Blum and A. Boischot 1957, *The Observatory*, **77**, 205.
O. B. Slee 1956, *The Observatory*, **76**, 228.
D. E. Blackwell 1956, *M.N.*, **116**, 56.
A. Hewish 1957, *The Observatory*, **77**, 151.
F. Link 1951, *Bull. Astr. Czech.*, **3**, 6.

MEASUREMENT OF THE PROFILE OF A LUNAR WRINKLE RIDGE

Gilbert Fielder

(Received 1958 June 17)

Summary

A lunar wrinkle ridge has been measured uniquely by means of a method which involves measuring the changing length of a shadow cast across it by a neighbouring mountain. Probable errors in the positions of points are ± 330 m in the plane of the surface, and only ± 14 m along normals to the surface. The profile of the wrinkle ridge shows that it cannot be regarded as a wave front of solidified lava.

---

1. *Principle of the method.*—In essentials the method is that which McMath, Petrie and Sawyer (1937) proposed and used to obtain cross-sections of parts of Theophilus. Cine photographs are taken of the surrounds of a lunar mountain which is casting a shadow either at local sunrise or at local sunset. The length of the shadow is measured on every good negative and, the instant of each exposure being known, it is possible to reduce the measurements to differences in vertical height of the country across which the shadow-tip travels.

2. *Equipment employed.*—The telescope used for these observations was the $f/30$, 60 cm refractor of the Observatory of the Pic-du-Midi. At the prime focus, the image of full Moon is about 16 cm in diameter, and the depth of focus is about 1 mm at $\lambda = 560$ mμ. A passband of only about 150 A, which centred on this wave-length, was necessary partly because of the characteristics of the film which was selected and partly because the secondary spectrum of the objective is such that the longitudinal aberration is zero at 585 mμ, and the curve rises rather steeply to either side of this point, so that to have utilized light of shorter wave-length than 550 mμ, or of greater wave-length than 630 mμ, would have necessitated the use of even smaller passbands and exposures increased beyond reasonable limits.

Since the experiments were concerned essentially with photography of the terminator regions, where contrasts are very low, it was necessary to select an emulsion having as high a contrast as possible, compatible with a grain size smaller than the best seeing disk. Tests showed that resolution was limited by scintillation, and not by grain-size. Of eight emulsions tested, each in conjunction with five different filters, four different developing agents, and differing times of development at constant temperature, the best proved to be Ilford 5G91 in spite of the rather long exposure time of $\frac{3}{4}$ sec which had to be employed. This was used in conjunction with the Chance glass filter OY2 (yellow) and was developed for 40 minutes in Microphen or Promicrol at 20 °C.

A 35 mm film holder for 30 m of film was adapted to automatic lunar cine-photography. The obscurator used was a self re-cocking Zeis Ikon tri-metal leaf shutter, which yielded a clear aperture 2·5 cm in diameter when fully opened.

Elementary considerations showed that a sufficiently large rate of taking pictures was one per minute. A 1 r.p.m. synchronous motor was therefore arranged to operate the shutter by means of a cam, shown in Plate 8. This motor also wound on the film. The cam closed and opened a microswitch which was wired in series with a solenoid and 24 volt d.c. supply. In the closed position of the shutter the solenoid core, which was linked mechanically with the shutter lever, was held out of the solenoid by the shutter spring. When the microswitch was closed, the core plunged into the solenoid, opening the shutter. The duration of the exposure depended only upon the pre-set position of a timing lever which was attached to the shutter; the speed was continuously variable from 1 sec up to 1/100 sec, and there was a setting for a "time" exposure.

The smaller of the visible cog-wheels in Plate 8, fixed to the spindle of the motor and carrying the cam, had a quarter of its total number of teeth removed. Thus, in operation, the motor was running continuously but the driven (larger) cog-wheel was at rest for 25 per cent of the time; it was an easy matter to arrange the system so that the shutter was opened and closed only within the interval during which the film was stationary. In addition, the geometry of the cog-wheels and sprocket was chosen so that a suitable frame-spacing was obtained.

The film-holder was mounted on a specially constructed optical bench of steel which was fixed rigidly to the eyepiece end of the telescope. Focusing was achieved with the aid of a reflex system by sliding the film-holder along this optical bench. The observer viewed the image of the Moon in the plane of the scratches on a clear strip of film placed in position for normal photography, behind a pressure plate in the film-holder. This was made possible by having a hole 0·9 cm in diameter in the pressure plate. The images were viewed with a compound microscope mounted on the lid of the film-holder. When the images of the scratches on the film and of the Moon were sharply defined and coincident, the film-holder was clamped rigidly to the optical bench. The film-holder was then loaded with a roll of film, and the assumption was made that the depth of focus was of sufficient magnitude to accommodate any change of focus during a night's work. This assumption was not disproved.

The time of the first exposure was noted and successive frames were spaced by nearly equal intervals of one minute of time. (Slight corrections to the synchronous motor had to be effected because of mains' fluctuations.) A finder was used for guiding.

3. *Reductions of the film.*—The instrument which was selected for measuring shadow lengths on the negatives of the film was a Mark II Automatic Recording Microdensitometer, manufactured by Joyce, Loebl and Company, of Newcastle-upon-Tyne. Orientation of each transparency was effected rapidly, since the translucent table which carried it could be rotated about a vertical axis as well as displaced in two horizontal mutually perpendicular directions. It was an easy matter to align a pointed shadow with the line of scanning.

The measured shadow lengths were converted into seconds of arc, s. It may be shown that, at a given instant,

$$s \doteqdot \frac{56207(1+h)\sin\phi}{\operatorname{cosec} p - c}\{\sin A - \sqrt{\sin^2 A - h(2-3h)}\}, \tag{1}$$

where A (degrees) is the altitude of the Sun at a point P, on the Moon's surface, defined by the selenographical coordinates (λ_P, β_P) of the mountain peak which

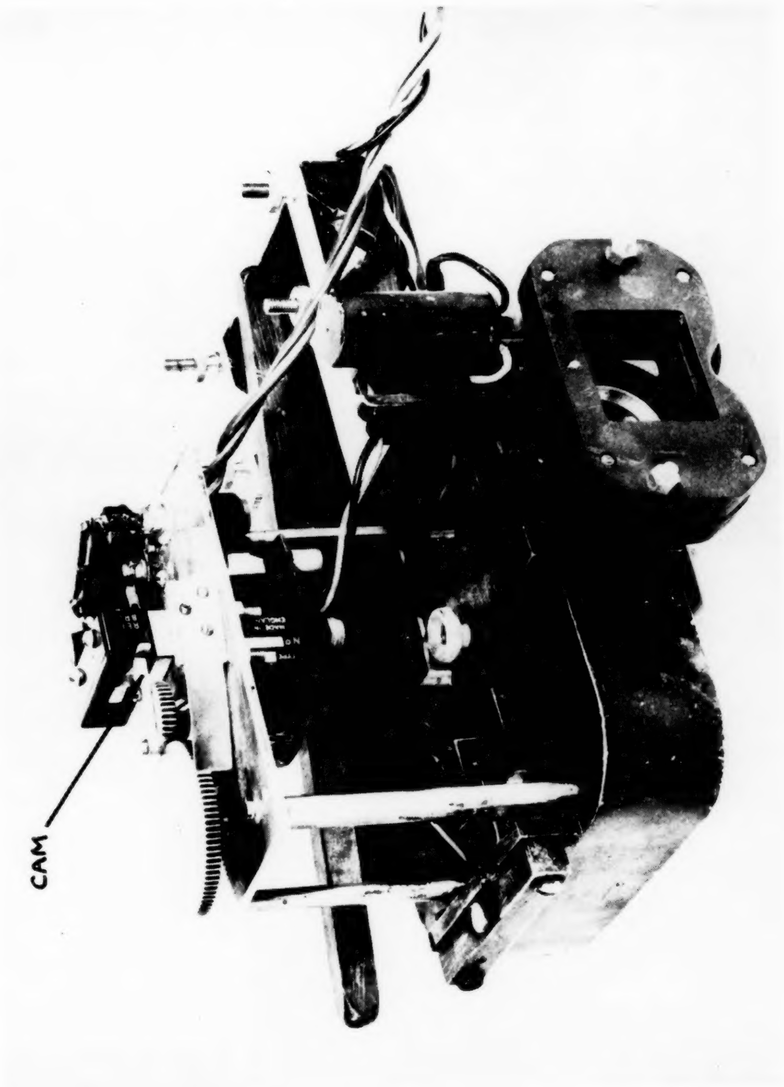

Gilbert Fielder, Measurement of the profile of a lunar wrinkle ridge.

N

is
qu
ϕ
pe
T

wl

is
by
β_I
is
fr

ar
wi
si
T
as

ob
du
in

A
to

Fr

In

Si
of
(5

$\pm$
sy

is casting the shadow, p is the equatorial horizontal parallax of the Moon, the quantity $(\operatorname{cosec} p - c)$ is the distance between the observer and the point P, ϕ is the phase angle, and h is the difference in height of the top of the mountain peak and the tip of the shadow, measured in units of the Moon's mean radius. The principal terms in c have been discussed in a paper by MacDonald (1931).

Solving equation (1) for h,

$$h \doteqdot \frac{s}{E}\left(\sin A - \frac{1}{2}\frac{s}{E}\right), \tag{2}$$

where

$$E \equiv \frac{56207 \sin\phi}{\operatorname{cosec} p - c}.$$

4. *Results and estimated errors.*—The particular peak of concern in this paper is that near to the southern termination of the lunar Alps. It is designated β by Wesley and Blagg (1935) and has selenocentric coordinates $\lambda_P = +6^\circ{\cdot}03$, $\beta_P = +31^\circ{\cdot}00$, taken from the same I.A.U. map. The wrinkle ridge in question is that which, at a mean distance of some 30 km east of peak β, runs roughly from north to south. The profile of the wrinkle ridge has been plotted in Fig. 1.

The measured section, which cuts roughly east to west, indicates that there are minor ridges running along the top of the broad-based wrinkle ridge. The width of the base of the ridge is of the order of 20 km. Also, the country on *both* sides of the wrinkle ridge is lower than the crests of the ridge by at least 100 m. These facts seem to indicate that the wrinkle ridge is not a frozen wave of lava, as Baldwin (1949) has suggested.

Profiles of the eastern slopes (broken lines) of this wrinkle ridge were not obtained because the hills themselves shielded the sunlight from these regions during sunrise. However, the western slopes of the ridge are seen to be vertical, in places, and undercuts in these parts are not excluded.

An estimate of the most probable diameter of the seeing disk gave $\sim 0''{\cdot}33$ arc. As a first approximation, therefore, it is thought reasonable to take the error in s to be $\delta s = \pm 0''{\cdot}16$ (i.e. ± 330 m).

The estimated error in h is then given by

$$\delta h = \frac{\partial h}{\partial s}.\delta s + \frac{\partial h}{\partial A}.\delta A + \frac{\partial h}{\partial E}.\delta E. \tag{3}$$

From equation (2),

$$\frac{\partial h}{\partial s} \doteqdot \frac{\sin A}{E} - \frac{s}{E^2}. \tag{4}$$

In equation (4) s/E^2 is essentially positive. Hence,

$$\left(\frac{\partial h}{\partial s}\right)_{\max} = \frac{\sin A}{E}. \tag{5}$$

Since A and E are quantities which have been computed to the desired degree of accuracy, $\delta A = \delta E \simeq 0$, and using these conditions, together with condition (5), in equation (3),

$$(\delta h)_{\max} = \frac{\sin A}{E}.\delta s. \tag{6}$$

Using $\delta s = \pm 0''{\cdot}16$, it follows that the estimated error in h does not exceed ± 14 m. It should be noted that the assumption has been made that any systematic errors having their origin in the photographic emulsion have been

neglected, and hence the quoted error should be considered to be a provisional estimate, only.

Peak β towered to a height of 1390 m above the arbitrary zero level shown in Fig. 1; but the exact radius of the arbitrary reference surface is not known and it is necessary to refer the height of the peak to some point on the ridge. The peak is 1290 ± 14 m above the highest point of the wrinkle ridge, and 1440 ± 14 m above the lowest point measured. On subtraction, these figures give 150 ± 28 m for the greatest difference in the altitudes of points on and adjacent to the wrinkle ridge.

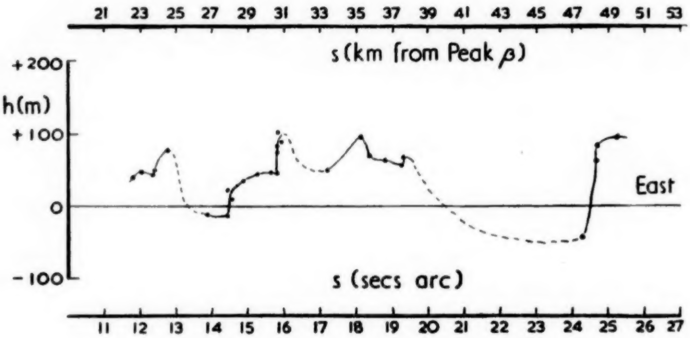

Fig. 1.—*Profile of a wrinkle ridge.*

5. *Acknowledgments.*—Professor Z. Kopal directed this work and he and Dr J. Ring of Manchester University very willingly sacrificed a great deal of their time to advise me. Workshop facilities were provided at Manchester by Dr H. J. J. Braddick, and at the Pic-du-Midi by the Director of the Observatory, Dr J. Rösch, who liberally granted us some four months of observing time. M. M. Gentili and Dr A. H. Batten were very helpful when assistance was required in the Observatory, and the cosmic ray group from Imperial College, who were working there under the direction of Professor C. Butler, kindly loaned us photographic processing equipment.

All the computation for this paper was undertaken by Mr C. G. Fielder, to whom I am deeply grateful. The work was performed as part of a programme of lunar topographical studies which was launched by the University of Manchester.

Department of Astronomy,
The University,
Manchester, 13:
1958 *June.*

References

Baldwin, R. B., 1949, *The Face of the Moon*, Chicago.

MacDonald, T. L., 1931, "On the Determination of Relative Lunar Altitudes", *J. Brit. Astr. Assoc.*, **41**, 367–379.

McMath, R. R., Petrie, R. M. and Sawyer, H. E., 1937, "Relative Lunar Heights and Topography by means of the Motion Picture Negative", *Publ. Obs. Univ. Mich.*, **6**, 67–76.

Wesley, W. H. and Blagg, M. A., 1935, *Map of the Moon*, I.A.U., Lond.

A SHORT METHOD FOR THE DISCOVERY OF NEPTUNE

R. A. Lyttleton

(Received 1958 September 25)

Summary

The mathematical basis is described of a method for the discovery of Neptune that involves far less numerical calculation. The time of heliocentric conjunction can be found solely from considerations of the discrepancy in the longitude of Uranus. This information alone makes prediction possible within less than 15° on the basis of Bode's law. By finding the distance in a circular orbit appropriate to the best fit of the observations a prediction can be made comparable in accuracy with that achieved by Le Verrier. It is shown how by suitable combination of the equations of condition the number of unknowns can be reduced to three (as compared with eight in the original methods) for any assumed mean distance, and the same process removes certain awkward features that would otherwise enter for orbits near the 2 : 1 resonance.

---

1. *Introduction.*—It is an outstanding question of interest in relation to the discovery of Neptune whether in fact there could have been devised any much less laborious method that would have achieved the prediction with an accuracy comparable with that attained by Adams ($2\frac{1}{2}^\circ$) and Le Verrier (1°). Such a method is described in the present paper as to its theoretical basis; the details of its numerical application have been given in full elsewhere*. The whole of the present investigation was inspired by discussions between the author and J. E. Littlewood following the 1946 centenary celebrations of the original discovery, and the procedure here described in Section 2 for estimating the time of heliocentric conjunction, which is the first step of the present method, is due principally to him†.

It is helpful first to explain briefly why the original methods were so extensive, and for this the one used by Le Verrier will be sufficient‡. All perturbations by known planets having been dealt with, the unknowns that have to be solved for consist of the four corrections necessary to the existing elements assigned to the orbit of Uranus, δa (or δn), δe, $\delta\epsilon$, and $\delta\varpi$; the four elements of the (coplanar) orbit of Neptune, a', e', ϵ', and ϖ'; and also the mass m' of the unknown planet; making apparently *nine* in all. The quantities e' and ϖ' can be replaced by $h' = e'\cos\varpi'$, $k' = e'\sin\varpi'$, as is usual, and h' and k' then occur only *linearly* in the perturbations in longitude of Uranus§. But a' and ϵ' do not occur linearly, while m' multiplies everything throughout. The mean distance a' was assigned (with considerable inaccuracy, it will be recalled) by means of Bode's law, but ϵ' occurs trigonometrically as $\begin{smallmatrix}\cos\\ \sin\end{smallmatrix}\,\epsilon'$, $\begin{smallmatrix}\cos\\ \sin\end{smallmatrix}\,2\epsilon'$, etc. To determine a first

* *Vistas in Astronomy*, Vol. III, 1959, Pergamon Press, London.

† For Prof. Littlewood's own account of the problem see his *A Mathematician's Miscellany*, pp. 117–134, Methuen, 1953.

‡ For a more detailed account of Le Verrier's method see: F. Tisserand, *Mécanique Céleste*, I, Ch. 23, Paris 1889; W. M. Smart, *Celestial Mechanics*, p. 259, Longmans, 1953.

§ Tisserand, *Mécanique Céleste*, Vol. I, p. 378.

approximation to ϵ', with a view eventually to having linear equations, Le Verrier took in turn 40 values for ϵ' spaced at 9° intervals covering the whole possible range from 0° to 360°, and for each value solved by least squares 18 consolidated equations of condition relating to 1690–1845, now in seven variables. It was then possible to select that value of ϵ' giving the best fit to the whole series of observations. Using this, he then proceeded to improve the solution to arrive finally at a set of "best" elements for Neptune.

The quantity ϵ' is closely associated with the longitude of the unknown planet, and the first step of the method to be described in this paper leads to an equivalent but even more specific piece of information concerning the unknown planet, namely the time of heliocentric conjunction with Uranus.

2. *Determination of the time of conjunction.*—The fact that the rate of change of angular momentum, dh/dt, must vanish at conjunction would enable the instant to be found were it not that $h=r^2\,dv/dt$ is not itself sufficiently well determined because of its strong dependence on the radius vector r. But an alternative procedure is possible that depends only on considerations of the longitude, and is one that involves little calculation in application.

In undisturbed elliptic motion we have for the heliocentric longitude, in standard notation,

$$v = nt+\epsilon+2e\sin(nt+\epsilon-\varpi), \tag{1}$$

to the first order in the eccentricity. We note that for Uranus $e=0{\cdot}047$. If the elements are in error as a result of small perturbations depending on the mass m' of the unknown planet (Sun $=1$), the resulting error in v will be given by

$$\Delta v = t\Delta n+\Delta\epsilon+2\Delta e\sin(nt+\epsilon-\varpi)+2e(\Delta\epsilon-\Delta\varpi)\cos(nt+\epsilon-\varpi)$$
$$+2et\Delta n\cos(nt+\epsilon-\varpi), \tag{2}$$

and on the right-hand side, from consideration of the equations of motion, the first four terms are of order m', while the last term is of order em' and so is much smaller than the others. Hence if we agree to neglect this last term we can write, with an obvious notation,

$$\Delta v = m'(a_0+bt+c\cos nt+d\sin nt) \tag{3}$$

for any discrepancy in longitude due to perturbations, correct to the present order.

Consider now the elliptic orbit E best fitting the observations of Uranus (after allowing for all known perturbations). The observations will not in fact be properly representable by E because they contain effects of the unknown body m'. Writing $v_E(t)=$ calculated heliocentric longitude of Uranus in ellipse E, $v(t)=$ actual heliocentric longitude determined from observation, then the well-known discrepancies in longitude, which constitute the observational material to be explained, are given by

$$\delta(t)=v(t)-v_E(t). \tag{4}$$

The values of $\delta(t)$ from 1690–1840 were the quantities utilized by Adams* and have been used in applying the present method. Le Verrier had observational data from 1690–1845.

Next, denoting by t_0 the instant of heliocentric conjunction that we wish to find, let E_0 denote the instantaneous, or osculating, elliptic orbit of Uranus

* *Coll. Works*, I, p. 11, Cambridge, 1896.

corresponding to t_0, and $v_0(t)$ the longitude of Uranus in this instantaneous orbit. Also let the perturbations produced by m' since time t_0 be denoted by $w(t)$, so that

$$w(t) = v(t) - v_0(t).$$

Then we have from (4)

$$\delta(t) = (v_0 - v_E) + w, \tag{5}$$

and in this both terms are of order m'. Since we are proposing to neglect all terms of order em', then in calculating $w(t)$ both orbits E and E_0 can be regarded as circular, and therefore $w(t)$ will take equal and opposite values at times equally separated on the two sides of conjunction. So if τ measures time from conjunction $w(t_0 - \tau) = -w(t_0 + \tau)$, or writing

$$W(\tau) = w(t) = w(t_0 + \tau) \tag{6}$$

then $W(\tau)$ is an odd function of τ. The analytical form of W is given below by (11) but is not required for the present purpose of finding t_0.

Now to the first term on the right in (5), the form (3) will clearly be applicable, and so

$$\delta(t) = m'\{a_0 + bt_0 + b\tau + c\cos(nt_0 + n\tau) + d\sin(nt_0 + n\tau)\} + W(\tau),$$

which may be written, introducing new constants, in the form

$$\delta(t_0 + \tau) = A + B(1 - \cos n\tau) + \{C\tau + D\sin n\tau + W(\tau)\}. \tag{7}$$

Since $W(\tau)$ is an odd function, we also have

$$\delta(t_0 - \tau) = A + B(1 - \cos n\tau) - \{C\tau + D\sin n\tau + W(\tau)\}.$$

Hence, since $\delta(t_0) = A$, it follows that neglecting terms of order em' the function given by

$$\rho(\tau) = \frac{\delta(t_0 + \tau) - 2\delta(t_0) + \delta(t_0 - \tau)}{1 - \cos n\tau} = B \tag{8}$$

will be constant.

This result provides the following simple rule for determining the approximate time of conjunction: *Select an instant t_0, calculate the second difference $\delta(t_0 + \tau) - 2\delta(t_0) + \delta(t_0 - \tau)$ for a number of values of τ, divide each by $(1 - \cos n\tau)$, and the resulting quantity will be (approximately) constant if t_0 has been selected at conjunction.*

The result of applying this rule to the observational data $\delta(t)$ (Adams, *loc. cit.*) is shown in Fig. 1. The quantity $\rho(\tau)$ turns out to be most nearly constant for a value of t_0 of about 1822·3. This time for the heliocentric conjunction in longitude differs by only just over six months from the actual value 1821·74.

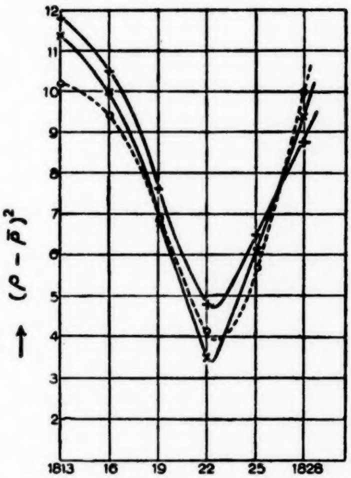

FIG. 1.—*Graph showing degree of constancy of $\rho(\tau)$. The ordinate represents the root mean value of $(\rho - \bar{\rho})^2$ plotted at t_0* = 1813, 1816, 1819, 1822, 1825, and 1828. *The different curves correspond to different weightings. For each the minimum occurs at about* 1822·3.

+ equal weightings of $\rho(\tau)$;
× weightings increasing with τ;
○ weights increasing and then decreasing.

3. *Prediction purely from a knowledge of conjunction.*—On the basis of the unknown planet being in a circular orbit, it is a simple matter once the time of conjunction is available to calculate its longitude for any assumed size of orbit. Even on the crude assumption of Bode's law, viz. $a'/a=2$, the longitude so predicted for the date of discovery is only about 13° behind the actual position. The actual planet would have been well inside a zodiacal belt 30° long by 10° wide centred on this place, which was the kind of region Airy suggested should be searched by Challis.

The foregoing procedure can be carried out with a minimum of arithmetical labour, taking at most a few hours, but the question arises, in view of the serious failure of Bode's law, which had it held would have made discovery almost triflingly easy by the present method, whether any better estimate of a'/a can be reached without unduly extensive calculation. For this purpose, Bode's law is dropped and instead we assume always a circular orbit for the unknown body, which is at least an equally valid assumption to make for any planetary orbit.

4. *Equations for finding an improved value of a'.*—On this basis then, the perturbations in longitude of Uranus are given by*

$$P(t) = -m' \sum_{1}^{\infty} F_i \sin i\{(n'-n)t+\epsilon'-\epsilon\} + m'e \sum_{-\infty}^{+\infty} G_i \sin\,[i\{(n'-n)t+\epsilon-\epsilon\}+nt+\epsilon-\varpi] \tag{9}$$

wherein

$$F_i = \frac{i(z_i^2+3)}{z_i^2(1-z_i^2)}\,aA^{(i)} + \frac{2z_i}{z_i^2(1-z_i^2)}\,a^2\frac{\partial A^{(i)}}{\partial a},$$

$z_i = i(1-n'/n)$, and $A^{(i)}$ is a certain infinite series in a/a'; while a similar form gives G_i. Unless a definite numerical value is adopted for a/a' there is clearly therefore no possibility of arriving at linearized equations, and this plainly must have been the great attraction of Bode's law.

The assumption of a circular orbit and knowledge of the time of conjunction immediately reduce the number of unknowns associated with Neptune to *two*, namely m' and a', and also remove altogether the awkward feature otherwise produced by the appearance of ϵ' trigonometrically, for once conjunction is known t can be measured from it. Also since e is small, the terms in $m'e$ in (9) are small compared with those solely in m', and the perturbations can be calculated as if Uranus itself moved in a circular orbit. The principal terms in $m'e$ can however readily be included for higher accuracy. Accordingly, if from now on the time is measured from conjunction, the whole expression for the discrepancies in heliocentric longitude will be of the form

$$\delta v = \delta\epsilon + t\delta n + \delta\alpha \sin nt + \delta\beta \cos nt + P(t) \tag{10}$$

wherein now

$$P(t) = -m' \sum_{1}^{\infty} F_i \sin i(n-n')t = -m' \sum_{1}^{\infty} F_i \sin iD, \tag{11}$$

say. If, for any assumed value of a/a', direct comparison of (10) with the observations is made, the variables are now only *five* in number, $\delta\epsilon$, δn, $\delta\alpha$, $\delta\beta$, and m', already a considerable reduction on the number used by Adams and

* Tisserand, Vol. I, p. 365.

Le Verrier, though practical application would require solution for a number of values of a/a'. But it is possible to eliminate the variables $\delta\alpha$ and $\delta\beta$, as we shall next explain.

5. ***Further reduction of the number of unknowns.***—In view of the unavoidable feature that a series of values of a/a' must be taken, it is convenient to take advantage of a simple regrouping of the equations of condition that has the effect of removing $\delta\alpha$ and $\delta\beta$, as well as a certain other important consequence. For this, we note the simple identities

$$\frac{\sin}{\cos}(x+\theta)+\frac{\sin}{\cos}(x-\theta)-\frac{\sin}{\cos}x=(2\cos\theta-1)\frac{\sin}{\cos}x \tag{12}$$

in which, if $\theta=60^\circ$, the right-hand sides vanish.

Now for Uranus $2\pi/n=84{\cdot}015$ years, and accordingly 60° of longitude is described by the planet in almost exactly 14 years. Hence if instead of a particular observation (discrepancy in longitude), $f(t)$ say, we adopt

$$f(t+14)+f(t-14)-f(t),$$

where t is now measured in years, then the terms in $\delta\alpha$ and $\delta\beta$ will disappear.

This device is of course no more than a regrouping of the equations of condition, incidentally reducing their number since, to some extent, 14 years are lost at each end of the range of available observations. But as will be shown later it simultaneously has the important effect of making the method safely applicable near the resonance $n/n'=2$ (for which $a/a'=0{\cdot}63$ approximately) where in fact the coefficient F_2 can become very large.

Under this regrouping, the terms $\delta\epsilon+t\delta n$ come out the same, but the terms in $P(t)$ have to be adjusted as to their coefficients. For the term in $\sin D$, for instance,

$$\begin{aligned} D+\theta &= (n-n')(t+14) \qquad \text{where} \quad n\,.\,14=60^\circ \\ &= D+(1-n'/n)60^\circ. \end{aligned}$$

So, writing $\nu=n'/n$, we have $\theta=(1-\nu)60^\circ$, and hence to transform $P(t)$ the coefficient F_1 has to be multiplied by $2\cos\{(1-\nu)60^\circ\}-1$, the coefficient F_2 has to be multiplied by $2\cos\{(1-\nu)120^\circ\}-1$, and so on. With these conversion factors applied, we can write, denoting the new coefficients by f_i,

$$Q(t)\equiv P(t+14)+P(t-14)-P(t)=m'\sum f_i\sin iD, \tag{13}$$

and the revised equations of condition take the form

$$\delta\epsilon+t\delta n+Q(t)=\delta v(t+14)+\delta v(t-14)-\delta v(t), \tag{14}$$

and these, for each selected a/a', involve now only *three* unknowns, namely $\delta\epsilon$, δn, and m'.

The procedure adopted was therefore to set up these modified equations of condition for each of a short series of values of a/a', and solve by least squares to find what value of the ratio of axes gives the best fit to the observations.

6. ***Effect of the transformation on the coefficient F_2.***—The following table shows the values of F_1, F_2, F_3, F_4 for an appropriate set of values of a/a'.

TABLE I

Coefficients of terms in $P(t)=m'\Sigma F_i \sin iD$

a/a'	$\sin D$	$\sin 2D$	$\sin 3D$	$\sin 4D$
0·50	− 5·738	1·429	0·141	0·031
0·55	− 7·432	3·380	0·299	0·068
0·60	− 9·911	15·712	0·672	0·154
0·65	−13·718	−38·422	1·692	0·366
0·70	−19·944	−18·655	5·461	0·967

It will be noticed that F_2 becomes very large in magnitude as the resonance $n'/n=2$, or $a/a'=0·63$, is approached from either side. The expression (9), or (11), for the perturbations in longitude is not of course applicable for exact resonance, at which the coefficient F_2 would become infinite. Now to avoid excessive calculation of the various F_i for different a/a', it would obviously be convenient if we could interpolate within the above table, but in the case of F_2 interpolation from only a few values is not possible with much accuracy because of the resonance. (All these coefficients are nowadays available in tabular form*, but as they were not so to Adams and Le Verrier any comparison of methods must suppose the F_i to be calculated as part of the work.)

But the conversion factor $2\cos\theta-1$ vanishes at the resonance when the coefficient F_2 has its infinity through the factor $1-z_i=2\nu-1$ in its denominator. But it is easily seen that the expression

$$\frac{2\cos\{(1-\nu)120^\circ\}-1}{2\nu-1}$$

has limit $\pi/\sqrt{3}$ as $\nu\to\frac{1}{2}$, and the coefficient f_2 passes smoothly through the resonance value without singularity, as the following table of the transformed coefficients shows:

TABLE II

Coefficients of terms in $Q(t)=m'\Sigma f_i \sin iD$

a/a'	$\sin D$	$\sin 2D$	$\sin 3D$	$\sin 4D$
0·50	− 3·208	−0·814	−0·266	−0·087
0·55	− 4·664	−1·290	−0·469	−0·176
0·60	− 6·877	−2·052	−0·821	−0·345
0·65	−10·382	−3·299	−1·436	−0·666
0·70	−16·165	−5·471	−2·558	−1·284

The smooth trend of these coefficients makes sufficiently accurate interpolation for other intermediate values of a/a' easily possible, for it is mainly the general form of the curve represented by $Q(t)$ as a/a' changes that matters, and our aim is to find that value of a/a' giving the closest fit to the (adjusted) observations. Another feature of this table is that the coefficients corresponding to $\sin 5D$ and $\sin 6D$ can also be roughly estimated for any given a/a' from inspection of the general run of the earlier coefficients.

7. *The solution giving the best fit.*—The equations of condition (14) have been set up and solved for a series of seven different values of a/a' ranging from 0·50 (Bode's law) to 0·65. The mean square value of the resulting sets of residuals for each solution is shown plotted against a'/a in Fig. 2, from which it is seen that there is a pronounced minimum at just about $a'/a=1·6$, and there is obviously

* *Yale Trans.*, VI and VII, Cambridge, 1932.

little point in endeavouring to improve on the round figure of 1·6 for the ratio of axes. This corresponds to a mean distance for the unknown planet of 30·71 a.u. compared with the true value of 30·07.

The longitude thereby predicted for the date of discovery is readily found to be 329°·4 compared with the actual value of 328°·4. The error of the present method is therefore about 1° ahead of the true position, whereas that of Le Verrier was just under 1° behind.

Consistently with the closeness of a' to the true value, the present method also gives a closer value of the mass of the unknown body than was obtained by either Le Verrier or Adams. The value found is $m'/\odot = 1/25\,000$ in round figures.

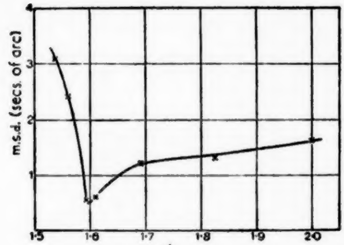

FIG. 2.—*Curve of mean square residuals computed for a number of values of a'/a. The best fit is seen to occur at about $a'/a = 1 \cdot 6$.*

8. *Prediction at a date other than* 1846.—The orbital elements (and mass) obtained by the various methods, adopting the better of the two solutions given by Adams, are as follows.

TABLE III

	Adams	Le Verrier	Present method	Neptune
a	37·25	36·15	30·71	30·07
e	0·1206	0·1076	0	0·0086
ϖ	299°	285°	—	44°
$\odot/m'$	6670	9350	25500	19300
Longitude at discovery (equinox 1950)	330°·9	327°·4	329°·4	328°·4

It is a simple matter to find the longitude that these solutions would predict at any other time than 1846·73, the time of discovery. The three curves of Fig. 3 show the difference between the longitude calculated in turn from the above values and the actual longitude of Neptune. It is evident from the curves that some element of good fortune entered into the predictions to make them as good as they were. Le Verrier's solution appears superior to that of Adams, and his prediction would have been better still at a somewhat earlier date (supposing the same material to have been available, which could not in fact have been so) since the error changes sign at about 1842. Both solutions place the unknown planet *ahead* of the true position in the earlier part of the range, so that with a'/a assumed nearly equal to 2, the hypothetical planet will move more slowly than the actual one and therefore must eventually coincide with it in longitude. For Adams' solution this does not occur till as late as 1856. But their orbits were intended to fit the observations prior to 1840 in Adams' case, and 1845 in Le Verrier's, so comparison can only properly be made for times earlier than discovery. This shows that the errors implied by Adams' solution are on the whole roughly twice as great as those of Le Verrier's. (A possible reason for this is discussed below.) On the other hand the circular solution arrived at by the present method shows an accuracy comparable with that of Le Verrier's orbit, but persisting over a much longer range in time. The three

curves show that $\pm 1^\circ$ accuracy would be obtained by Adams' solution only for about 5 years, by Le Verrier's solution for about 12 years, while for the present solution it would obtain for about 24 years.

The orbits arrived at by Adams and Le Verrier both exhibit the curious feature that their difference in longitude from the true position is at its least fairly near the time of prediction—six years earlier for Le Verrier and nine years later for Adams. Why this place of "best fit" should have come near the crucial time seems something of a puzzle when the observations utilized extended back some 150 years. It may well be that the latest observations were of particularly strong influence, but in any event it would seem that some element of good fortune attended the degree of closeness of the actual prediction.

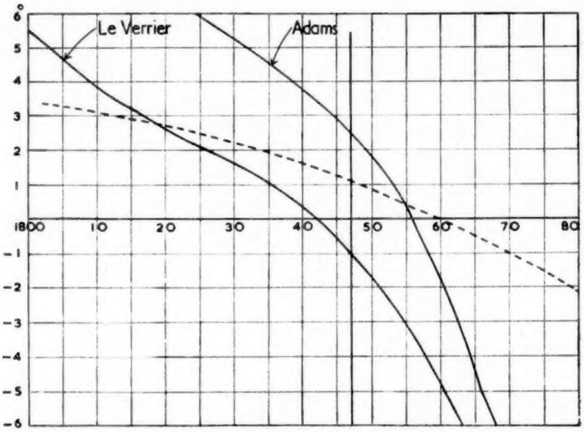

FIG. 3.—*Showing the amounts by which the orbits of Adams, Le Verrier, and the circular orbit solution differ from the true position of Neptune.*

9. *Other points.*—The weaker agreement of Adams' orbit with the actual one seems very probably to arise from what appears to be an invalid step made by him at the very outset of his work. Adams says (*loc. cit.*, I, p. 11) "It is easily seen that the series expressing the corrections of mean longitude in terms of the corrections applied to the elements of the orbit, is more convergent than that which gives the correction of the *true* longitude, and the same thing is true for the perturbations of the mean longitude, as compared with those of the true. The corrections found above were accordingly converted into corrections of mean longitude by multiplying each of them by the factor r^2/ab." Now whereas such a relation as that here claimed subsists between the true longitude and the mean longitude in an *undisturbed* orbit in virtue of the equation

$$r^2 \frac{dv}{dt} = h = nab,$$

which may be written

$$(r^2/ab)\, dv = n\, dt = dl, \tag{15}$$

there would seem no validity in supposing that in perturbed motion the variation in true longitude Δv and that in mean longitude Δl are similarly related.

No such relation seems known in celestial mechanics. We have in any case that

$$v = \int hr^{-2}\,dt, \qquad l = nt + \epsilon,$$

and so for a variation Δ, in which all the elements are changed,

$$\Delta v = \int (r^{-2}\Delta h - 2hr^{-3}\Delta r)\,dt, \qquad \Delta l = t\Delta n + \Delta\epsilon,$$

and that the ratio of these cannot reduce to a form independent of the variations of the elements, such as (15), seems evident. But the actual case is more complex still because the discrepancies involve also the corrections to the orbit of Uranus. The validity of this step has also been queried by E. W. Brown*.

In his paper E. W. Brown also was concerned with the possibility of finding some simple criterion for the prediction of an unknown planet, and the method he proposed therein rests on consideration of the series $-m'\sum F_i \sin iD$ for the principal perturbations in longitude, naturally enough, as here. Brown's discussion shows how the general trend of this function (with changing a/a'), rather than its precise value at all stages, is sufficient to estimate the position of the unknown planet, though he applies the method on the basis that the first three terms of this function are adequate. Independent preliminary determination of the instant of conjunction is not included in his method, and one gets the impression that this could be a considerable defect when it comes to application. There is difficulty in being certain, however, from the actual work given in his paper, since the present author has not found it possible to recover the numerical values he gives for several of the various coefficients. At all events, Brown himself reaches the conclusion that his method predicts conjunction as occurring *close to* 1840, which in fact is almost 90° from the true position, and would lead to a longitude at the time of discovery some 27° ahead of the actual place of Neptune, even assuming a circular orbit at exactly the right distance. Nevertheless, the general theory behind Brown's method would appear to be sound, though, handicapped as it would be in detailed application by lack of knowledge of conjunction, to reach a prediction of accuracy comparable with those of Adams and Le Verrier might very well require considerable numerical labour.

St. John's College,
Cambridge:
1958 *September* 19.

* *M.N.*, **92**, 93, 1931. See Section 14.

STELLAR GROUPS. III. THE SPACE MOTIONS OF SOME MAIN SEQUENCE DWARFS

Olin J. Eggen

(Communicated by the Astronomer Royal)

(Received 1958 September 8)

Summary

Using photoelectrically determined magnitudes and colours, photometric parallaxes have been determined for 359 stars with known radial velocity and proper motion that have been spectroscopically classified as main sequence dwarfs on the Mt Wilson or Yerkes Observatory systems. These parallaxes have been used to compute the **U**, **V**, **W**-vector space motions of the stars. The stars were subdivided according to the size of the W-motion (perpendicular to the galactic plane) and the motions plotted in the U, V-plane in Figs. 2 to 5. These figures suggest that the distribution of space motions, at least for small values of W, is not random.

Introduction.—In previous papers of this series (Eggen 1958*a*, *b*; Papers I and II) several widely scattered stars were assigned to five groups—the Hyades, Sirius, ζ Herculis, ϵ Indi and 61 Cygni groups—on the basis of the apices and total amounts of their apparent motions. This method—which we will call the "convergent-point method"—of choosing group members has the advantage that the parallaxes, which are accurately known for very few stars, are not used. After the members of the above-mentioned groups were chosen by the convergent-point method, the distances computed for the individual stars, from the group motion, were shown to agree satisfactorily with those derived from the observed parallaxes, within the very wide limits of uncertainty of most of the latter. Also, several tests, discussed in Papers I and II, indicated that far too many stars satisfied the requirements for group membership to be the result of chance coincidences of apparent motion. Nevertheless, the reality of the groups will remain in doubt until the space motions of the individual stars can be examined and the design of the present paper is to explore the possibility of using photometric parallaxes for this purpose.

Photometric parallaxes.—In a previous paper (Eggen 1956) photometric parallaxes were computed for 285 main sequence stars with annual proper motion exceeding $0''\cdot5$. In addition to the correctness of the fundamental assumption that main sequence stars later than, say, G0 have a unique colour–luminosity relation, the accuracy of such parallaxes depends upon (1) the accuracy of the colours and magnitudes, (2) the freedom of the observed colour from contamination by interstellar reddening or the presence of a companion star, and (3) the validity of the assumption that a star is a main sequence dwarf. There is some evidence, mainly from open clusters (Eggen 1955), that (*a*) spectral classification on either the Mt Wilson or Yerkes system—at least in the range from G0 to K5—can

distinguish the main sequence dwarfs from the subdwarfs and subgiants; and (*b*) the colour–luminosity relation for these main sequence dwarfs, in the same spectral range, is given by $M_V = +2^m\cdot56 + 5\cdot84(P-V)_E$, for all values of $(P-V)_E$ between $+0^m\cdot5$ and $+1^m\cdot24$. Therefore, using all of the magnitudes and colours determined on the $(P, V)_E$-system, or reducible to that system, photometric parallaxes have been determined for the 359 stars in Table I. The parallaxes for stars with annual proper motion greater than $0''\cdot5$ have been taken from the previous publication (Eggen 1956) where a comparison with the trigonometric values is given; a few values have been altered on the basis of more recent magnitudes and colours.

Space motions.—Table I contains all stars for which (1) spectral classification of dG1 to dK5 inclusive, or G1 V to K5 V inclusive, has been assigned by Joy (cf. Wilson 1953) or by the Yerkes observers, respectively; (2) radial velocities are known; and (3) photoelectric magnitudes and colours, $+0^m\cdot5 < (P-V)_E \geqslant 1^m\cdot24$, are available. Also included are a few objects which, although just outside the spectral range given above, have colours in the accepted range. The radial velocities were taken from Wilson's catalogue (1953) except for a few published since that compilation was made. Many of the Yerkes MK classifications are by Roman (1955) but some additional classifications by Morgan and others have also been taken from the literature. In the main the Yerkes and Mt Wilson classifications agree for stars classified at both observatories, but two or three subdwarfs, on the Mt Wilson system, have been classified as main sequence objects by Miss Roman, who has also classified as subgiants or giants a half-dozen stars later than G5 which were called dwarfs at Mt Wilson; in all cases of doubt about the luminosity class, the star has been omitted from Table I. Visual binaries have also been excluded except when the difference in visual magnitude is known to be less than one or two tenths, in which case "AB" follows the HD number in Table I and the parallax was computed for the mean component; double-lined spectroscopic binaries have been excluded. The proper motions were, in decreasing order of preference, taken from the GC, Yale zone catalogues, Cincinnatti catalogues, and some unpublished Greenwich results. Of the stars which otherwise meet the requirements stated above, colours and magnitudes are available for about 90 per cent of those with annual proper motions in excess of $0''\cdot5$, 50 per cent of those with smaller proper motions but with radial velocity exceeding 50 km/sec, and only about 25 per cent of the remaining stars.

Because of the manner in which the stars in Table I have been selected, the parallaxes undoubtedly represent, within the framework of the assumptions, the most consistent set available at present. The uncertainties in the proper motions and in the radial velocities, which are all of quality *a*, *b*, or *c* (Wilson 1953), will cause some blurring of the space motions as will uncertainties in the colour, where the probable error of $0^m\cdot01$ leads to an error of 2 per cent in the parallax, but gross inaccuracies in the space motions will only arise from an error in the assumption that the star is a main sequence dwarf. The space motions, which are all referred to the Sun, are given in the vectors: **U** (directed away from the galactic centre; $l=148°$, $b=0°$), **V** (in the direction of galactic rotation; $l=58°$, $b=0°$), and **W** (perpendicular to the galactic plane; $b=90°$).

All of the stars in Table I are plotted in the U, V-plane in Fig. 1; the filled circles represent stars with positive values of W and the cross at $U=+11$ and $V=-17$ km/sec represents the velocity of the local standard of rest with respect

TABLE I

Space motions of 359 main sequence dwarfs

HD/BD	π_{pt} (0″·001)	*U*	*V* km/sec	*W*	HD/BD	π_{pt} (0″·001)	*U*	*V* km/sec	*W*
166	75	+ 16	− 20	− 10	− 7°699	73	+ 64	+ 23	− 16
245	21	+ 29	− 96	− 45	24916	71	− 5	− 2	− 16
834	51	+ 28	− 3	− 9	25329	34	+ 76	−297	+ 35
3443	64	+ 89	− 49	− 18	25680	60	+ 29	− 12	− 7
3628	33	+108	− 39	+ 43	+32°719	22	+163	−193	− 54
3651	111	− 36	− 20	+ 11	26965	193	− 96	− 12	− 46
3765	65	− 21	− 78	− 22	27274	82	+ 32	− 4	+ 44
3795	63	+ 26	− 50	+ 51	+24°659	26	+ 79	− 28	+ 37
4628	124	0	− 53	− 12	28343	62	− 34	+ 12	+ 15
4747	61	+ 38	− 15	− 6	+55°900	38	+ 74	− 42	+ 35
5133	69	+ 37	− 20	− 6	29400	28	− 33	− 62	+ 43
5351	36	+ 54	− 84	− 29	29587	29	+137	− 57	+ 18
+63°137	67	+ 82	− 63	+ 29	30003AB	38	+ 22	− 14	− 6
8262	38	+ 54	− 39	+ 8	30455	37	+ 49	− 55	− 24
9407	51	− 46	− 4	0	30495	87	+ 20	− 6	0
9540	68	+ 9	− 22	+ 3	31501	29	+ 59	− 71	+ 52
9770AB	50	+ 20	− 2	− 30	32147	125	+ 1	− 53	− 13
10126	35·5	+ 99	+ 2	+ 3	32923	74	+ 23	− 21	+ 24
10145	32	+ 95	− 52	− 11	+55°960	13	− 49	−133	−110
10307	94·5	+ 33	− 25	+ 1	+29°847	18	− 65	− 15	− 6
10436	73	− 43	− 26	− 44	34673	68	+ 79	− 56	+ 16
10476	142	− 35	− 24	+ 4	36003	82	− 74	+ 2	− 18
10780	106	+ 22	− 16	− 5	36283	20	+ 29	− 77	− 62
13043	38	− 63	− 21	+ 3	36435	54	− 10	− 4	− 18
13435	92	+ 13	− 12	+ 36	36443	22	− 55	− 94	− 12
13445	85	+106	− 79	− 20	37008	44	− 46	+ 25	− 52
13783	22·5	− 53	+ 14	−105	37394	90	+ 12	− 21	− 13
14214	60	+ 48	+ 9	+ 4	37706	46	− 43	− 14	− 23
14412	64	+ 13	+ 34	− 10	38230	53	− 25	− 65	+ 10
+70°169	27	+ 62	− 86	+ 8	38392	115	− 18	+ 5	− 11
+ 4°415	18	−165	− 78	− 66	39881	50	− 15	− 55	+ 10
16160	147	+ 71	+ 1	+ 33	+26°1067	22·5	− 90	− 43	− 75
16591	69·5	+ 19	− 29	− 37	42618	41	− 64	− 14	+ 8
16619	20·5	+ 19	− 36	− 40	42807	53	− 6	− 26	− 5
+48°739	23	− 49	−105	− 51	43147	21·5	− 4	− 50	− 86
17155	39	− 43	− 60	− 12	43834	112	− 18	− 30	− 13
17925	105	+ 16	− 19	− 10	45289	48	+ 86	− 22	− 4
18702	38	+ 84	− 64	− 17	47752	58	− 51	− 19	− 2
18757	45	+ 64	− 79	− 25	+47°1355	57	+ 50	− 44	− 26
19305	68	− 31	− 60	− 1	50281	118	− 1	+ 14	− 21
20165	47	− 11	− 58	+ 9	+40°1758	46	+ 49	− 44	+ 11
20630	111	+ 22	− 4	− 5	50806	71	+ 9	− 79	− 10
20766	68	+ 86	− 54	+ 22	51219	37·5	− 43	− 48	− 34
20794	170	+ 75	− 93	− 26	51608	31	− 20	− 35	− 27
21197	80	− 40	− 23	− 17	55458	33	− 28	+ 17	− 74
22049	321	+ 4	+ 7	− 19	56274	27	+ 92	+ 3	− 61
22496	78	+ 36	− 24	− 13	+33°1505	44	− 70	− 49	+ 3
23439AB	31·5	+112	−155	− 93	+46°1264	22	+ 47	− 50	− 66
23484	70	+ 33	− 16	− 16	+50°1435	14	− 74	− 18	− 20
24002	30	− 43	−100	− 11	60298	36	−130	− 20	− 47
24331	35	+ 90	+ 8	− 10	− 1°1792	21	− 4	− 77	+ 11
24451	66	+ 47	− 14	− 2	61606	66·5	− 28	− 2	− 9
24616	65	+ 50	− 69	− 62	+54°1175	45	+ 28	− 50	− 16

TABLE I (*cont.*)

HD/BD	π_{pt} (0″·001)	U	V km/sec	W	HD/BD	π_{pt} (0″·001)	U	V km/sec	W
62613	59	+ 10	+ 8	− 37	+29°2279	58	+ 87	− 30	− 34
63685	40	+ 31	− 31	0	107582	21	+ 5	−113	− 40
64606	39	+ 80	− 57	− 7	107596	58	− 31	− 27	+ 27
65430	42	− 45	− 53	− 15	108754	17	+ 8	−164	− 93
65583	44	+ 12	−121	− 41	+ 9°2639	58	+ 23	− 66	− 3
66171	21	+104	− 59	− 4	109200	55	+ 40	− 20	− 28
68017	43	+ 51	− 66	− 44	110463	44	− 15	+ 3	− 5
68788	33	+ 59	− 52	− 23	110833	77	+ 16	− 17	+ 13
+31°1781	51·5	+ 21	− 70	− 30	111515	26	− 45	− 96	− 56
69830	83·5	− 27	− 58	− 10	112758	44	+ 82	− 35	+ 14
70352	28·5	+ 41	− 51	+ 22	112943	36·5	+ 83	− 50	− 5
+33°1694	26	− 64	−106	− 66	113101	19	+ 93	− 69	− 33
71881	31	+ 30	− 45	+ 1	114060A	26	+ 56	− 6	+ 3
72614	33	+ 78	− 82	+ 4	114703	30	+ 86	− 78	+ 7
72673	78	+ 90	+ 5	− 26	115404	91	− 38	+ 9	− 1
73393	26·5	+ 72	− 50	− 6	115617	132	+ 21	− 43	− 29
73667	46	− 21	− 44	− 34	116012	37	+ 71	− 15	− 4
74377	38	+ 8	− 78	− 48	116495AB	51·5	+ 49	− 9	− 33
74576	91	+ 26	− 14	0	117635	43	+106	− 17	− 16
74842	45	− 21	− 10	− 20	119070	20	+ 30	− 43	− 28
75530	18	− 13	−120	− 94	+ 7°2692	28	+ 70	− 66	− 15
75632AB	83	+ 86	+ 8	− 19	120690	54	+ 31	− 48	− 9
75732	105	+ 34	− 14	− 1	+13°2721	50	− 21	− 68	− 4
78558	32	+ 61	− 65	− 52	122742	64	− 10	− 13	− 22
79096	59·5	+ 63	− 4	+ 6	124752	29·5	− 21	+ 9	− 14
79969AB	56	− 24	− 37	− 15	125072	109	+ 33	− 12	− 27
84035	70	− 15	− 56	− 4	125161B	33·5	+ 34	− 13	− 14
84737	86	− 6	− 4	+ 13	125455	49	+ 42	− 50	+ 8
85512	94·5	− 33	+ 9	− 4	+30°2512	74	+ 25	− 51	− 19
86728	87	+ 50	− 34	+ 28	126053	61	− 24	− 18	− 42
87884	34	+ 26	− 4	− 19	127506	45	+ 54	− 25	+ 8
88371	20	+121	− 23	+ 21	127871	32	− 73	− 43	− 10
233719	33·5	− 26	−103	+ 16	+34°2541	46	+ 78	− 51	− 18
89668	36	+ 72	− 55	− 30	129747	20	+ 70	− 4	− 6
89777	16	+169	− 41	+ 10	+17°2785	53	− 69	− 62	+ 27
90711	38	+ 27	− 54	− 19	130669	25	+ 42	− 49	− 78
+56°1458	81	+ 14	− 2	+ 7	130871	32	+ 67	− 66	+ 13
+46°1635	72	+ 41	− 43	+ 9	130992	59	+ 89	− 49	− 19
+42°2163	17	+145	−143	− 90	131511	96	+ 35	− 15	− 17
95128	90	+ 21	− 1	+ 4	131582	35	+ 82	− 81	+ 28
97584	71	+ 28	0	− 9	132142	39·5	+113	− 59	+ 26
98281	41	− 87	+ 11	+ 31	134319	20	+ 33	− 16	+ 4
100623	85	+ 57	+ 21	+ 17	134331	36·5	+ 3	− 4	− 13
101349	25	+ 28	− 11	− 10	135101B	37·5	+ 83	− 36	+ 16
101501	102	− 6	− 22	+ 8	− 3°3746	32	+148	− 48	0
101581	73	+ 39	− 27	+ 7	135204AB	44·5	+ 97	−128	− 1
102158	21	+106	− 92	+ 28	136202B	41·5	− 88	− 10	− 19
102345	105	+ 61	− 38	+ 6	136274	31	+ 43	− 81	+ 23
104304	98	− 16	− 12	− 13	136352	73	+117	− 43	+ 36
104556	77	+ 3	− 40	− 9	136834	49	+ 23	− 53	− 18
104988	30	+ 75	− 39	+ 5	137826	20	+ 20	− 68	+ 16
+22°2442	13	+133	− 50	− 26	138549	29	0	− 28	+ 20
106116	37	+ 89	− 4	+ 26	139323	60	+ 36	− 61	− 35
106156	36	− 46	− 26	− 20	139777	50	+ 14	− 22	0
106210	33	− 45	− 60	− 51	140901	72	+ 16	− 31	+ 6

TABLE I (*cont.*)

HD/BD	π_{pt} (0″·001)	U	V km/sec	W	HD/BD	π_{pt} (0″·001)	U	V km/sec	W
143291	32	+111	− 79	+ 28	172310	23	− 93	− 19	− 27
143761	75	− 43	− 26	+ 19	+31°3330	39	− 99	− 6	− 36
144287	47·5	+ 92	− 12	+ 18	174080	67	− 2	− 27	− 24
144515	30	+ 66	− 72	+ 9	229590	50·5	− 27	− 48	+ 14
144579	56	+ 41	− 65	− 11	175541	46	− 20	+ 3	+ 2
144628	58	− 40	− 12	+ 24	230409	12	−179	+172	− 16
144872	39·5	− 76	+ 1	− 3	178126	37	− 80	− 71	− 7
+35°2774	30	− 95	− 18	− 28	178428	59	− 25	− 1	− 15
145417	43	+ 90	−153	− 44	179957AB	46·5	+ 58	− 40	+ 33
145675	85	− 16	− 7	− 7	+41°3306	25·5	− 69	−134	− 88
145958AB	39	− 52	− 13	− 19	+33°3433	33	+114	− 22	+ 28
146233	79	− 24	− 15	− 21	182488	78	+ 23	− 13	− 2
148530	22	− 80	− 78	− 41	183255	46	+ 95	− 46	− 12
148653AB	46	+ 60	− 12	+ 14	231683	22	+ 13	− 62	− 9
149661	105	+ 3	− 1	− 29	184467	81	− 35	+ 5	+ 21
149957	41	− 53	− 8	− 43	184700	18	− 32	− 84	− 20
150248	37	− 59	− 28	− 14	185144	180	− 31	+ 46	− 22
150437	30	− 12	− 10	− 13	186427	61	− 12	− 29	− 1
151188AB	36	− 3	− 16	+ 1	186858AB	48	− 37	− 6	− 23
151288	112	+ 28	− 13	− 15	225732	48	− 35	− 9	− 24
151337	61	− 24	− 19	+ 4	189087	36·5	+ 43	− 13	+ 7
151877	30·5	− 53	− 31	+ 4	189567	58	+ 70	− 30	− 45
152391	60·5	− 85	−111	+ 6	190007	92	+ 22	− 18	+ 15
152792	43·5	− 39	0	− 7	190067	47	− 54	− 28	− 19
154345	52·5	+ 82	− 6	− 34	190404	52	−105	− 57	+ 30
154363	86	− 45	− 71	+ 19	190406	67	− 37	− 18	+ 7
154577	56	− 35	+ 32	+ 20	191069	25	− 3	− 64	− 55
155456	36	+ 60	− 35	+ 3	191408	140	+118	− 56	+ 47
+42°2810	30	− 61	−104	+113	191785	55	+ 30	− 29	+ 57
155885AB	157	− 1	− 37	− 8	192031	22	− 74	− 55	+ 30
156274	117	− 30	+ 23	− 32	192310	128	+ 71	− 12	− 13
156802	26·5	+ 69	− 55	− 40	193202	66	+ 31	− 23	+ 20
157214	67	− 28	− 81	− 64	194640	58	− 2	− 43	− 6
157750	26	+ 21	− 19	− 12	195987	55	+ 21	− 6	+ 34
157881	138	+ 4	− 53	− 11	196761	61	+ 69	+ 22	+ 9
158633	65·5	− 4	− 54	+ 10	196794	38	+ 57	− 29	− 8
+31°3025	15	+ 66	−111	+ 79	197076	49·5	+ 40	− 18	+ 15
159222	48	+ 30	− 50	− 6	197214	43	+ 10	− 27	+ 10
159868	41	+ 28	− 27	+ 13	197484	16	− 23	− 61	− 2
160346	80	− 19	− 2	+ 12	+19°4499	40	− 44	− 26	− 5
+71°851	38	+ 40	− 16	+ 13	199476	33	+ 86	− 60	− 7
160691	107	+ 13	− 4	− 1	+12°4499	42	+ 81	+ 3	− 13
161198	40·5	− 71	− 36	− 5	200779	73	+ 16	− 74	+ 7
161848	25	+ 54	−129	+ 52	201091AB	296	+ 89	− 54	− 5
162756	28	+104	− 80	− 30	202123	26	− 85	+ 38	0
164922	56·5	− 50	+ 9	− 37	202457	54·5	+ 52	− 30	− 4
165401	42	+ 84	− 90	− 37	204587	53·5	+105	− 68	− 9
166348	82	+ 12	− 18	− 16	204814	34	+ 78	− 84	+ 4
166620	87	− 19	− 31	0	205067	30	+ 41	− 19	− 3
169822	30	− 34	− 77	− 11	205390	65	+ 5	− 22	− 38
170493	67	+ 42	− 31	− 21	205855	29·5	− 77	− 25	+ 22
170357	20	+ 54	−104	+ 53	+24°4460	21	−126	− 85	− 8
170657	72	+ 40	− 26	+ 7	+ 4°4762	13·5	+ 91	− 44	− 33
171314	45	− 64	− 4	+ 6	209100	280	+ 78	− 40	+ 5
171627	93	− 26	− 3	− 10	209742	33·5	+ 53	− 46	− 24

TABLE I (*cont.*)

HD/BD	π_{pt} (0″·001)	U	V km/sec	W	HD/BD	π_{pt} (0″·001)	U	V km/sec	W
210144	40	− 81	− 24	+ 4	219249	28	+ 41	+ 2	− 16
210193	27	+ 20	− 15	− 24	219709	38	+ 12	− 36	− 17
+22°4567	23	−100	− 7	+ 71	219953	24·5	+114	−100	− 30
210918	55·5	+ 46	− 67	− 19	220339	75	+ 27	+ 17	− 36
213042	80	− 10	− 59	− 18	221354	68	+ 60	− 53	− 12
214059	24	+ 52	− 51	− 59	221818	26	+ 14	− 60	+ 11
214385	24·5	+ 55	− 11	− 83	221830	38	+ 51	−102	+ 59
214749	79	+ 19	− 7	− 12	221914	32	+ 97	− 40	+ 13
214759	47	+ 35	− 16	+ 4	222237	89·5	− 32	− 75	− 23
216054	33	− 61	− 16	+ 10	222794	39	+ 28	− 84	+ 50
216777	24·5	+ 97	− 55	− 17	222935	34	+131	− 12	− 55
216803	130	+ 2	− 7	− 14	223238	29	+ 45	− 36	− 2
217014	85	+ 11	− 28	+ 16	223498	26	+ 88	− 28	+ 19
+68°1345	24	+109	− 75	+ 5	223778	112	+ 11	− 6	− 1
217357	110	− 28	+ 15	− 4	224383	25·5	+ 61	− 74	+ 3
219134	175	+ 45	− 37	− 11	224618	21	+229	−136	− 6
219175B	25	+ 94	− 55	− 11					

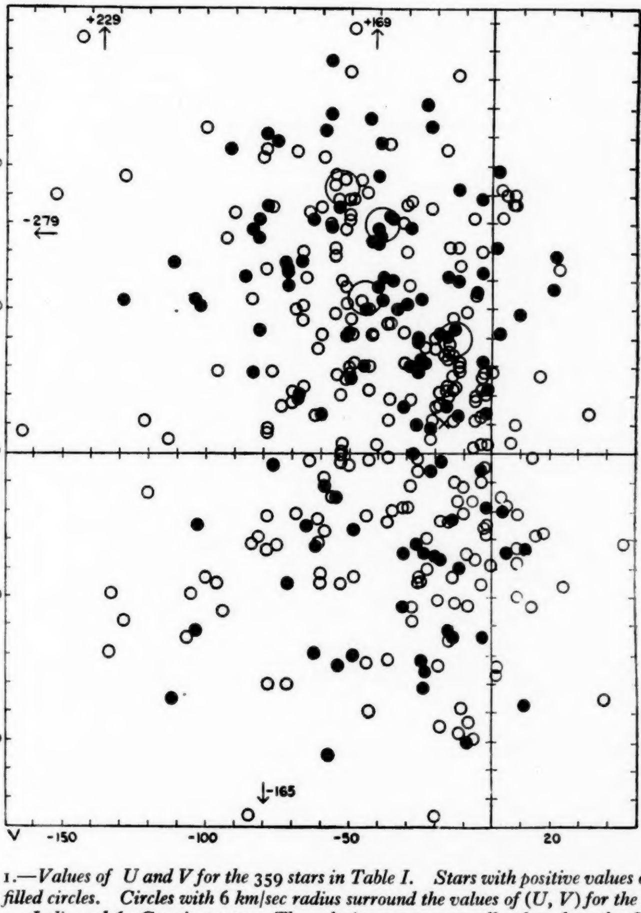

FIG. 1.—*Values of U and V for the 359 stars in Table I. Stars with positive values of W are plotted as filled circles. Circles with 6 km/sec radius surround the values of (U, V) for the Hyades, ζ Herculis, ε Indi, and 61 Cygni groups. The velocity vectors are all referred to the Sun; the cross at U = +11 and V = −17 km/sec represents the velocity of the standard of rest for the nearby stars. The arrows indicate stars falling outside the boundaries of the diagram.*

to the Sun (Woolley 1958 *a*). The values of (U, V, W) for the Hyades, ζ Herculis, ϵ Indi and 61 Cygni, taken from Papers I and II are the following:

	U	V	W
61 Cyg	+92	−53	− 6 km/sec
ϵ Ind	+79	−39	+ 6
ζ Her	+54	−45	−26
Hyades	+40	−18	− 2

These values of U and V are shown in Fig. 1 as the centres of circles with a radius of 6 km/sec.

It is of interest to examine the distribution of points in Fig. 1 for the presence of regularities and therefore, in an effort to reduce any blurring effect that might arise from the inclusion of all values for W, the material in Fig. 1 has been subdivided as follows:

Fig. 2: $W = 0$ to -20 km/sec,
Fig. 3: $W = +1$ to $+20$,
Fig. 4: $W < -20$,
Fig. 5: $W > +20$.

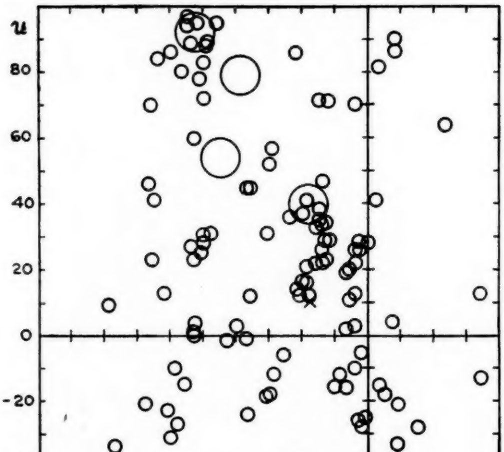

FIG. 2.—*Values of U and V for the stars with W from 0 to −20 km/sec. The symbols are as in Fig. 1. A few stars fall outside the limits of the figure.*

A few stars falling outside the limits of each of these diagrams are not plotted. The values of $|W| > 50$ km/sec in Figs. 4 and 5 are indicated by filled circles. Since the Sun's motion in W, with respect to the local standard of rest, is -7 km/sec (Woolley 1958 *a*), the limits for W in Figs. 2 and 3 become $+7$ to -13 and $+8$ to $+28$ km/sec, respectively, referred to that standard. The values of (U, V) for the four groups of high velocity have been marked in Figs. 2 to 5

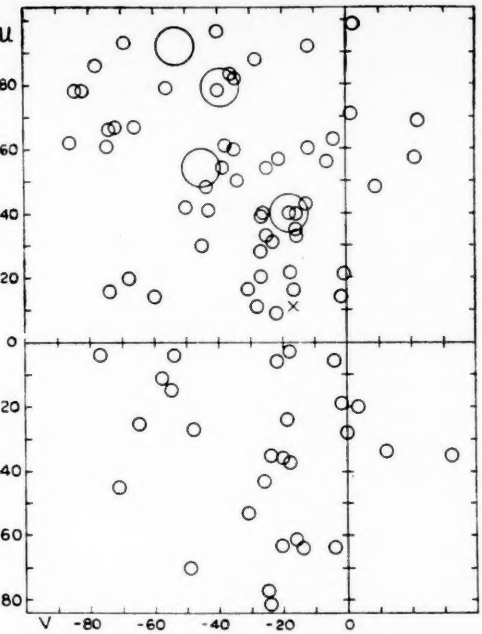

FIG. 3.—*Values of U and V for the stars with W between* $+1$ *and* $+20$ *km/sec. The symbols are as in Fig.* 1; *a few stars fall outside the limits of the figure.*

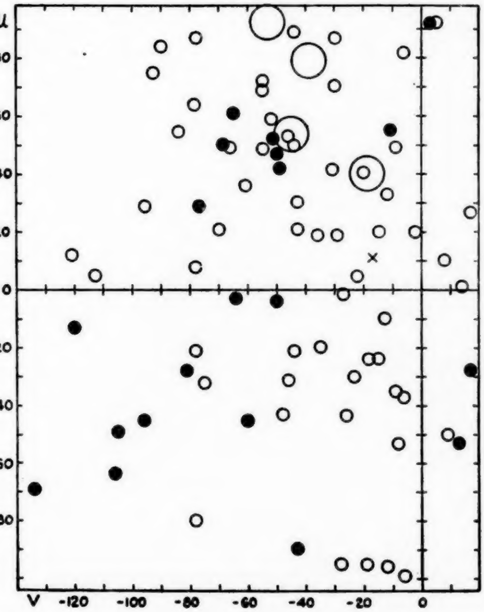

FIG. 4.—*Values of U and V for stars with values of* $W < -20$ *km/sec. The filled circles indicate stars with* $W < -50$ *km/sec; the other symbols are as in Fig.* 1. *A few stars fall outside the limits of the figure.*

as in Fig. 1. For comparison with Fig. 2 the values of U and V derived from the trigonometric parallaxes of the stars in Gliese's (1957) list of objects within 20 parsecs of the Sun and with $W = 0$ to -20 km/sec have been plotted in Fig. 6; a few stars fall outside the limits of this diagram.

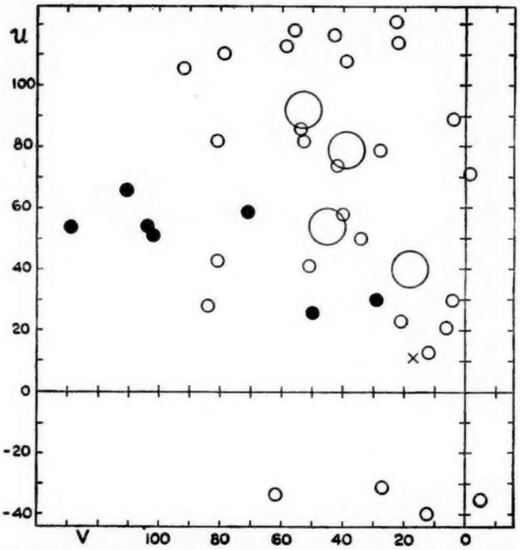

FIG. 5.—*Values of U and V for stars with W > +20 km/sec. The filled circles indicate stars with W > +50 km/sec; the other symbols are as in Fig. 1. A few stars fall outside the limits of the diagram.*

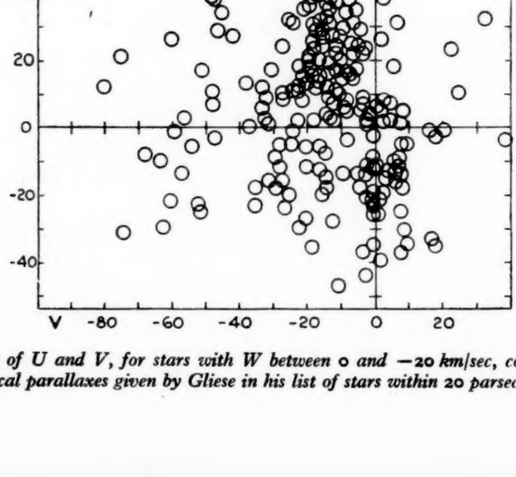

FIG. 6.—*Values of U and V, for stars with W between 0 and −20 km/sec, computed from the trigonometrical parallaxes given by Gliese in his list of stars within 20 parsecs of the Sun.*

In comparing Figs. 2 and 6 it must be remembered that, although the material used in both diagrams is nearly complete for stars within 20 parsecs, which are, in the main, low velocity stars, the larger number in Fig. 6 results from the use of all spectral types. On the other hand, the stars in Fig. 2 that are more distant than 20 parsecs are largely high velocity objects. The apparent regularity in the distribution of the low velocities suggested by Fig. 2 may indicate the blurring effect of inaccurate parallaxes used in constructing Fig. 6, but the reality of the two chains of stars, with V near -5 and -18 km/sec, separated by a lane, needs confirmation by a larger sample of stars; observations of magnitude and colour for this purpose are now in progress. In any case, the apparent connection of the Hyades with the chain at V near -18 km/sec may be partly accidental since finer subdivisions in the values of M can break up the chain and remove the Hyades from the figure. This effect is better illustrated, perhaps, in the case of 61 Cygni. The value of (U, V) for 61 Cygni, for which $W=-6$ km/sec, falls in a rather densely populated region of Fig. 2 while the values for ζ Herculis and ϵ Indi, both of which have W's outside the range shown in the figure, fall in unpopulated regions. The ten stars, including 61 Cygni, which fall in the range, $U=+80$ to $+100$ km/sec and $V=-40$ to -60 km/sec are the following, arranged in order of increasing photometric parallax (in units of $0''\cdot001$):

HD	π_{pt}	U	V	W
216777	24·5	+97	−55	−17
219175B	25	+94	−55	−11
10145	32	+95	−52	−11
199476	33	+86	−60	− 7
112943	36·5	+83	−50	− 5
64606	39	+80	−57	− 7
183255	46	+95	−46	−12
130992	59	+89	−49	−19
3443	64	+89	−49	−18
Mean	...	+90	−53	−12
61 Cyg	296	+92	−53	− 6

The mean values of U and V for the nine stars are nearly identical with those for 61 Cygni but the values of W differ by 6 km/sec. Since the apex of the apparent motion of 61 Cygni was used in selecting—by the convergent-point method—the group members in Paper II, and the value of (A, D) used in that method is sensitive to W, more group members perhaps would have been found if the mean value of W given above had been used. However, tolerances far wider than those used in Paper II would be necessary to include, by the convergent-point method, all of the above stars in the 61 Cygni group. The question arises as to the spread in U and V, as well as in W, that can be tolerated in considering stars as members of groups. The answer, of course, depends upon both the definition of "group" and the relation of the groups to the general dynamics of the galaxy (Woolley 1958*b*) and will not be discussed here.

A suggestive clumping of stars in Fig. 2 occurs near $(U, V)=(26, -50)$. Some of these stars had previously been associated, by the convergent-point method (the θ Centauri group), with a group moving toward $A=6^h\ 12^m$, $D=-27^\circ\cdot2$ with a velocity of 60 km/sec. The six stars that form this group in Fig. 2 are the following:

HD/BD	π_{pt}	U	V	W
90711	38	+27	−54	−19
+54°1175	45	+28	−50	−16
159222	48	+30	−50	− 6
136834	49	+23	−53	−18
120690	54	+31	−48	− 9
+30°2512	74	+25	−51	−19

The following additional stars, among those within 20 parsecs of the Sun, may also belong to the same group:

Name	π_e	U	V	W	π_{tr}
θ Cen	60	+26	−48	− 5	76Y(8), 39C(7)
+37°748	64	+28	−47	−19	83M(10), 51V(16)
GAZ 82°1111	110	+30	−48	−19	93M(12), 104Yk(10), 106G(12)
+18°638	112	+27	−54	−11	99M(10), 104V(12)
Wolf 359	400	+26	−46	−19	404W(6), 397V(4)

The values of π_e given above are those used in computing the space motions; the trigonometric parallaxes, with the observatory designations and weights, are taken from the Yale catalogue (Jenkins 1952).

In comparing Figs. 2 and 6 it is interesting to note the near absence of stars in the former that might belong to the Sirius group (Paper I) for which $(U, V, W) = (-14, 0, -12)$ while the latter shows a heavy concentration of group members. The scarcity of dwarf members of this group, with colours in excess of $+0^{m}\cdot5$, was noted in Paper I and seems to be confirmed by the present comparison since bluer stars are contained in the material used to construct Fig. 6 but not in that used for Fig. 2.

Since the division point of $W=0$, used to separate the stars in Figs. 2 and 3 is an arbitrary one, we might expect some of the features of Fig. 2 to appear also in Fig. 3. This seems to be the case, but there are some curious differences—the chain of stars in Fig. 2 with V near -5 km/sec and with small values of U does not appear in Fig. 3, indicating the relatively small range of W for these stars. Members of the Hyades group, for which $W=-2$, appear in both figures but they are accompanied in Fig. 3 by a chain with V near -25 km/sec. Members of the ϵ Indi group, absent from Fig. 2, appear in Fig. 3 as expected since the value of W for this group is $+6$ km/sec. The distribution of the points in Figs. 4 and 5 is more featureless than that of Figs. 2 and 3 but there are too few stars to permit any detailed discussion. Some of the regularities in the distribution of points in Figs. 2 and 3 have previously been suspected by Dyer (1956), in the distribution of the velocities of M-type dwarfs, and by Vyssotsky (1951), in the distribution of the velocities of the A-type stars and the K-type giants.

Summary.—Photometric parallaxes have been derived for a selected list of 359 main sequence dwarfs with colours, $(P-V)_E$, between $+0^{m}\cdot5$ and $+1^{m}\cdot24$. These parallaxes have been used to compute the space motions (U, V, W) of the stars. Although the stellar groups, whose members were chosen by the convergent-point method in Papers I and II, appear in the distribution of space motions of these stars, that distribution shows (*a*) the limitations of the convergent-point method of defining group membership and (*b*) the need for a dynamical definition of stellar groups.

The space motions in Table I were computed at least once by the author and once by either Misses L. Mather or A. Heather, using desk calculators, or Messrs A. E. Carter and D. A. Harragan, of the Nautical Almanac Office, using Hollerith punch card machines. I am greatly indebted to the Astronomer Royal for many stimulating discussions.

Royal Greenwich Observatory,
Herstmonceux Castle,
Hailsham, Sussex:
1958 *September* 1.

References

Dyer, E. R., Jr., 1956, *A. J.*, **61**, 228.
Eggen, O. J., 1955, *A. J.*, **60**, 407; *Lick Obs. Bull.*, No. 539.
Eggen, O. J., 1956, *A. J.*, **61**, 462; *Lick Obs. Bull.*, No. 548.
Eggen, O. J., 1958 *a*, *M.N.*, **118**, 65.
Eggen, O. J., 1958 *b*, *M.N.*, **118**, 154.
Gliese, W., 1957, *Mitt. Heidelberg Astr. Rechen Inst.*, **8**.
Jenkins, L. 1952, *General Catalogue of Trigonometric Stellar Parallaxes* (Yale University Observatory).
Roman, N. G., 1955, *Ap. J. Supplement Series, II*, **195**.
Vyssotsky, A. N., 1951, *A. J.*, **56**, 62.
Wilson, R. E., 1953, *General Catalogue of Stellar Radial Velocities*, Carnegie Inst. of Wash. Publ. No. 601.
Woolley, R. v. d. R., 1958 *a*, *M.N.*, **118**, 45.
Woolley, R. v. d. R., 1958 *b*, *Vistas in Astronomy*, III, Ed. A. Beer, London.

ENERGY LEVELS AND TRANSITION PROBABILITIES OF Fe IV

R. H. Garstang

(Communicated by the Director of the University of London Observatory)

(Received 1958 September 17)

Summary

Estimates have been made of the quantum mechanical parameters of the $3d^5$ configuration of Fe IV, and the energy levels of this configuration have been calculated. Transition probabilities have been computed for magnetic dipole and electric quadrupole radiation for transitions between the levels of the $3d^5$ configuration. A search is made for [Fe IV] lines in the spectrum of RR Telescopii, and a number of identifications are suggested.

1. *Introduction.*—The absence of any term analysis of the Fe IV spectrum prevents precise predictions of the wave-lengths of forbidden lines which might be of astrophysical interest. The positions of a few terms were estimated by Edlén (**1**) and, more recently, by Glad (**6**). Edlén pointed out that the ^4G–^4F multiplet should occur in the visible region of the spectrum, but that as it required a rather high excitation energy it would probably not be very strong. Swings and Struve (**12**) suggested that a line λ 5040·1 in RY Scuti should be attributed to [Fe IV]; they pointed out that this line also occurs in AX Persei (**12**), NGC 6572 and NGC 7027 (**18**) and in Nova RR Pictoris (1925) (**13**) and suggested that it might belong to the ^4G–^4F multiplet. Swings (**14**) suggested that some unidentified lines in RY Scuti might also be due to [Fe IV]. Thackeray (**15**) noted the presence of a number of unidentified lines in RR Telescopii, between λ 4835 and λ 5288 and in the infra-red, some of which he suggested were due to [Fe IV]; excitation conditions in RR Telescopii were favourable to the production of this ion. In a later paper (**16**) Thackeray quoted Edlén's identification of lines at $\lambda\lambda$ 4868, 4900, 4906, 4918, 7189 and 7221 as due to [Fe IV], but the transitions involved in these lines were not specified. The object of the present paper is to examine whether quantum mechanical calculations can contribute to the identification and analysis of the Fe IV spectrum. We shall compute all the energy levels of the lowest configuration ($3d^5$) of this ion, using as a starting point the predictions of a few terms by Glad (**6**), and then obtain the transition probabilities of forbidden lines between these levels. Having found the lines which should be strong we shall attempt to identify them in the spectrum of RR Telescopii. This paper has the further object of providing transition probability data for a type of configuration (d^5) which has not been studied previously in this connection; it also fills an important gap in the data for ionized iron, and forms the fifth and penultimate paper in the writer's programme on transition probabilities of forbidden lines of elements in the first long period (**2, 3, 4, 5**).

2. *Method of calculation.*—The theoretical formulae for the electrostatic energies of levels in the $3d^5$ configuration have been given by Racah (**9**) and by Ishidzu and Obi (**8**). Corrections of the form $\alpha L(L+1)$ and βQ were added

to the theoretical formulae along the lines of the work of Trees (e.g. (**17**)) and Racah (**10**). The matrices of spin–orbit interaction for the d^5 configuration have been computed by Greyber (**7**); a copy of his results was sent to the writer by R. E. Trees, together with four corrections to Greyber's work found by Trees.

The centres of gravity of five terms ^{6}S, ^{4}G, ^{4}P, ^{4}D and ^{4}F, were predicted by Glad (**6**). Our theoretical formulae contain five parameters, and these five parameters were chosen to fit these five terms. This is a somewhat dangerous procedure, in that it forces a fit which may be unjustified, and no check on this is possible if no other terms are known. No better procedure suggests itself at the present time. The spin–orbit parameter ζ_d was estimated by linearly interpolating $\zeta_d^{\frac{1}{2}}$ between Fe III and Fe V (**3**). The adopted parameters are listed in Table I. Using these parameters the complete energy matrices were set up. Their eigenvalues and eigenvectors were calculated. The smaller matrices were treated by hand computation; the three largest matrices were handled on an electronic computer. The line strength matrices were obtained in the usual way from Shortley's formulae for magnetic dipole radiation (**11**) and the present writer's results for electric quadrupole radiation (**2**). The eigenvectors of the energy matrices form the transformation matrices from LS-coupling to intermediate coupling; this transformation was carried out for the two types of radiation. The final stage in the calculations was the conversion of the line strengths, obtained in atomic units, into transition probabilities. For this work the electric quadrupole radial integral

$$s_q = \int_0^\infty r^2 P^2(3d)\,dr$$

was calculated by D. F. Mayers from his unpublished self-consistent field, with exchange, wave function. He obtained $s_q = 1{\cdot}14$, and this value was used in the present paper.

3. *Results.*—The final energies are given in Table II. It is difficult to estimate the accuracy of these energy levels. Previous experience suggests that many of the intervals between the levels of one term should be accurate to about 50 cm^{-1}, but that some will be substantially worse; most of the intervals between the terms should be accurate to about 500 cm^{-1}, but a few will almost certainly be less accurate. This accuracy is rather low for the purpose of identifying predicted wave-lengths of spectral lines with observed transitions. In particular, the lines of a multiplet which extends over a very small range of wave-length may not be predicted in the correct relative positions in the spectrum. This is largely due to the vanishing of diagonal spin–orbit interactions in the half-closed configuration $3d^5$. The observed term-intervals are second-order perturbations. The spin–orbit interaction still causes first-order perturbations in the wave functions, so that we should get reasonable estimates of the transition probabilities of forbidden lines between levels of different terms. Fortunately, three of the terms which are of most interest ($^2_5$D, $^2_3$F and ^{2}H) are predicted to have large term-intervals, and it is highly probable that, for example, lines from the level $^2H_{5\frac{1}{2}}$ to the ^{4}G term will be at shorter wave-lengths than $^2H_{4\frac{1}{2}}$–^{4}G transitions. This is of importance when searching for identifications in celestial spectra.

TABLE I

Adopted parameters (in cm⁻¹)

A	37656
B	1075
C	3884
α	104
β	182
ζ_d	468

TABLE II

Calculated energy levels

Term	J	Energy	
^6S	$2\frac{1}{2}$	0	
^4G	$2\frac{1}{2}$	32213	30
	$3\frac{1}{2}$	32243	20
	$4\frac{1}{2}$	32263	− 9
	$5\frac{1}{2}$	32254	
^4P	$\frac{1}{2}$	35259	− 87
	$1\frac{1}{2}$	35172	− 77
	$2\frac{1}{2}$	35095	
^4D	$\frac{1}{2}$	38389	64
	$1\frac{1}{2}$	38453	15
	$2\frac{1}{2}$	38468	−163
	$3\frac{1}{2}$	38305	
^2I	$5\frac{1}{2}$	47218	78
	$6\frac{1}{2}$	47296	
^2_5D	$1\frac{1}{2}$	49589	−485
	$2\frac{1}{2}$	49104	
^2_3F	$2\frac{1}{2}$	51864	−626
	$3\frac{1}{2}$	51238	
^4F	$1\frac{1}{2}$	52595	− 43
	$2\frac{1}{2}$	52552	−103
	$3\frac{1}{2}$	52449	− 35
	$4\frac{1}{2}$	52414	
^2H	$4\frac{1}{2}$	55959	476
	$5\frac{1}{2}$	56435	
^2_5G	$3\frac{1}{2}$	56872	411
	$4\frac{1}{2}$	57283	
^2_5F	$2\frac{1}{2}$	60316	28
	$3\frac{1}{2}$	60344	
^2S	$\frac{1}{2}$	65501	
^2_3D	$1\frac{1}{2}$	73182	53
	$2\frac{1}{2}$	73235	
^2_3G	$3\frac{1}{2}$	82193	−2[illegible]
	$4\frac{1}{2}$	82171	
^2P	$\frac{1}{2}$	98588	−49
	$1\frac{1}{2}$	98539	
^2_1D	$1\frac{1}{2}$	107018	−39
	$2\frac{1}{2}$	106979	

The transition probabilities of selected multiplets are listed in Table III. We have included all transitions from and between levels up to ^4D; most multiplets from the next five terms are given, only a few very weak multiplets being omitted. From the next five terms only the strongest multiplets are given, and from the highest two terms all multiplets have been omitted. In all, 75 multiplets have been omitted; this omission seems justified for reasons of economy, having regard to the unlikely need for data concerning these weak

transitions from high-energy levels. It is, as always, difficult to assess the accuracy of these transition probabilities. As mentioned above they are mostly due to first-order perturbations, and should be moderately reliable. There is, however, one cause of uncertainty which does not usually apply but which is of importance here. The unknown errors in the energies may introduce errors in the transition probabilities in two ways. First, the assumed positions of the terms enter into the calculation of the transformation matrices, and thence into the line strengths. Secondly, the conversion from line strengths to transition probabilities involves the third and fifth powers of the frequencies of the transitions. The first source of error will chiefly affect transitions between different terms. There is little that can be done to eliminate this source of error until an observational analysis of the Fe IV spectrum becomes available. The second source of error affects transitions within a term and between close terms, but has a relatively small effect on transitions in the visible spectrum between well-separated terms. There are a number of transitions for which the transition probabilities are small because of the frequency factors (ν^3 or ν^5) but the line strengths from which they were computed are large. In order that these line strengths may be obtained in a few cases which may be of interest, the corresponding transition probabilities have been retained in Table III.

Among the results it is worth noticing the high degree of metastability possessed by the ^{4}G levels. The line strengths of the ^{6}S–^{4}G transitions are so small that they could not be computed without a special investigation; the strengths came out as zero to the last figure retained in the calculations. An attempt was made to carry one section of the calculations to higher numerical accuracy and this led to a value of about 10^{-5} for the probability of the magnetic dipole transition $^6S_{2\frac{1}{2}}$–$^4G_{2\frac{1}{2}}$. A similar attempt for the $^6S_{2\frac{1}{2}}$–$^4G_{3\frac{1}{2}}$ transition led to an upper limit of 10^{-7}. Although these values are rather uncertain—one cannot say without a great deal of extra work whether they are sensitive to changes of the parameters in the calculation—it does seem that the ^{4}G levels of the $3d^5$ configuration are highly metastable.

The weakness of the ^{4}P–^{4}F multiplet is not entirely unexpected: it has zero electric quadrupole line strength in LS-coupling in the $3d^5$ configuration. But one might have expected rather larger magnetic dipole strengths. There is probably little prospect of finding it in celestial spectra.

There are no strong sextet–doublet transitions and, as Edlén pointed out, no transitions at all to the sextet ground state which are in the accessible region of the spectrum.

4. *Tentative identification of* [Fe IV] *lines.*—One of the striking results which emerges on examination of Table III is the intensity of some of the magnetic dipole transitions. Indeed, almost all the strong transitions requiring less than 8 volts energy are magnetic dipole transitions, with the exception of the ^{4}G–^{4}F transition, and even in this multiplet magnetic dipole transitions make substantial contributions to the total transition probabilities. Such searches as have been made for [Fe IV] lines in celestial objects have of necessity been confined to those multiplets whose positions were roughly predicted by Edlén (1), together with an examination of the behaviour of unidentified lines with varying excitation conditions (for example in novae). Now that we can pick out from Table III

TABLE III

Transition probabilities for selected multiplets of [Fe IV]

All entries in this Table are probabilities of spontaneous emission. Units: reciprocal seconds. The letters ' v.s. ' denote a line with a very small strength. See text for details of multiplets omitted from this Table.

Transition		A_m	A_q
^6S–^4G	$2\frac{1}{2}$–$2\frac{1}{2}$	10^{-5}:	$< 10^{-9}$
	$2\frac{1}{2}$–$3\frac{1}{2}$	$< 10^{-7}$	$< 10^{-9}$
	$2\frac{1}{2}$–$4\frac{1}{2}$	...	$< 10^{-9}$
^4G–^4G	$2\frac{1}{2}$–$3\frac{1}{2}$	1.1×10^{-6}	7.5×10^{-20}
	$2\frac{1}{2}$–$4\frac{1}{2}$	...	9.9×10^{-19}
	$3\frac{1}{2}$–$4\frac{1}{2}$	3.5×10^{-7}	3.8×10^{-20}
	$5\frac{1}{2}$–$4\frac{1}{2}$	2.6×10^{-8}	1.6×10^{-21}
	$3\frac{1}{2}$–$5\frac{1}{2}$	...	6.5×10^{-22}
^6S–^4P	$2\frac{1}{2}$–$2\frac{1}{2}$	1.4	3.9×10^{-5}
	$2\frac{1}{2}$–$1\frac{1}{2}$	0.88	1.5×10^{-5}
	$2\frac{1}{2}$– $\frac{1}{2}$	...	v.s.
^4G–^4P	$2\frac{1}{2}$–$2\frac{1}{2}$	6.8×10^{-5}	1.4×10^{-9}
	$3\frac{1}{2}$–$2\frac{1}{2}$	1.5×10^{-5}	2.3×10^{-9}
	$4\frac{1}{2}$–$2\frac{1}{2}$	...	6.4×10^{-10}
	$2\frac{1}{2}$–$1\frac{1}{2}$	8.6×10^{-6}	8.5×10^{-10}
	$3\frac{1}{2}$–$1\frac{1}{2}$	...	1.3×10^{-9}
	$2\frac{1}{2}$– $\frac{1}{2}$	...	3.4×10^{-10}
^4P–^4P	$2\frac{1}{2}$–$1\frac{1}{2}$	1.1×10^{-5}	4.9×10^{-16}
	$2\frac{1}{2}$– $\frac{1}{2}$	...	1.2×10^{-13}
	$1\frac{1}{2}$– $\frac{1}{2}$	3.7×10^{-5}	7.4×10^{-15}
^6S–^4D	$2\frac{1}{2}$– $\frac{1}{2}$	...	1.8×10^{-4}
	$2\frac{1}{2}$–$1\frac{1}{2}$	0.038	6.2×10^{-4}
	$2\frac{1}{2}$–$2\frac{1}{2}$	0.051	1.0×10^{-3}
	$2\frac{1}{2}$–$3\frac{1}{2}$	2×10^{-4}	1.1×10^{-3}
^4G–^4D	$2\frac{1}{2}$– $\frac{1}{2}$	...	1.0×10^{-7}
	$2\frac{1}{2}$–$1\frac{1}{2}$	2.8×10^{-4}	6.6×10^{-7}
	$3\frac{1}{2}$–$1\frac{1}{2}$	...	6.0×10^{-7}
	$2\frac{1}{2}$–$2\frac{1}{2}$	5.8×10^{-4}	7.2×10^{-7}
	$3\frac{1}{2}$–$2\frac{1}{2}$	v.s.	1.1×10^{-6}
	$4\frac{1}{2}$–$2\frac{1}{2}$	...	6.7×10^{-7}
	$2\frac{1}{2}$–$3\frac{1}{2}$	7.6×10^{-5}	5.2×10^{-8}
	$3\frac{1}{2}$–$3\frac{1}{2}$	7.6×10^{-4}	6.8×10^{-7}
	$4\frac{1}{2}$–$3\frac{1}{2}$	6.3×10^{-4}	1.5×10^{-6}
	$5\frac{1}{2}$–$3\frac{1}{2}$	...	1.7×10^{-7}
^4P–^4D	$\frac{1}{2}$– $\frac{1}{2}$	0.058	...
	$1\frac{1}{2}$– $\frac{1}{2}$	0.034	6.9×10^{-6}
	$2\frac{1}{2}$– $\frac{1}{2}$	...	9.9×10^{-7}
	$\frac{1}{2}$–$1\frac{1}{2}$	1.4×10^{-3}	1.8×10^{-6}
	$1\frac{1}{2}$–$1\frac{1}{2}$	0.039	3.3×10^{-6}
	$2\frac{1}{2}$–$1\frac{1}{2}$	0.018	3.4×10^{-6}
	$\frac{1}{2}$–$2\frac{1}{2}$	...	3.1×10^{-6}
	$1\frac{1}{2}$–$2\frac{1}{2}$	3.5×10^{-3}	1.5×10^{-7}
	$2\frac{1}{2}$–$2\frac{1}{2}$	0.022	5.5×10^{-6}
	$1\frac{1}{2}$–$3\frac{1}{2}$	...	2.9×10^{-6}
	$2\frac{1}{2}$–$3\frac{1}{2}$	0.038	4.9×10^{-6}

TABLE III (*continued*)

Transition		A_m	A_q
^4D–^4D	3½–1½	...	$3{\cdot}1\times10^{-14}$
	3½–2½	$1{\cdot}3\times10^{-4}$	$8{\cdot}7\times10^{-14}$
	½–1½	$1{\cdot}0\times10^{-5}$	$1{\cdot}2\times10^{-15}$
	½–2½	...	$1{\cdot}9\times10^{-19}$
	1½–2½	$1{\cdot}3\times10^{-7}$	$1{\cdot}9\times10^{-19}$
^4G–^2I	3½–5½	...	$1{\cdot}0\times10^{-6}$
	4½–5½	$3{\cdot}0\times10^{-3}$	$3{\cdot}3\times10^{-7}$
	5½–5½	$5{\cdot}1\times10^{-3}$	$3{\cdot}2\times10^{-7}$
	4½–6½	...	$1{\cdot}6\times10^{-6}$
	5½–6½	$1{\cdot}6\times10^{-4}$	$7{\cdot}1\times10^{-6}$
^2I–^2I	5½–6½	$5{\cdot}9\times10^{-6}$	$1{\cdot}9\times10^{-16}$
^4G–^2_5D	2½–1½	0·010	$3{\cdot}7\times10^{-3}$
	3½–1½	...	$1{\cdot}3\times10^{-3}$
	2½–2½	0·13	$3{\cdot}3\times10^{-4}$
	3½–2½	0·12	$5{\cdot}9\times10^{-4}$
	4½–2½	...	$2{\cdot}1\times10^{-4}$
^4P–^2_5D	½–1½	0·065	$7{\cdot}0\times10^{-6}$
	1½–1½	0·25	$2{\cdot}0\times10^{-5}$
	2½–1½	0·069	$7{\cdot}3\times10^{-6}$
	½–2½	...	$1{\cdot}1\times10^{-7}$
	1½–2½	0·10	$5{\cdot}9\times10^{-6}$
	2½–2½	0·54	$2{\cdot}8\times10^{-6}$
^2_5D–^2_5D	2½–1½	$1{\cdot}5\times10^{-3}$	$6{\cdot}4\times10^{-11}$
^4G–^2_3F	2½–2½	0·21	$4{\cdot}5\times10^{-3}$
	3½–2½	0·47	$8{\cdot}1\times10^{-3}$
	4½–2½	...	$4{\cdot}1\times10^{-3}$
	2½–3½	0·015	$2{\cdot}7\times10^{-5}$
	3½–3½	0·080	$2{\cdot}3\times10^{-4}$
	4½–3½	0·50	$4{\cdot}6\times10^{-4}$
	5½–3½	...	$1{\cdot}4\times10^{-4}$
^4P–^2_3F	½–2½	...	$2{\cdot}4\times10^{-5}$
	1½–2½	0·013	$1{\cdot}5\times10^{-5}$
	2½–2½	0·087	$7{\cdot}1\times10^{-5}$
	1½–3½	...	$2{\cdot}0\times10^{-5}$
	2½–3½	5×10^{-4}	$2{\cdot}5\times10^{-7}$
^4D–^2_3F	½–2½	...	$5{\cdot}4\times10^{-4}$
	1½–2½	0·021	$3{\cdot}0\times10^{-4}$
	2½–2½	0·022	$7{\cdot}1\times10^{-4}$
	3½–2½	$7{\cdot}2\times10^{-4}$	$1{\cdot}9\times10^{-4}$
	1½–3½	...	$2{\cdot}3\times10^{-5}$
	2½–3½	0·034	$2{\cdot}8\times10^{-5}$
	3½–3½	0·10	$3{\cdot}3\times10^{-5}$
^2_5D–^2_3F	1½–2½	0·035	$1{\cdot}8\times10^{-7}$
	2½–2½	0·090	$9{\cdot}2\times10^{-8}$
	1½–3½	...	$5{\cdot}9\times10^{-9}$
	2½–3½	0·023	$1{\cdot}7\times10^{-7}$

Table III (*continued*)

Transition		A_m	A_q
$^2_3$F–$^2_3$F	3½–2½	$3\cdot0\times10^{-3}$	$1\cdot0\times10^{-10}$
^{4}G–^{4}F	2½–1½	0·14	0·18
	3½–1½	...	0·071
	2½–2½	0·19	0·064
	3½–2½	$9\cdot4\times10^{-4}$	0·11
	4½–2½	...	0·061
	2½–3½	0·014	$4\cdot1\times10^{-3}$
	3½–3½	0·13	0·067
	4½–3½	0·039	0·15
	5½–3½	...	0·040
	2½–4½	...	$8\cdot7\times10^{-5}$
	3½–4½	$2\cdot3\times10^{-3}$	$3\cdot8\times10^{-3}$
	4½–4½	0·073	0·045
	5½–4½	0·11	0·21
^{4}P–^{4}F	½–1½	$1\cdot5\times10^{-4}$	$4\cdot1\times10^{-4}$
	1½–1½	$1\cdot5\times10^{-4}$	$1\cdot6\times10^{-3}$
	2½–1½	v.s.	$5\cdot6\times10^{-4}$
	½–2½	...	$1\cdot3\times10^{-4}$
	1½–2½	$2\cdot4\times10^{-3}$	$4\cdot6\times10^{-4}$
	2½–2½	$5\cdot3\times10^{-3}$	$1\cdot4\times10^{-3}$
	1½–3½	...	$6\cdot5\times10^{-4}$
	2½–3½	$1\cdot1\times10^{-3}$	$9\cdot9\times10^{-4}$
	2½–4½	...	$8\cdot8\times10^{-4}$
^{4}D–^{4}F	½–1½	0·10	$8\cdot3\times10^{-3}$
	1½–1½	0·16	0·016
	2½–1½	0·039	$4\cdot5\times10^{-3}$
	3½–1½	...	$1\cdot9\times10^{-4}$
	½–2½	...	$7\cdot7\times10^{-3}$
	1½–2½	0·023	$4\cdot1\times10^{-3}$
	2½–2½	0·18	0·012
	3½–2½	0·028	$2\cdot1\times10^{-3}$
	1½–3½	...	$8\cdot5\times10^{-3}$
	2½–3½	$9\cdot4\times10^{-3}$	$9\cdot2\times10^{-3}$
	3½–3½	0·10	0·011
	2½–4½	...	$5\cdot7\times10^{-3}$
	3½–4½	0·14	0·023
$^2_5$D–^{4}F	1½–1½	0·015	$9\cdot5\times10^{-10}$
	2½–1½	$1\cdot8\times10^{-4}$	$3\cdot5\times10^{-8}$
	1½–2½	$6\cdot9\times10^{-3}$	$3\cdot1\times10^{-8}$
	2½–2½	0·022	$4\cdot0\times10^{-9}$
	1½–3½	...	$1\cdot6\times10^{-10}$
	2½–3½	0·021	$1\cdot8\times10^{-8}$
	2½–4½	...	$7\cdot0\times10^{-10}$
^{4}F–^{4}F	4½–3½	$1\cdot4\times10^{-6}$	$9\cdot8\times10^{-18}$
	4½–2½	...	$3\cdot5\times10^{-15}$
	3½–2½	$5\cdot8\times10^{-5}$	$1\cdot2\times10^{-18}$
	3½–1½	...	$4\cdot8\times10^{-15}$
	2½–1½	$4\cdot6\times10^{-6}$	$8\cdot8\times10^{-18}$

TABLE III (*continued*)

Transition		A_m	A_q
^{4}G–^{2}H	$2\frac{1}{2}$–$4\frac{1}{2}$	...	$1{\cdot}9\times10^{-8}$
	$3\frac{1}{2}$–$4\frac{1}{2}$	0·13	$3{\cdot}4\times10^{-5}$
	$4\frac{1}{2}$–$4\frac{1}{2}$	0·042	$4{\cdot}8\times10^{-4}$
	$5\frac{1}{2}$–$4\frac{1}{2}$	0·56	$1{\cdot}3\times10^{-3}$
	$3\frac{1}{2}$–$5\frac{1}{2}$	...	v.s.
	$4\frac{1}{2}$–$5\frac{1}{2}$	0·61	$7{\cdot}8\times10^{-5}$
	$5\frac{1}{2}$–$5\frac{1}{2}$	0·47	v.s.
^{4}D–^{2}H	$2\frac{1}{2}$–$4\frac{1}{2}$	...	$3{\cdot}2\times10^{-5}$
	$3\frac{1}{2}$–$4\frac{1}{2}$	$1{\cdot}5\times10^{-3}$	$3{\cdot}2\times10^{-4}$
	$3\frac{1}{2}$–$5\frac{1}{2}$	...	v.s.
^{2}I–^{2}H	$5\frac{1}{2}$–$4\frac{1}{2}$	0·060	$4{\cdot}4\times10^{-4}$
	$6\frac{1}{2}$–$4\frac{1}{2}$	...	$8{\cdot}6\times10^{-6}$
	$5\frac{1}{2}$–$5\frac{1}{2}$	0·18	$2{\cdot}4\times10^{-5}$
	$6\frac{1}{2}$–$5\frac{1}{2}$	0·094	$5{\cdot}9\times10^{-4}$
^{4}F–^{2}H	$2\frac{1}{2}$–$4\frac{1}{2}$	...	$7{\cdot}6\times10^{-8}$
	$3\frac{1}{2}$–$4\frac{1}{2}$	$2{\cdot}4\times10^{-3}$	$7{\cdot}1\times10^{-8}$
	$4\frac{1}{2}$–$4\frac{1}{2}$	$6{\cdot}1\times10^{-3}$	$3{\cdot}5\times10^{-8}$
	$3\frac{1}{2}$–$5\frac{1}{2}$	...	$1{\cdot}6\times10^{-7}$
	$4\frac{1}{2}$–$5\frac{1}{2}$	v.s.	$3{\cdot}2\times10^{-7}$
^{2}H–^{2}H	$4\frac{1}{2}$–$5\frac{1}{2}$	$9{\cdot}4\times10^{-4}$	$2{\cdot}2\times10^{-10}$
^{4}G–$^2_5$G	$2\frac{1}{2}$–$3\frac{1}{2}$	v.s.	$8{\cdot}5\times10^{-5}$
	$3\frac{1}{2}$–$3\frac{1}{2}$	v.s.	$7{\cdot}0\times10^{-4}$
	$4\frac{1}{2}$–$3\frac{1}{2}$	0·077	$2{\cdot}4\times10^{-3}$
	$5\frac{1}{2}$–$3\frac{1}{2}$	...	$3{\cdot}3\times10^{-4}$
	$2\frac{1}{2}$–$4\frac{1}{2}$	...	$2{\cdot}5\times10^{-6}$
	$3\frac{1}{2}$–$4\frac{1}{2}$	0·064	$1{\cdot}3\times10^{-4}$
	$4\frac{1}{2}$–$4\frac{1}{2}$	$4{\cdot}2\times10^{-3}$	$1{\cdot}3\times10^{-3}$
	$5\frac{1}{2}$–$4\frac{1}{2}$	v.s.	$4{\cdot}6\times10^{-3}$
^{2}I–$^2_5$G	$5\frac{1}{2}$–$3\frac{1}{2}$	...	$7{\cdot}7\times10^{-6}$
	$5\frac{1}{2}$–$4\frac{1}{2}$	0·036	$1{\cdot}3\times10^{-4}$
	$6\frac{1}{2}$–$4\frac{1}{2}$	...	$3{\cdot}2\times10^{-6}$
$^2_3$F–$^2_5$G	$2\frac{1}{2}$–$3\frac{1}{2}$	0·013	$4{\cdot}4\times10^{-9}$
	$3\frac{1}{2}$–$3\frac{1}{2}$	0·026	$1{\cdot}6\times10^{-8}$
	$2\frac{1}{2}$–$4\frac{1}{2}$	...	$2{\cdot}5\times10^{-8}$
	$3\frac{1}{2}$–$4\frac{1}{2}$	$7{\cdot}0\times10^{-3}$	$4{\cdot}1\times10^{-7}$
^{4}F–$^2_5$G	$1\frac{1}{2}$–$3\frac{1}{2}$	...	$5{\cdot}8\times10^{-10}$
	$2\frac{1}{2}$–$3\frac{1}{2}$	0·013	$1{\cdot}1\times10^{-9}$
	$3\frac{1}{2}$–$3\frac{1}{2}$	0·020	$5{\cdot}5\times10^{-10}$
	$4\frac{1}{2}$–$3\frac{1}{2}$	$9{\cdot}7\times10^{-4}$	$9{\cdot}5\times10^{-11}$
	$2\frac{1}{2}$–$4\frac{1}{2}$	...	$6{\cdot}8\times10^{-8}$
	$3\frac{1}{2}$–$4\frac{1}{2}$	0·017	$8{\cdot}3\times10^{-9}$
	$4\frac{1}{2}$–$4\frac{1}{2}$	0·048	$1{\cdot}1\times10^{-8}$
^{2}H–$^2_5$G	$4\frac{1}{2}$–$3\frac{1}{2}$	$3{\cdot}2\times10^{-3}$	$2{\cdot}0\times10^{-8}$
	$5\frac{1}{2}$–$3\frac{1}{2}$	...	$2{\cdot}9\times10^{-11}$
	$4\frac{1}{2}$–$4\frac{1}{2}$	0·013	$1{\cdot}9\times10^{-9}$
	$5\frac{1}{2}$–$4\frac{1}{2}$	$2{\cdot}5\times10^{-3}$	$1{\cdot}5\times10^{-8}$

TABLE III (*continued*)

Transition		A_m	A_q
$^2_5$G–$^2_5$G	$3\frac{1}{2}-4\frac{1}{2}$	$6\cdot0 \times 10^{-4}$	$1\cdot1 \times 10^{-10}$
$^2_3$F–$^2_5$F	$2\frac{1}{2}-2\frac{1}{2}$	$7\cdot9 \times 10^{-4}$	$9\cdot3 \times 10^{-4}$
	$3\frac{1}{2}-2\frac{1}{2}$	0·047	$3\cdot0 \times 10^{-4}$
	$2\frac{1}{2}-3\frac{1}{2}$	0·051	$1\cdot2 \times 10^{-4}$
	$3\frac{1}{2}-3\frac{1}{2}$	$1\cdot3 \times 10^{-4}$	$2\cdot0 \times 10^{-3}$
^{4}F–$^2_5$F	$1\frac{1}{2}-2\frac{1}{2}$	0·098	$6\cdot8 \times 10^{-8}$
	$2\frac{1}{2}-2\frac{1}{2}$	0·016	$3\cdot1 \times 10^{-5}$
	$3\frac{1}{2}-2\frac{1}{2}$	0·027	$7\cdot2 \times 10^{-7}$
	$4\frac{1}{2}-2\frac{1}{2}$	...	$1\cdot1 \times 10^{-7}$
	$1\frac{1}{2}-3\frac{1}{2}$	...	$3\cdot3 \times 10^{-9}$
	$2\frac{1}{2}-3\frac{1}{2}$	0·026	$5\cdot4 \times 10^{-6}$
	$3\frac{1}{2}-3\frac{1}{2}$	0·013	$7\cdot0 \times 10^{-6}$
	$4\frac{1}{2}-3\frac{1}{2}$	0·11	$4\cdot7 \times 10^{-8}$
$^2_5$F–$^2_5$F	$2\frac{1}{2}-3\frac{1}{2}$	$2\cdot8 \times 10^{-7}$	$3\cdot5 \times 10^{-19}$
^{4}P–^{2}S	$\frac{1}{2}-\frac{1}{2}$	0·11	...
	$1\frac{1}{2}-\frac{1}{2}$	0·73	$3\cdot3 \times 10^{-6}$
	$2\frac{1}{2}-\frac{1}{2}$	...	$2\cdot0 \times 10^{-5}$
^{4}D–^{2}S	$\frac{1}{2}-\frac{1}{2}$	0·078	...
	$1\frac{1}{2}-\frac{1}{2}$	0·010	$1\cdot1 \times 10^{-4}$
	$2\frac{1}{2}-\frac{1}{2}$	...	$2\cdot2 \times 10^{-4}$
^{4}D–$^2_3$D	$\frac{1}{2}-1\frac{1}{2}$	0·63	v.s.
	$1\frac{1}{2}-1\frac{1}{2}$	0·22	v.s.
	$2\frac{1}{2}-1\frac{1}{2}$	0·090	v.s.
	$3\frac{1}{2}-1\frac{1}{2}$	...	v.s.
	$\frac{1}{2}-2\frac{1}{2}$	...	v.s.
	$1\frac{1}{2}-2\frac{1}{2}$	0·027	v.s.
	$2\frac{1}{2}-2\frac{1}{2}$	0·16	v.s.
	$3\frac{1}{2}-2\frac{1}{2}$	0·72	v.s.
$^2_5$D–$^2_3$D	$1\frac{1}{2}-1\frac{1}{2}$	v.s.	0·11
	$2\frac{1}{2}-1\frac{1}{2}$	v.s.	0·037
	$1\frac{1}{2}-2\frac{1}{2}$	v.s.	0·031
	$2\frac{1}{2}-2\frac{1}{2}$	v.s.	0·096
$^2_5$F–$^2_3$D	$2\frac{1}{2}-1\frac{1}{2}$	0·10	$7\cdot1 \times 10^{-3}$
	$3\frac{1}{2}-1\frac{1}{2}$	...	$1\cdot3 \times 10^{-3}$
	$2\frac{1}{2}-2\frac{1}{2}$	0·18	$1\cdot3 \times 10^{-3}$
	$3\frac{1}{2}-2\frac{1}{2}$	0·10	$7\cdot2 \times 10^{-3}$
^{2}I–$^2_3$G	$5\frac{1}{2}-3\frac{1}{2}$	...	4·2
	$5\frac{1}{2}-4\frac{1}{2}$	v.s.	0·12
	$6\frac{1}{2}-4\frac{1}{2}$	...	4·1
$^2_5$D–$^2_3$G	$1\frac{1}{2}-3\frac{1}{2}$	...	0·28
	$2\frac{1}{2}-3\frac{1}{2}$	v.s.	0·027
	$2\frac{1}{2}-4\frac{1}{2}$	...	0·24
$^2_5$G–$^2_3$G	$3\frac{1}{2}-3\frac{1}{2}$	v.s.	0·40
	$4\frac{1}{2}-3\frac{1}{2}$	$5\cdot3 \times 10^{-3}$	0·028
	$3\frac{1}{2}-4\frac{1}{2}$	0·029	0·033
	$4\frac{1}{2}-4\frac{1}{2}$	0·017	0·29
$^2_5$F–$^2_3$G	$2\frac{1}{2}-3\frac{1}{2}$	0·091	0·055
	$3\frac{1}{2}-3\frac{1}{2}$	0·22	$7\cdot1 \times 10^{-3}$
	$2\frac{1}{2}-4\frac{1}{2}$	...	$2\cdot9 \times 10^{-3}$
	$3\frac{1}{2}-4\frac{1}{2}$	0·10	0·058

a number of other multiplets which might be expected to be strong and for which the predicted wave-lengths are in the accessible region of the spectrum, a further search for [Fe IV] lines is justified.

Of the multiplets listed in Table III, 18 lie in the accessible spectrum. Six of these are rather weak, and are unlikely to be identifiable without precise wave-lengths. (These are ^{4}G–^{2}I, ^{4}P–^{4}F, ^{4}D–^{2}H, ^{4}G–$^2_5$G, ^{4}D–^{2}S and $^2_5$G–$^2_3$G.) The strongest lines of the remaining 12 multiplets are listed in Table IV, together with the wave-lengths predicted for their lines and the quantities $(2J_{\text{upper}}+1)A$ which are proportional to the strengths of the lines. Lines with $(2J+1)A<0{\cdot}25$ have been omitted from Table IV; data for these lines can easily be obtained from Tables II and III.

TABLE IV

Stronger [Fe IV] lines in the accessible spectrum

Transition		Predicted		Possible identification in RR Telescopii (1954)		
		λ	Intensity $(2J+1)A>0{\cdot}25$	λ	Int.	Notes
^{4}G–$^2_5$D	2½–2½	5920	0·8	5911	3	1
	3½–2½	5931	0·7	5911	3	1
^{4}P–$^2_5$D	½–1½	6978	0·3			
	1½–1½	6936	1·0	6997	4	2
	2½–1½	6899	0·3			
	1½–2½	7178	0·6	7221	3	3
	2½–2½	7138	3·2	7189	3	3
^{4}G–$^2_3$F	2½–2½	5089	1·3	5033	10	4
	3½–2½	5097	2·9	5041	15	4
	3½–3½	5265	0·6			
	4½–3½	5270	4·0	5233	16	4
^{4}P–$^2_3$F	2½–2½	5963	0·5	5911	3	1
^{4}D–$^2_3$F	2½–3½	7831	0·3			
	3½–3½	7732	0·8			
^{4}G–^{4}F	2½–1½	4905	1·3	4868	8	5
	3½–1½	4912	0·3			
	2½–2½	4916	1·5	4868	8	5
	3½–2½	4923	0·7			
	4½–2½	4928	0·4			
	3½–3½	4948	1·6	4900	8	5
	4½–3½	4953	1·5	4900	8	5
	5½–3½	4951	0·3			
	4½–4½	4961	1·2	4918	4	5, 7
	5½–4½	4959	3·2	4906	12	5, 7
^{4}D–^{4}F	½–1½	7039	0·4			
	1½–1½	7071	0·7			
	2½–2½	7100	1·2	7221	3	3
	3½–3½	7070	0·9			
	3½–4½	7088	1·6	7189	3	3

TABLE IV (*continued*)

Transition		Predicted λ	Intensity	Possible identification in RR Telescopii (1954) λ	Int.	Notes
		$(2J+1)A > 0{\cdot}25$				
^{4}G–^{2}H	$3\frac{1}{2}$–$4\frac{1}{2}$	4217	1·3	4209	7	6
	$4\frac{1}{2}$–$4\frac{1}{2}$	4220	0·4			
	$5\frac{1}{2}$–$4\frac{1}{2}$	4218	5·6	4206	10	6
	$4\frac{1}{2}$–$5\frac{1}{2}$	4137	7·3	4152	8	6, 7
	$5\frac{1}{2}$–$5\frac{1}{2}$	4135	5·6	4152	8	6, 7
^{4}P–^{2}S	$1\frac{1}{2}$– $\frac{1}{2}$	3297	1·5			
$^2_5$D–$^2_3$D	$1\frac{1}{2}$–$2\frac{1}{2}$	4239	0·4			
	$2\frac{1}{2}$–$2\frac{1}{2}$	4144	0·6			
$^2_5$F–$^2_3$D	$2\frac{1}{2}$–$1\frac{1}{2}$	7742	0·4			
	$2\frac{1}{2}$–$2\frac{1}{2}$	7741	1·1			
	$3\frac{1}{2}$–$2\frac{1}{2}$	7757	0·6			
$^2_5$F–$^2_3$G	$2\frac{1}{2}$–$3\frac{1}{2}$	4571	1·2			
	$3\frac{1}{2}$–$3\frac{1}{2}$	4577	1·8			
	$3\frac{1}{2}$–$4\frac{1}{2}$	4575	1·6			

Notes to Table IV

1. The three identifications of λ 5911 are all plausible.

2. Plausible. Thackeray's suggestion of [Ti III] is doubtful.

3. λ 7221 and λ 7189 might belong to either ^{4}P–$^2_5$D or to ^{4}D–^{4}F. If the former is correct, the computed transition probability of λ 7189 may be too high. According to Thackeray, Edlén considers both lines as definitely [Fe IV].

4. Highly probable identification.

5. The four lines $\lambda\lambda$ 4868, 4900, 4906 and 4918, which Edlén ascribes to [Fe IV], almost certainly belong to the ^{4}G–^{4}F multiplet. The identification of individual transitions is difficult. It seems likely that λ 4906 is the $5\frac{1}{2}$–$4\frac{1}{2}$ transition, but the other suggested identifications are very uncertain. The small spread of wave-length in this multiplet hinders the identification of the lines.

6. λ 4152 may represent either or both of the transitions $4\frac{1}{2}$–$5\frac{1}{2}$ and $5\frac{1}{2}$–$5\frac{1}{2}$. The identifications of λ 4209 and λ 4206 are both plausible.

7. If λ 4152 is a blend of $^4G_{4\frac{1}{2},\,5\frac{1}{2}}$–$^2H_{5\frac{1}{2}}$ then the two ^{4}G levels must be relatively close in energy, and in that case λ 4906 and λ 4918 cannot both be correctly identified. If λ 4152 is a blend, the identification of λ 4918 is a problem. If λ 4152 is not a blend, it should be accompanied by a companion of comparable strength. There is no obvious way out of this difficulty.

The star RR Telescopii in 1954 was undoubtedly (**16**) the best object in the sky for a search for [Fe IV] lines. We have examined Thackeray's list of wave-lengths and intensities, with special attention to unidentified lines and to lines which increased substantially in intensity from 1953 to 1954. The results of this search are contained in Table IV, and some detailed comments are appended to that table. There are a number of lines in RR Tel whose wave-lengths agree with those of certain predicted lines, within the probable limits of error of the calculations, and for which the observed and predicted intensities are in tolerable agreement. There is a good chance that some or all of these lines are due to [Fe IV]. There is of course no certainty about the suggested

identifications: only a laboratory analysis can decide as to the correctness of the suggestions. An attempt to use the data of Table IV to provide a partial term analysis of Fe IV was not very successful; the number of identifications made is inadequate.

5. *Conclusion.*—This paper has presented data on the energy levels and transition probabilities of forbidden lines of Fe IV, and a number of identifications with lines in RR Tel have been suggested. The numerical data in this paper are of rather lower accuracy than data in earlier papers by the writer because the calculations are not based directly on observed energy levels. Nevertheless, even if the suggested identifications are not correct, the results of this paper should give a reliable indication as to the transitions of importance in ions with $3d^5$ configurations. It is hoped that the work described above will stimulate some experimental spectroscopist to make a renewed attempt to produce and analyse the Fe IV spectrum.

Acknowledgments.—The writer is greatly indebted to Dr R. E. Trees for supplying a copy of the spin–orbit matrices computed by Greyber and for sending his own corrections to the matrices. Thanks are due to Dr D. W. N. Stibbs and Mr D. F. Mayers for diagonalizing three matrices on the DEUCE computer, and to Mr Mayers for supplying his estimate of the quadrupole radial integral.

University of London Observatory,
Mill Hill Park, London, N.W.7:
1958 *September* 15.

Note added in proof.—Since the above paper was written Professor Edlén has kindly sent to the author further details of the identifications referred to by Thackeray (**16**). Analysis of measurements in the vacuum-ultraviolet which had been made in connection with work on Fe III enabled six quartet terms to be established. Among these are the ^{4}G, ^{4}D and ^{4}F terms of the $3d^5$ configuration, and these allowed the identification of individual forbidden transitions. Professor Edlén has given permission for his results to be published here. The energy levels found by him are listed in Table V; to facilitate comparison they are in the same order as in Table II. In all cases the calculated term intervals

TABLE V

Relative energy levels of Fe IV derived by Edlén from a partial analysis of the vacuum-ultraviolet spectrum

Term	J	Energy		Term	J	Energy	
$3d^5\ ^4$G	$3\frac{1}{2}$	60		$3d^4 4s\ ^4$D	$2\frac{1}{2}$	106100	
			−4				501
	$4\frac{1}{2}$	56			$3\frac{1}{2}$	106601	
			−56				
	$5\frac{1}{2}$	0					
				$3d^4 4p\ ^4$F	$2\frac{1}{2}$	164093	
							218
					$3\frac{1}{2}$	164311	
							293
$3d^5\ ^4$D	$2\frac{1}{2}$	6698			$4\frac{1}{2}$	164604	
			−163				
	$3\frac{1}{2}$	6535					
				$3d^4 4p\ ^4$D	$1\frac{1}{2}$	169843	
							246
$3d^5\ ^4$F	$2\frac{1}{2}$	20599			$2\frac{1}{2}$	170089	
			−144				277
	$3\frac{1}{2}$	20455			$3\frac{1}{2}$	170366	
			−75				
	$4\frac{1}{2}$	20380					

agree with the observed ones within the accuracy of 50 cm^{-1} mentioned in the paper, and the intervals between terms agree within 500 cm^{-1}. The wave-lengths

of the forbidden lines in the ^4G–^4F and ^4D–^4F multiplets of the $3d^5$ configuration have been calculated from the observed energy levels and are listed in Table VI.

TABLE VI

Wavelengths of forbidden lines calculated from observed energy levels of the $3d^5$ configuration

Transition		λ	Identification in RR Tel λ	Int (1954)
^4G–^4F	$3\frac{1}{2}$–$2\frac{1}{2}$	4867·4	4868·2:	8:
	$4\frac{1}{2}$–$2\frac{1}{2}$	4866·5		
	$3\frac{1}{2}$–$3\frac{1}{2}$	4901·8	4900·2	8
	$4\frac{1}{2}$–$3\frac{1}{2}$	4900·8	4900·2	8
	$5\frac{1}{2}$–$3\frac{1}{2}$	4887·4		
	$3\frac{1}{2}$–$4\frac{1}{2}$	4919·9		
	$4\frac{1}{2}$–$4\frac{1}{2}$	4918·9	4918·1	4
	$5\frac{1}{2}$–$4\frac{1}{2}$	4905·4	4906·2	12
^4D–^4F	$2\frac{1}{2}$–$2\frac{1}{2}$	7191·7	7189	3
	$3\frac{1}{2}$–$2\frac{1}{2}$	7108·4		
	$2\frac{1}{2}$–$3\frac{1}{2}$	7267·0		
	$3\frac{1}{2}$–$3\frac{1}{2}$	7181·9		
	$2\frac{1}{2}$–$4\frac{1}{2}$	7306·9		
	$3\frac{1}{2}$–$4\frac{1}{2}$	7220·8	7221	3

In Table VI we have also included those identifications in RR Telescopii which are now firmly established. It is gratifying to note that four of the suggested identifications in the ^4G–^4F multiplet have been confirmed. The problem mentioned in note 3 to Table IV is resolved: λ7189 and λ7221 belong to ^4D–^4F. There remains the problem of identifying $^4P_{2\frac{1}{2}}$–$^2_5D_{2\frac{1}{2}}$, which if the computed transition probabilities are correct ought to be of considerable strength; possibly it contributes to λ7171.

References

(1) B. Edlén, *Les Novae et les naines blanches*, Actualités Sci. et Industrielles, No. 895, 1941.
(2) R. H. Garstang, *Proc. Camb. Phil. Soc.*, **53**, 214, 1957.
(3) R. H. Garstang, *M.N.*, **117**, 393, 1957.
(4) R. H. Garstang, *Proc. Camb. Phil. Soc.*, **54**, 383, 1958.
(5) R. H. Garstang, *M.N.*, **118**, 234, 1958.
(6) S. Glad, *Ark. f. Fys.*, **10**, 291, 1955.
(7) H. D. Greyber, *Thesis*, University of Pennsylvania, 1953.
(8) T. Ishidzu and S. Obi, *J. Phys. Soc. Japan*, **5**, 124, 1950.
(9) G. Racah, *Phys. Rev.*, **62**, 438, 1942.
(10) G. Racah, *Phys. Rev.*, **85**, 381, 1952.
(11) G. H. Shortley, *Phys. Rev.*, **57**, 225, 1940.
(12) P. Swings and O. Struve, *Ap. J.*, **91**, 546, 1940.
(13) P. Swings and O. Struve, *Ap. J.*, **96**, 468, 1942.
(14) P. Swings, *J. Opt. Soc. America*, **41**, 153, 1951.
(15) A. D. Thackeray, *The Observatory*, **74**, 90, 1954.
(16) A. D. Thackeray, *M.N.*, **115**, 236, 1955.
(17) R. E. Trees, *Phys. Rev.*, **85**, 382, 1952.
(18) A. B. Wyse, *Ap. J.*, **95**, 356, 1942.

THE PHOTO-ELECTRIC LIGHT CURVE OF RT SCULPTORIS

G. G. Cilliè and E. M. Lindsay

(Received 1958 August 13)

Summary

With the 60-inch Rockefeller reflector of the Boyden Observatory photo-electric light curves have been obtained in blue and yellow light for the eclipsing variable RT Sculptoris. The two maxima are unequal and are not flat-topped in any way. There has been a slight shortening of the period of this star during the past 50 years and assuming the decrease to be linear we find the following light elements which best fit the observations:

$$\text{Min.} = \text{JD } 2423736^{\text{d}}{\cdot}51145 + (0^{\text{d}}{\cdot}51156702 - 1{\cdot}0568 \times 10^{-10}E)E.$$

The variability of the star, RT Sculptoris, CoD $-26°179$, CPD $-26°43$, position $00^{\text{h}}\,31^{\text{m}}\,30^{\text{s}}$, $-26°\,13'{\cdot}5$ (1900) was discovered on Harvard plates by Ida Whiteside (1) who gave the following light elements:

$$\text{Min.} = 2411736^{\text{d}}{\cdot}114 + 0^{\text{d}}{\cdot}511574E.$$

The star varied between photographic magnitudes 9·64 at maximum and 10·47 and 9·84 at the two minima. The first maximum was flatter and of longer duration than the second and it was considered that the star was of the β Lyrae type. Miss Whiteside's material consisted of 276 photographic observations over the period 1891–1907, and since her first observation was on JD 2411736·436 her epoch must have been found by using the determined period and extrapolating backwards. From 1891 to 1899 only thirty estimates were available. The residuals from these and a few others were larger on the whole than from the rest. It was considered, however, that they did not show any systematic difference which would indicate a changing period and that they were due to the plates having been taken with a different instrument.

Shapley (2) discussed Miss Whiteside's observations, determined orbital elements, and gave ranges of primary and secondary minima of $0^{\text{m}}{\cdot}71$ and $0^{\text{m}}{\cdot}20$ respectively.

In 1925 Schilt (3) published some further observations of this star from measurements with the thermopile-microphotometer on 326 plates taken by Hertzsprung on sixteen nights at the end of 1924. The quality of many of the plates was rather poor due to spots and irregularities in the film and the determination of the magnitudes of the variable was uncertain in some cases as a consequence of the large irregularities in the galvanometer readings of the comparison star. Schilt found that in comparison with the earlier observations the secondary minimum had shifted $0^{\text{d}}{\cdot}026$ towards the following primary minimum. He also found that the first maximum is higher and broader than the second one and that the descent towards secondary minimum is steeper than the rise from secondary minimum, a result that is confirmed by our photo-electric observations. Schilt determined a "normal minimum" at JD 2424147·298. This minimum, together with that of Miss Whiteside's,

gave an "improved period" of $0^{d}\cdot51156935$. Thus his light elements for RT Sculptoris are:

$$\text{Min.} = 2411736\cdot114 + 0^{d}\cdot51156935E.$$

In 1928 Dugan (4) gave the following light elements:

$$\text{Min.} = 2423736\cdot51145 + 0^{d}\cdot511569633E.$$

These were determined by using Miss Whiteside's original epoch and two well-determined minima by himself, using the polarizing photometer on 1923 December 7 (JD 2423761) and 1924 November 26 (JD 2424116). The dispersion in Dugan's observations were rather larger than usual and their distribution not normal. Systematic errors of some unknown type were present. Dugan concluded that any irregular variation in the comparison star or in one of the components of the variable would be pretty well ironed out by observations. In attempting to compute the physical dimensions of the system he found it impossible to obtain elements which predict the light curve satisfactorily.

TABLE I

Primary minima of RT Sculptoris

	Date of run	Observed time of prim. min.	Wt.	Min. $= 2423736\cdot51145 + 0^{d}\cdot51156471E$ Calc. min.	O–C	Min. $= 2411736\cdot114 + (0\cdot51157183 - 1\cdot0245 \times 10^{-10}E')E'$ Calc. min.	O–C
		243....		243....	d	243....	d
1952	July 28/29	4222·56596	4	4222·5649	+0·0011	4222·5678	−0·0018
1954	September 5/6	4991·44630	3	4991·4466	−0·0003	4991·4465	+0·0001
	September 28/29	5014·46611	4	5014·4670	−0·0009	5014·4666	+0·0004
	October 14/15	5030·32572	2	5030·3256	+0·0001	5030·3251	+0·0006
	October 15/16	5031·35012	2	5031·3487	+0·0014	5031·3483	+0·0018
	October 16/17	5032·37130	5	5032·3718	−0·0005	5032·3713	0·0000

In communications to Dugan, Adams and Joy gave the spectral classification of RT Sculptoris as A5n and they found that the two spectra were of nearly equal intensity, that of the star receding between primary and secondary minima being perhaps a little fainter.

As Dugan pointed out, and as will be seen from the above, all observers have remarked on some peculiarities of the observations. It is also to be noted that any "improved" periods have been based on Miss Whiteside's original epoch and obtained on the assumption that the period is constant. In view of the uncertainties with regard to this system, the star was put on the programme of the Linnell-King photo-electric photometer attached to the 60-inch Rockefeller reflector of the Boyden Observatory in 1951. All told, 1986 comparisons—1064 in blue light and 922 in yellow light—were made in the course of 1951, 1952 and 1954 with the nearby star CoD $-26°193$ ($9^{m}\cdot1$) = CPD $-26°49$ ($9^{m}\cdot8$).

Well-observed primary minima of RT Sculptoris were obtained on six nights, and using Dugan's fundamental epoch we obtain the best mean-square fit with the following light elements:

$$\text{Min.} = 2423736\cdot51145 + 0^{d}\cdot51156471E.$$

In Table II we summarize the various determinations of the period of RT Sculptoris up to date, the first two being determined with the fundamental

epoch of Whiteside and the last two with that given by Dugan. From Table II, as indeed we suspected from rough plots of our observations, it is evident that the period of RT Sculptoris has been slowly decreasing during the past 50 years. So far as one can judge, the decrease has been steady and roughly linear with time. Hence we try to fit a formula of the following type to the observed primary minima,

$$\text{Min.} = T_0 + (P_0 - aE')E',$$

where T_0 is some fundamental epoch, a a constant, E' the number of cycles calculated from T_0 and P_0 may be termed the "original period". Using Whiteside's fundamental epoch, Schilt's "normal minimum" and our own minimum of 1954 October 16/17, we obtain the light elements:

$$\text{Min.} = 2411736{\cdot}114 + (0{\cdot}51157183 - 1{\cdot}0245 \times 10^{-10}E')E'.$$

The minima predicted with this formula at the time of our observations and the residuals when these are compared with the observed times are given in the last two columns of Table I. The actual period of RT Sculptoris at any particular time (or epoch E') is given by

$$P_0 - 2aE' = 0^{\text{d}}{\cdot}51157183 - 2{\cdot}049 \times 10^{-10}E'.$$

At the time of our observations in 1954 October, the period of RT Sculptoris was $0^{\text{d}}{\cdot}51156249$ and we use this to compute a "normal minimum" at that time. It comes out at JD 2435019·58244 at the epoch $E' = 45514$ calculated from Whiteside's original epoch.

TABLE II

Determinations of the period of RT Sculptoris

Observer	Period
	d
Whiteside	0·511574
Schilt	·51156935
Dugan	·511569633
Cillié and Lindsay	·51156471

We now recalculate the constants in the formula for the minima of RT Sculptoris, namely,

$$\text{Min.} = T_0'' + (P_0'' - a''E'')E'',$$

taking as $T_0'' = 2423736{\cdot}51145$, which is Dugan's fundamental epoch, and making use of Whiteside's fundamental epoch and our own "normal minimum". This gives for RT Sculptoris,

$$\text{Min.} = \text{JD } 2423736{\cdot}51145 + (0^{\text{d}}{\cdot}51156702 - 1{\cdot}0568 \times 10^{-10}E'')E''.$$

Schilt's normal minimum gives an O–C residual of $-0^{\text{d}}{\cdot}0017$ with this formula, which is not surprising and about the same residual found by Dugan when he tried to fit Schilt's normal minimum to his own observations.

Our observations of the primary minima of RT Sculptoris prove that the period of the star has in all probability been steadily decreasing during the past 50 years. No doubt this change of period has something to do with Dugan's difficulty in interpreting the light curve satisfactorily. Secondary minima of RT Sculptoris fall half-way between primary minima according to our observations. The weighted mean phase of secondary minimum is 0·4984.

In Tables III and IV we give the normal points in blue and in yellow light for the light curve of RT Sculptoris. These have been computed in the usual way by using our final light elements. The period changes very slowly, so that even for the duration of our observations the period of the star changed very little and we had no difficulty in combining our observations into normal points.

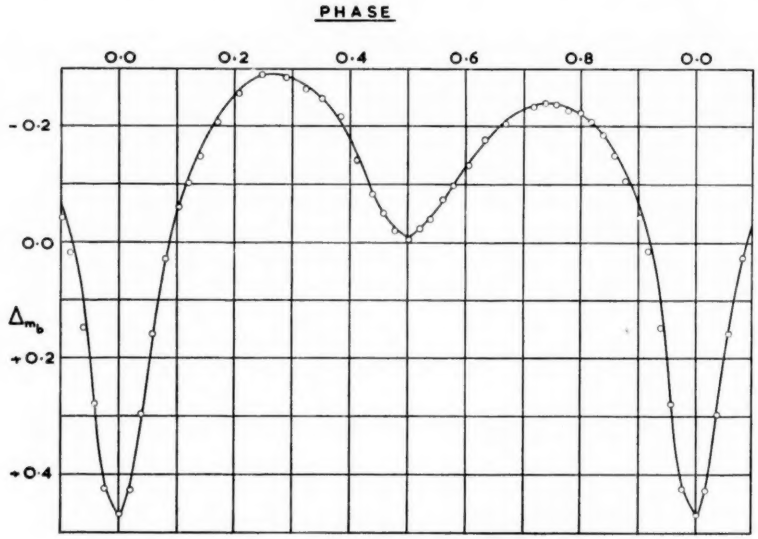

FIG. 1.—*Blue light curve of RT Sculptoris.*

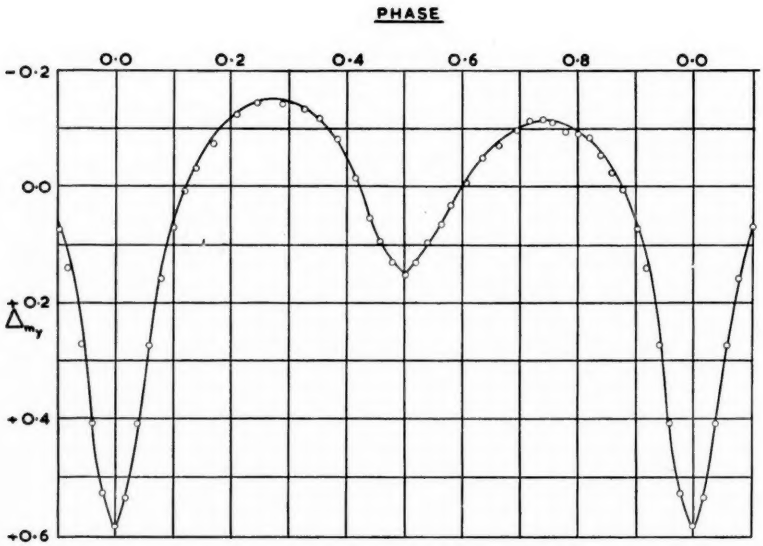

FIG. 2.—*Yellow light curve of RT Sculptoris.*

TABLE III

Blue light curve of RT Sculptoris

Phase (period)	Δm_b	M.e. of normal pt.	Wt.	Phase (period)	Δm_b	M.e. of normal pt.	Wt.
0·0008	$+0^m·470$	$\pm0^m·002$	43	0·5621	$-0^m·073$	$\pm0^m·002$	18
·0191	·426	·003	39	·5792	·099	·002	18
·0385	·296	·002	24	·6051	·134	·003	26
·0585	·155	·003	28	·6335	·177	·003	28
·0829	+0·024	·005	21	·6698	·205	·003	26
·1006	−0·060	·005	25	·7193	·234	·004	15
·1214	·104	·005	16	·7395	·241	·003	27
·1396	·149	·003	23	·7582	·239	·003	24
·1717	·208	·003	23	·7796	·228	·002	26
·2093	·258	·002	20	·8000	·224	·003	33
·2480	·289	·003	20	·8195	·208	·003	20
·2912	·285	·003	15	·8389	·185	·002	42
·3245	·267	·002	17	·8613	·149	·002	36
·3534	·250	·002	27	·8798	·105	·002	37
·3856	·217	·003	28	·9018	−0·043	·002	40
·4152	·145	·004	21	·9177	+0·018	·003	25
·4399	·084	·004	24	·9397	·145	·004	34
·4606	·051	·004	18	·9589	·278	·003	36
·4818	·020	·002	28	0·9783	+0·422	±0·003	37
·5011	·006	·005	19				
·5213	·024	·003	19				
0·5402	−0·040	±0·003	19				

TABLE IV

Yellow light curve of RT Sculptoris

Phase (period)	Δm_y	M.e. of normal pt.	Wt.	Phase (period)	Δm_y	M.e. of normal pt.	Wt.
0·0001	$+0^m·581$	$\pm0^m·003$	31	0·5402	$+0^m·096$	$\pm0^m·004$	18
·0188	·533	·003	27	·5629	·066	·003	16
·0394	·408	·003	19	·5799	+0·033	·002	18
·0595	·272	·004	22	·6066	−0·005	·003	22
·0804	·158	·005	15	·6343	·049	·002	19
·0998	·070	·004	23	·6628	·070	·002	25
·1213	+0·008	·005	13	·6976	·099	·003	16
·1399	−0·033	·003	18	·7179	·112	·003	15
·1703	·076	·003	22	·7403	·113	·003	24
·2099	·122	·003	20	·7583	·110	·003	19
·2466	·146	·003	19	·7800	·093	·004	22
·2900	·145	·003	18	·8000	·090	·003	28
·3259	·133	·002	17	·8196	·084	·004	16
·3532	·117	·002	24	·8401	·055	·002	30
·3851	·081	·002	24	·8608	−0·024	·002	29
·4152	−0·016	·005	23	·8783	+0·006	·003	28
·4399	+0·053	·006	21	·9015	·074	·003	32
·4589	·094	·005	12	·9178	·139	·004	26
·4810	·129	·002	28	·9408	·270	·003	27
·5012	·149	·005	18	·9604	·405	·003	28
0·5201	+0·131	±0·004	16	0·9789	+0·524	±0·003	30

Our light curve confirms previous observations in connection with this very interesting star. We find primary minimum deeper by $0^m·48$ in blue light and $0^m·44$ in yellow light than secondary minimum. The descent into secondary minimum is steeper than the subsequent ascent, as first pointed out by Schilt.

The maxima do not appear to be flat-topped in any way, but they are slightly unequal. "Primary maximum", i.e. the maximum following primary minimum, exceeds "secondary maximum" by $0^{m}\cdot05$ in blue and $0^{m}\cdot035$ in yellow light. In this, as indeed in other respects, there seems to be a considerable similarity between the eclipsing systems RT Sculptoris and V 525 Sagittarii (**5**). The only significant difference we find is the gradually changing period of RT Sculptoris. Over the last 50 years the period of this star has decreased by something less than 1 second*.

In conclusion it is a pleasure to record our thanks to the staff of the Boyden Observatory for kind assistance while the programme was being carried out.

* The individual observations will be printed separately and distributed with Armagh Contribution Number 25.

Department of Mathematics,
University of Stellenbosch,
Union of South Africa:
1958 *August.*

Armagh Observatory,
N. Ireland.

References

(**1**) E. C. Pickering, *Harv. Circ.* No. 139, 1908.
(**2**) H. Shapley, *Princ. Univ. Obs. Contr.* 3, 1915.
(**3**) J. Schilt, *B.A.N.*, **3**, 63, 1925.
(**4**) R. S. Dugan, *Princ. Univ. Obs. Contr.* 8, 1928.
(**5**) G. G. Cillié and E. M. Lindsay, *M.N.*, **113**, 516, 1953.

RADIO EMISSION FROM ORION

H. Rishbeth

(Communicated by F. Graham Smith)

(Received 1958 July 30)

Summary

The Orion region has been surveyed at two wave-lengths by the Sydney "Mills Cross" radio telescopes. The radio emission from bright nebulae in the region appears to be of thermal origin; but a faint extended source in the region may emit non-thermally, and is perhaps associated with an extensive dark nebula. Radio and optical observations of the Orion Nebula, M42, are compared with the aid of a simple model.

---

1. *Introduction.*—The Orion region has long been recognized to be of great astrophysical interest, and a large literature dealing with it is now in existence. The outstanding object in the constellation is the Great Nebula, M42; many other emission nebulae excited by early-type stars are found in the vicinity.

The region offers a good opportunity for the comparison of optical and radio observations, both of which enable the "emission measure" to be determined provided that the radio-frequency radiation is of thermal origin. Differences between the optical and radio emission measures may thus be attributed to optical obscuration or to non-thermal radio emission. Evidence already available (e.g. (**1**)) suggests that emission nebulae emit thermally at radio wave-lengths, in contrast to other types of radio source which can only be explained in terms of a non-thermal emission mechanism.

Many radio observations of the Orion region have been made in recent years, and isophotes at decimetre wave-lengths have been published (**2, 3, 4**). This paper describes the results of high-resolution surveys at metre wave-lengths, obtained with the Mills Cross radio telescopes of the C.S.I.R.O. Radiophysics Laboratory near Sydney, N.S.W.

2. *Observations.*—The principles of the Mills Cross are now well known, and as the equipments have been described in detail (**5, 6**) only the salient details will be given here. The 1500 ft cross operates at a wave-length of 3·5 m (85·5 Mc/s); the second instrument, whose overall dimensions are about 3500 ft, operates at 15·2 m (19·7 Mc/s). The crosses are transit instruments and possess pencil-beam responses of approximately Gaussian form. The Orion region transits about 30° north of the zenith at Sydney, where the aerial responses are slightly elongated in declination; the half-power responses for the two systems are about $50' \times 60'$ and $85' \times 100'$ respectively.

The survey at 3·5 m covered an area of over four hundred square degrees; the records were of the scanning type previously described (**7**). Most of the area was covered twice, and a number of simple records of greater sensitivity were obtained to provide additional information about particular features. The reduction procedure outlined in another paper (**8**) was employed in the construction of isophotes, which are presented in Fig. 1. The discrete sources are substantially those of Mills and Slee (**7**).

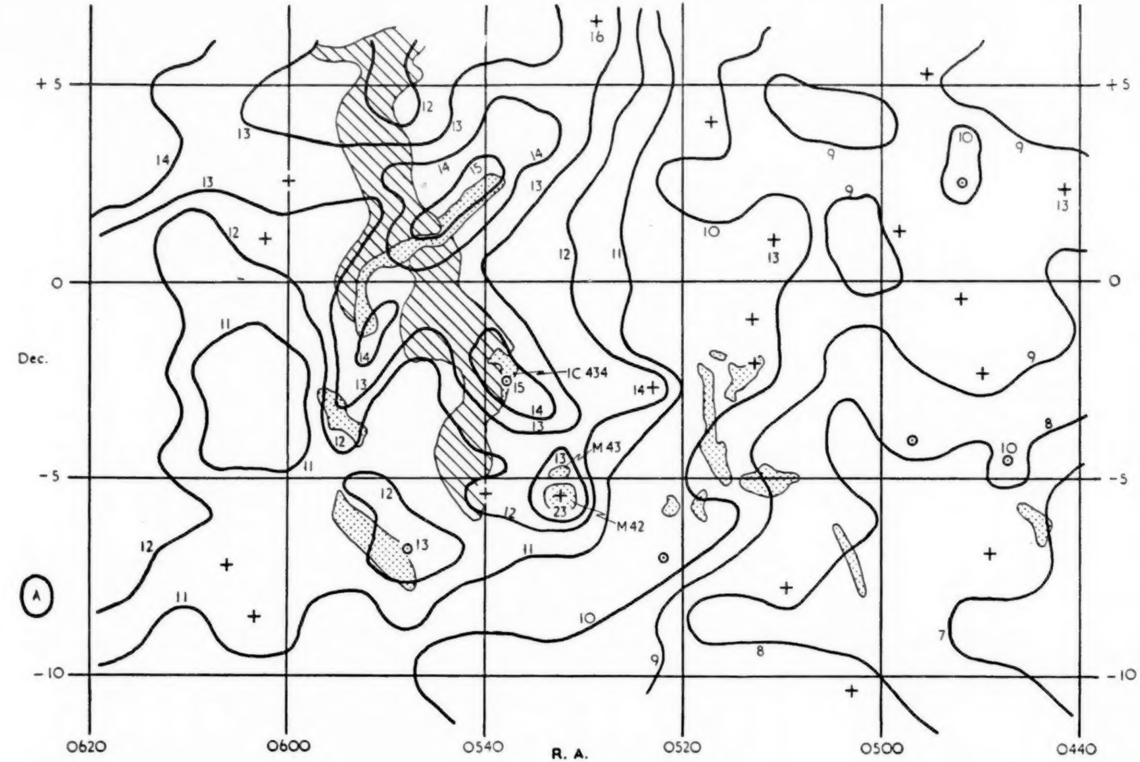

FIG. 1.—*Isophotes of the Orion region at 3·5 m wave-length.* 1950 *coordinates.* *Unit* 100 °*K.* *Many closed contours surrounding discrete sources are omitted, but the peak aerial temperatures of the principal sources are shown.*

+ = *Unresolved source.* ⊙ = *Extended source.*

A = *Half-power contour of aerial beam.* H II *regions (dotted) and dark nebulae (shaded) are taken from the Skalnote Pleso Atlas* (**9**). *Barnard's* H II *ring (Section* 5 (*b*)) *is contained within the rectangle formed by right ascensions* 0505 *and* 0555 *and declinations* +6° *and* −9°.

At 15 m wave-length, broadcast interference and ionospheric effects were troublesome and fewer records were obtained. Corrections for ionospheric refraction were estimated from daily observations of intense sources, and have been applied to the isophotes of Fig. 2.

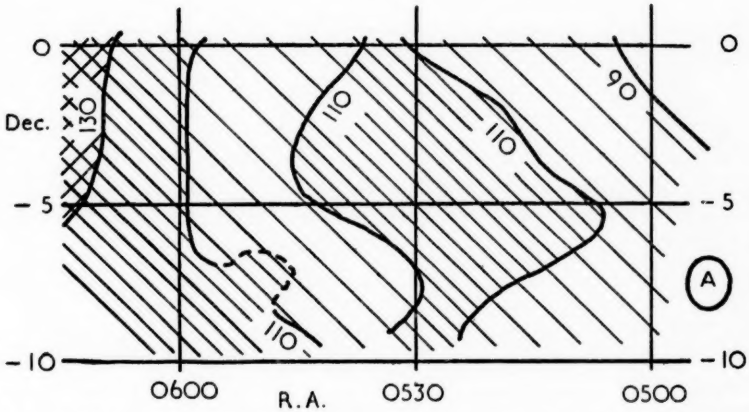

FIG. 2.—*Isophotes of the Orion region at 15 m wave-length. 1950 coordinates. Unit 1000 °K. A is the half-power contour of the aerial beam.*

3. *Theory.*—The theory of thermal radio emission by free-free transitions in ionized hydrogen has been discussed by Piddington (**10**) and Mills, Little and Sheridan (**11**). A few results are given here.

The optical depth τ of a region of ionized gas is proportional to its emission measure E, defined as $E = \int N^2 . dl$, where N is the electron density (in cm^{-3}) and l is the path length through the gas (in parsecs). The equation is:

$$\tau = \lambda^2 g(\lambda) . E T_e^{-3/2} \qquad (1)$$

where $g(\lambda)$ is a slowly-varying function of wave-length λ and T_e is the electron temperature, which is of the order of 10^4 °K in emission nebulae. Typical values of the quantity E/τ for various radio wave-lengths are given in Table I.

TABLE I

Values of E/τ

Wave-length	E/τ $T_e = 10\,000$ °K	$T_e = 20\,000$ °K
15·2 m	$7 \cdot 9 \times 10^2$	$2 \cdot 1 \times 10^3$
3·5	$1 \cdot 6 \times 10^4$	$4 \cdot 4 \times 10^4$
1·9	$5 \cdot 8 \times 10^4$	$1 \cdot 6 \times 10^5$
0·5	$9 \cdot 1 \times 10^5$	$2 \cdot 5 \times 10^6$
0·1	$2 \cdot 6 \times 10^7$	$7 \cdot 0 \times 10^7$

For optically thin objects, sufficiently extensive to fill the aerial beam, a simple relation connects the average emission measure and the increase of aerial beam temperature (ΔT_a) due to the source. It may easily be shown that under these conditions $\Delta T_a = \tau . T_e$, and substitution in (1) of the values $T_e = 10\,000$ °K, $\lambda = 3 \cdot 5$ m and $g(\lambda) = 5 \cdot 0$ gives

$$E = 1 \cdot 6 \Delta T_a. \qquad (2)$$

At 3·5 m wave-length, the emission nebulae in Orion are seen against a background of cosmic radio emission, whose brightness temperature is about 1000 °K. The above equation must be modified to take account of this, and becomes

$$E = 1{\cdot}8\Delta T_a. \tag{3}$$

The radiation from an emission nebula, small compared to the aerial beamwidth, is more conveniently specified by its flux density S, given by:

$$S \propto \int E\,.\,d\Omega = \int \frac{N^2\,.\,dV}{D^2} \tag{4}$$

where $d\Omega$, dV are elements of solid angle and volume respectively. D is the distance from the solar system. If the ionization is contained in a homogeneous sphere of radius a, as in the model of an H II region proposed by Strömgren (**12**), then

$$\int \frac{N^2\,.\,dV}{D^2} = \frac{4\pi I^3}{3D^2} \tag{5}$$

where $I^3 = N^2a^3$. I then depends upon the temperature of the exciting star: it is the quantity tabulated by Strömgren as a function of the spectral type of the star.

4. *The Orion Nebula*

(*a*) *A simple model of the Orion Nebula, M42.*—A simple thermal model of M42 can be constructed from available data. Spherical symmetry is assumed and the electron temperature is supposed uniform throughout the nebula. The distribution of electron density N is taken as a function of radial distance r such that

$$N^2 = N_1^2\,\mathrm{e}^{-r/a} + N_2^2\,\mathrm{e}^{-r/b}. \tag{6}$$

Two terms are necessary in order that the model shall resemble the optical appearance of M42. The first term represents the central nucleus of the nebula, whose brightness falls off very rapidly with increasing distance from the Trapezium cluster of exciting stars. The second term represents the extensive outer portion of the nebula. Its radial decrease of brightness is much slower, and is specified by the parameter b whose value is derived from the optical isophotes of Michelson (**13**). N_2 is chosen to give the observed flux density at 3·5 m wave-length, and then the parameters N_1, a of the central portion are determined from the measurements at centimetre and decimetre wave-lengths.

Values of these quantities are given in Table II, and the radial variation of emission measure is shown in Fig. 3: the two curves refer to models with electron temperatures of 10 000 °K and 20 000 °K. The radio spectra of the models are plotted in Fig. 4, together with the observed flux densities which are listed in Table III.

At centimetre wave-lengths the nebula is optically thin, but S decreases slowly with decreasing wave-length because of the logarithmic factor $g(\lambda)$ of equation (1). The probable error of the point at 3·2 cm is large, as the flux density quoted by Kaidanovski and others (**17**) is equal to the equipment sensitivity. A measurement by Haddock (**1**) suggests that the 3·2 cm flux density is higher, and closer to the 9·4 cm value. Recent work by Westerhout (**18**) gives the flux density at 22 cm as 520×10^{-26} w. m.$^{-2}$ (c/s)$^{-1}$ ± 20 per cent, in substantial agreement with the points shown on Fig. 4.

TABLE II

Model of M42 (equation (6), Section 4 (a))

Quantity	$T_e = 10\ 000\ ^\circ K$	$T_e = 20\ 000\ ^\circ K$
Assumed distance from the solar system (D)	500 pc	500 pc
Emission measure at centre	$7 \cdot 6 \times 10^6$	$1 \cdot 32 \times 10^7$
N_1	6200 cm^{-3}	8500 cm^{-3}
N_2	83 cm^{-3}	78 cm^{-3}
a	0·10 pc	0·092 pc
(angular equivalent)	(41″)	(38″)
b	1·0 pc	1·0 pc
(angular equivalent)	(6′·9)	(6′·9)
Mass:		
Central portion	30 $M_\odot$	30 $M_\odot$
Outer portion	400 $M_\odot$	400 $M_\odot$

If D is changed, then N_1, N_2 vary as $D^{-1/2}$; a, b as D; and the mass as $D^{5/2}$.

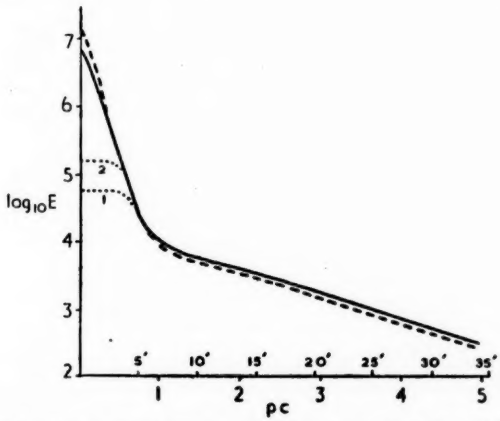

FIG. 3.—*Radial variation of emission measure E (cm⁻⁶ parsec) of the model of M42, for two values of electron temperature. For the lower scale (parsecs) a distance of 500 parsecs from the solar system is assumed.*

———— $T_e = 10\ 000\ ^\circ K$.
- - - - - - $T_e = 20\ 000\ ^\circ K$.
.... *Radial brightness variation at 1·9 m wave-length for* $T_e = 10\ 000\ ^\circ K$ (1) *and* $T_e = 20\ 000\ ^\circ K$ (2).

At wave-lengths greater than about 3 m the brightness temperature of the galactic background is appreciable in comparison to the electron temperature, so the apparent flux density is reduced. At 15 m the nebula should absorb the background radiation: the effect would be near the limit of detection of the equipment, and is not in fact observed.

There does not seem to be any non-thermal component in the radiation from M42. If such a component existed, it would be most prominent at long wave-lengths. An upper limit of 100×10^{-26} w. m.$^{-2}$ (c/s)$^{-1}$ can be set at 7·9 m (G. R. Whitfield, private communication), whereas the upper limit at 15 m is about 200×10^{-26} w. m.$^{-2}$ (c/s)$^{-1}$. With present techniques it is not significant that the spectrum of the model does not include both the 1·9 m and 3·5 m points.

TABLE III

Radio observations of the Orion Nebula, M42 (IAU source 05S0A)

Observer	Wave-length m	Freq. Mc/s	R.A. 1950 h m m	Dec. 1950 ° ′ ′	Flux 10^{-26} w.m.$^{-2}$(c/s)$^{-1}$
Rishbeth (present obs.)	3·5	85·5	05 32·5 ±0·2	−5 27±3	85
Baldwin, Archer (private communication)	1·9	160	05 32·8 ±0·2	−5 24±4	65
Seeger, Westerhout, van de Hulst (**2**)	0·75	400	05 32	−5	230
Piddington and Trent (**14**)	0·50	600	05 32	$-5\frac{1}{2}$	300
Denisse, Lequeux, Le Roux (**4**)	0·33	900	05 32	−5 30	420
Hagen, Lilley, McClain (**15**)	0·21	1420	05 32	−5 20	420
Haddock, Mayer, Sloanaker (**16**)	0·094	3200	05 33·0 ±0·2	−5 27±5	450
Kaidanovski, Kardashev, Shklovski (**17**)	0·032	9400	05 33	−5 27	270
Visual position of Trapezium stars	—	—	05 32·8	−5 25	—

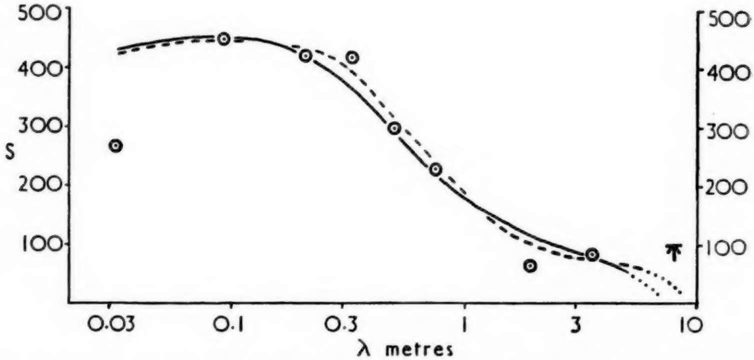

FIG. 4.—*Observed radio flux densities S of the Orion Nebula, M42, from Table III. Unit 10^{-26}w.m.$^{-2}$(c/s)$^{-1}$. The observation at 7·9 m is an upper limit. The curves show the spectra of the model of equation* (6) *for two values of electron temperature.*

———————— $T_e = 10\,000$ °*K.*

- - - - - - - - $T_e = 20\,000$ °*K.*

. . . . *These portions of the curves are dependent on the background temperature.*

Information concerning the angular size of the M42 source is given by the interferometric measurements of Mr S. Archer, of the Cavendish Laboratory, at 1·9 m. At this wave-length (see Fig. 3) the model has an optical depth of unity at a radius near the transition between the central peak and the outer portion, and so the observations provide a sensitive test of the validity of the model. The aerial spacings used were 27 λ in the north–south direction and 307 λ in the east–west direction; and the ratio of the corresponding Fourier components of the strip brightness distribution is certainly less than 0·2, and probably not more than 0·1. The values given by the model are 0·11 and 0·24 for electron temperatures of 10000 °K and 20000 °K respectively.

The model with $T_e = 10\,000\,°K$ thus accords with the 1·9 m result, but with $T_e = 20\,000\,°K$ the effective diameter is too small, and cannot be appreciably increased if the radio spectrum is to be preserved. Although this discussion relates to an exponential distribution of electron density, the result is not critically dependent on the choice of model, and it seems that the electron temperature of the nebula is probably less than 20 000 °K. This merely corroborates optical estimates, which are around 10 000 °K; but it is possible that with further technical progress radio methods will enable narrower limits to be set on the value.

(*b*) *Comparison with optical data.*—The overall shape of the M42 model, and the density of its outer portions, were chosen to suit optical data, while the emission measure of the central portion was determined from high-frequency radio observations. Further comparisons with optical data are possible.

Westerhout and Oort (**19**) give the emission measure at the centre of the nebula as 8×10^6, in agreement with the radio model. The emission measures of Johnson (**20**) are averaged over areas of $8' \times 18'$; similar averages taken from the model are comparable with his results, though somewhat smaller. The emission measure at the periphery of the model is consistent with the overall diameter recorded on long exposure photographs of M42.

Electron densities in the Orion nebula have been derived by Osterbrock (**21**) from measurements of the relative intensities of the $\lambda 3726$ and $\lambda 3729$ lines of O II. Within 5′ of the centre, the radial dependence of electron density agrees well with the parameter *a*, but the actual values measured by Osterbrock are greater by a factor of order five than those given by equation (6) with the adopted parameters. In the outer portion, more than 7′ from the centre, the ratio is roughly 20 : 1. However, the model takes no account of irregularities within the nebula, the presence of which may affect the comparison of the values of N (as given by the optical measurements) with the integral $\int N^2 . dl$.

Another test of the model comes from the application of Strömgren's (**12**) theory of the excitation of H II regions by O and B stars. The stars of the Trapezium cluster, at the centre of M42, range from O7 to B1 in spectral type; the value of the ionization parameter I (equation (5)) appropriate to their combined effect is found from Strömgren's Table 5 to be about 100. The theory assumes that the ionization density throughout the sphere is uniform; the nebula is far from uniform, but it is plausible that the actual value of I should be comparable with that given by the simple theory. In fact, the model gives $I = 60$.

It cannot be claimed that such an idealized model represents the true composition of the nebula. It takes no account of the irregular structure*, nor of the presence of the solid particles which are responsible for the optical continuum radiation of M42. It may however be concluded that the radio emission of the nebula can be explained in terms of a simple thermal model which agrees reasonably well with optical data.

5. *Other features of the Orion region*

(*a*) *The Horsehead group, IC 434, NGC 2023/4, etc.*—This group is situated in the vicinity of the stars ζ Orionis and σ Orionis, to the north of the Great Nebula, and takes its name from a well-known dark marking visible in IC 434.

* Much of the apparent irregularity of M42 may however be due to foreground obscuration.

It is a prominent source at 3·5 m: the peak is situated at R.A. $05^{h}37^{m}\cdot8 \pm 0\cdot3$, Dec. $-2°\,30' \pm 10'$ (1950), near the centre of IC 434. The integrated flux density is $(130 \pm 10) \times 10^{-26}$ w. m.$^{-2}$ (c/s)$^{-1}$, greater than that of M42.

The source is very extended: its half-power contour encloses an area of $3\frac{1}{2}$ square degrees, much greater than the aerial beam, and greater than the visible extent of the nebula, which suggests that part of the object may be hidden from view behind the obscuring matter found in its neighbourhood. The 3·5 m isophotes also suggest that the Horsehead and Great Nebulae may be linked by a ridge of emission.

The Horsehead Nebula has also been observed at 21 cm by Hagen, Lilley and McClain (**15**), using a 1° aerial beam; the flux density is 50×10^{-26} w. m.$^{-2}$ (c/s)$^{-1}$. This appears to be a peak value; if the source has the same angular size at 21 cm and 3·5 m the integrated flux densities at the two wave-lengths are similar, as would be expected if the radiation were thermal. Westerhout (**18**) obtains 95×10^{-26} w. m.$^{-2}$ (c/s)$^{-1}$ at 22 cm.

Assuming for simplicity that the radio source is an optically thin H II region, 500 parsecs from the solar system, and that it is roughly spherical in shape and of uniform electron density N, the 3·5 m results give $N \simeq 10$ cm^{-3} and a mass of about 700 $M_{\odot}$. The emission measure at the centre of this model is 1000, with $\tau = 0\cdot06$: the optical emission measure is given as 4000 (Westerhout and Oort (**19**)). The ionization parameter I (equation (5)) is about 40, which is consistent with excitation of this H II region by ζ Orionis (type B0) and σ Orionis (O9·5).

Such an H II region should appear in absorption at long wave-lengths, and should produce a dip equivalent to at least 40 000 °K on the 15 m records. This dip is not observed, although the sensitivity should be just enough to detect it. If it can be confirmed that the dip is much less than the expected value, it would suggest that some non-thermal emission is received from this direction at long wave-lengths; though it is possible that its source is unconnected with the Horsehead Nebula.

(*b*) *The H II ring of Barnard.*—This H II region is roughly in the form of an elliptical ring, $17° \times 12°$ overall, of which the major axis approximates to the galactic parallel of latitude $-18°$: the angular thickness of the ring is nowhere greater than about 1°. It encloses M42 and the Horsehead complex. The brightest parts of Barnard's Ring are in the following sector, towards the galactic equator: the preceding parts are extremely faint, and are barely visible in photographs by Lower (**22**) in which the brighter parts are heavily over-exposed. The maximum optical emission measure is about 2400 (**19**).

It is probable that the visible ring is the periphery of a three-dimensional structure. This interpretation is supported by observations of 21 cm line radiation by Menon (**23**), who detected at points inside the ring three concentrations of neutral hydrogen with different radial velocities. His results imply the existence of a central concentration of neutral hydrogen, surrounded by an expanding shell; assuming this shell to be spherical, he computes its thickness and inside radius to be 29 pc and 38 pc respectively, and the average density as 3·8 atoms cm^{-3}. The duration of expansion is estimated as a few million years.

The following part of Barnard's Ring is visible as a ridge on the 3·5 m contours, extending between declinations $+4°$ and $-7°$. The resolution is

inadequate to show much detail, but the observations yield values of $\int E.d\theta$, the integral of the emission measure along a declination scan across the ridge. The corresponding optical quantity cannot be accurately evaluated in the absence of isophotes but a very rough estimate gives a result three times the 3·5 m value. At 15 m a trough of absorption coincides in position with the bright parts of the ring: the maximum depth is about 30000 °K, and the estimated value of $\int E.d\theta$ is consistent with the 3·5 m result.

For comparison with the 21 cm results, the 3·5 m observations can be related to a model of a uniform transparent shell. With allowance for aerial smoothing, the thickness of this H II shell is found to be <15 pc: the maximum emission measure is about 1000, leading to an electron density $N \simeq 4$ in the bright portions of the ring. The preceding portions are unobservable at 3·5 m, and for these $N < 1 \cdot 5$.

Application of Strömgren's theory shows that the radiation of stars inside the H II ring is insufficient to produce the observed ionization (e.g. (**23**)). Instead, the radio observations suggest the presence of an H I shell expanding into a relatively stationary medium. At the boundary, a thin shell of H II ionization is formed by collisional excitation: this is most intense in low galactic latitudes, where the density of the surrounding medium is expected to be greatest. Comparison of 21 cm and 3·5 m data shows that in these regions the percentage ionization may be high. Comparison with optical data suggests that there is no appreciable non-thermal component in the 3·5 m radiation from the edge of the shell.

(*c*) *An extended source in Orion—"Orion X".*—The 3·5 m isophotes reveal an extensive area of faint emission covering much of the north-following part of Orion. A scan across the region at declination $-2° 17'$ is shown in Fig. 5, and it is evident that the received radiation is stronger in the centre of the Orion region, at about R.A. 0545—between the peaks at 0538 and 0552, due respectively to the Horsehead Nebula and Barnard's Ring—than outside the region, as at 0500 and 0605. This effect is visible on all scans between declinations $+5°$ and $-7°$. The contributions to the profiles of the other features can be estimated, as indicated in the figure: the separation is of course very rough, but if it is made for each scan an approximate contour diagram of the excess radiation can be built up. The maximum excess temperature is 150 °K, and the angular extent is estimated as 7° in R.A. by 12° in declination. The source will be referred to as "Orion X": it is perhaps associated with Barnard's Ring, but seems to extend outside the north-following boundary of the Ring.

Several observers have reported a faint extended source in this position (Table IV). Though the spectrum has not been measured accurately, there seems to be little variation of flux density with wave-length.

Such a spectrum is consistent with thermal radiation from an optically thin H II region, and this interpretation appears reasonable in view of the presence of faint Hα emission over much of the Orion region. Application of the assumptions previously made (Section 5 (*a*)) to the radio source gives $E \simeq 300$, $N \simeq 2$, and a mass of $10^4 M_{\odot}$. The ionization parameter I of equation (5) is about 100—equivalent to the radiation of sixty stars of type B0. It does not seem feasible to attribute the ionization of this object to the stars actually found in the region, especially as the emission nebulae previously discussed account for the ionizing radiation of several of the brightest stars; and it may be shown

that this deficiency remains if the radio source is supposed to be distinct from the Orion complex, and to lie closer to the solar system. If the object is thermal, its excitation must be collisional, and not due to stellar radiation.

Long wave-length observations, however, cast doubt on the classification of Orion X as a thermal source. It is seen in emission at 7·9 m, at which wave-length a faint H II region would scarcely be prominent as the background brightness temperature in this part of the sky is close to 10 000 °K. Moreover, if Orion X were an H II region it would have an optical depth of about 0·4 at 15 m and would thus produce appreciable absorption. The situation is complicated by the absorption due to Barnard's Ring; however, comparison of 15 m radiation from Orion with that from neighbouring areas in lower galactic latitudes yields no evidence of absorption in Orion X.

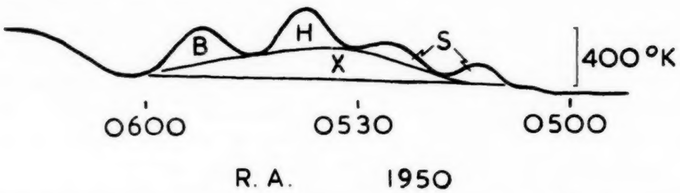

FIG. 5.—*Scan through the Orion region at declination* $-2°\ 17'$ ($\lambda = 3{\cdot}5$ *m*), *showing features:—*
H = *Horsehead Nebula, IC 434, etc.* (*Section* 5 (*a*)).
B = *Barnard's H II ring* (*Section* 5 (*b*)).
X = *Extended object " Orion X "* (*Section* 5 (*c*)).
S = *Discrete sources* (*Mills and Slee* 05–03, 05–06).
The radio brightness increases eastwards from R.A. 0600 *towards the galactic equator.*

TABLE IV

Observations of an extended radio source in Orion " Orion X " (*Section* 5 (*c*))

Observer	Wave-length m	R. A. 1950 h m	Dec. 1950 °	Diameter R.A. × Dec. °	Peak temp. °K	Total Flux 10^{-24} w.m.$^{-2}$ (c/s)$^{-1}$
Blythe (**24**)	7·9	05 40	+1	10 × 5	3000	13
Rishbeth (present observations)	3·5	05 40	−1	7 × 12	150	10
Bolton, Westfold, Stanley and Slee (**25**)	3·0	05 42	0	10 × 5*	—	15
Ko and Kraus (**26**)	1·2	05 42	0	9 × 9	40	(~14)†
Piddington and Trent (**14**)	0·5	05 42	−1	5 × 5	7	(~10)†

* Major axis parallel to galactic equator.
† Author's estimate.

These considerations do not conclusively disprove that Orion X is a thermal source, but they suggest that a non-thermal component may be present. It is therefore interesting that the extent of the radio source is similar to that of the dark nebula charted in the Skalnate Pleso Atlas (**9**) and indicated in Fig. 1. Such concentrations of interstellar dust in the vicinity of bright stars might afford suitable conditions for the production of non-thermal radiation.

(*d*) *Other objects in Orion.*—The emission nebula M43 lies about 30′ to the north of M42, and its dimensions are 42′ × 26′. At 3·5 m it is not resolved from M42, but a northward extension of the contours of the latter

is interpreted as the contribution of M43, which is assigned a flux density of $(20 \pm 5) \times 10^{-26}$ w. m.$^{-2}$ (c/s)$^{-1}$, a quarter of that of M42. With simplifying assumptions as before, the average electron density of M43 is found to be 25 cm^{-3}, the mass of order $50 M_{\odot}$, and the central emission measure 3000. The last figure seems too low for an object as bright as M43, but the total ionization gives $I \simeq 20$, quite consistent with excitation by the B1 star 42 Orionis. The optical brightness of M43 shows a rapid radial decrease from the central peak, and so the uniform model used to derive the above figures is not very appropriate, and gives order-of-magnitude estimates only.

Amongst the faint H II regions in Orion is a group a few degrees to the west of M42. Some of these nebulae are comparable in extent to the 3·5 m aerial beamwidth. With assumed emission measures of order 500, their flux densities should be about 10×10^{-26} w. m.$^{-2}$ (c/s)$^{-1}$, great enough for detection. A source of flux density of 14×10^{-26} w. m.$^{-2}$ (c/s)$^{-1}$, at R.A. 0513, Dec. $-2°$, may be identified with one H II region; whilst on examination of the isophotes the nebula at 0512, $-5°$ can be assigned the very small flux density of 3×10^{-26} w. m.$^{-2}$ (c/s)$^{-1}$, corresponding to an increase of 50° K.

A weak source at 0540, $-5\frac{1}{2}°$ coincides with a mass of filamentary structures prominent on the Palomar Sky Survey red-sensitive plate but barely discernible on the corresponding blue plate: this object is two degrees east of M42. The remaining discrete sources in the region do not seem to be associated with optical features and most of them are doubtless merely aligned by chance with the Orion complex.

A 15 m source is thought to exist at R.A. 0550, Dec. $-7°$ (see Fig. 2), but requires confirmation. It lies near a bright part of Barnard's Ring. If real, this source is non-thermal, on account of its high brightness temperature.

3·5 m records of the λ Orionis emission region, which is outside the area covered by Fig. 1, have also been examined. A weak extended source is present, but it does not correspond well to the optical features. The 3·5 m emission measure is about 800 at R.A. 0520, Dec. $+10°$, and 300 at 0528, $+10°$ (1950). The optical emission measure near the latter position is 3100 (**20**).

6. *Conclusions.*—Several emission nebulae in the Orion region have been observed at a wave-length of 3·5 m, and comparison with optical data indicates that the radio emission is thermal. In the case of M42, it is found that a simple thermal model can be made to agree with a variety of radio and optical observations. It is suggested, however, that the Horsehead group, IC 434 etc., may emit a non-thermal component of radiation at the longest wave-lengths.

In several cases the radio emission measures are less than the optical values. A similar result was found by the author for H II regions in the Vela-Puppis region (**8**). On the other hand, good agreement between optical and radio data has been found by previous observers, e.g. by Haddock (**1**) for the bright galactic nebulae in Sagittarius, and for the Rosette Nebula by Mills, Little and Sheridan (**11**). Many of the author's observations refer to very faint objects and the differences can largely be attributed to selection of the optical data; the optical emission measures of a nebula apply to the brightest parts, the radio observations to averages over finite areas.

A large faint extended source, referred to as Orion X, is detected in the region. Most of the radio data suggest that it may be an H II region with collisional excitation; but long wave-length observations, though not conclusive, favour

a non-thermal origin. The position and extent of this object suggest some correspondence to the extensive dark clouds in Orion, and to the H II ring of Barnard.

7. *Acknowledgments.*—The author wishes to express his thanks to Dr J. L. Pawsey, Mr B. Y. Mills and Mr C. A. Shain of the Radiophysics Laboratory, Sydney, for their guidance; and to Mr Shain for assistance with the observations at 15 m. He is also grateful for discussions with Dr F. G. Smith and other members of the Cavendish Laboratory.

The work described in this paper was carried out during the tenure of a Research Studentship awarded jointly by the Commonwealth Scientific and Industrial Research Organization in Australia and the Department of Scientific and Industrial Research in Great Britain.

Cavendish Laboratory,
Cambridge:
1958 *July* 29.

References

(1) F. T. Haddock, I.A.U. Symposium No. IV, p. 192, 1957, (C.U.P.).
(2) C. L. Seeger, G. Westerhout and H. C. van de Hulst, *B.A.N.*, **13,** 89, 1956.
(3) J. H. Piddington and G. H. Trent, *Aust. J. Phys.*, **9,** 481, 1956.
(4) J.-F. Denisse, J. Lequeux and E. Le Roux, *C.R. Acad. Sci. Paris*, **244,** 3030, 1957.
(5) B. Y. Mills, A. G. Little, K. V. Sheridan, and O. B. Slee, *Proc. I.R.E.*, **46,** 67, 1958.
(6) C. A. Shain, *Proc. I.R.E.*, **46,** 85, 1958.
(7) B. Y. Mills and O. B. Slee, *Aust. J. Phys.*, **10,** 162, 1957.
(8) H. Rishbeth, *Aust. J. Phys.*, **11,** 1958 (in the press).
(9) A. Becvar, " Atlas Coeli Skalnate Pleso II " (*Prirodovedecke Vydavatelstvi*: Prague, 1951).
(10) J. H. Piddington, *M.N.*, **111,** 45, 1951.
(11) B. Y. Mills, A. G. Little and K. V. Sheridan, *Aust. J. Phys.*, **9,** 218, 1956.
(12) B. Strömgren, *Ap. J.*, **89,** 526, 1939.
(13) N. N. Michelson, *Bull. Pulkovo. Astron. Obs.*, **19,** 69, 1953.
(14) J. H. Piddington and G. H. Trent, *Aust. J. Phys.*, **9,** 74, 1956.
(15) J. P. Hagen, A. E. Lilley and E. F. McClain, *Ap. J.*, **122,** 361, 1955.
(16) F. T. Haddock, C. H. Mayer and R. M. Sloanaker, *Nature*, **174,** 176, 1954.
(17) N. L. Kaidanovski, N. S. Kardashev and I. S. Shklovski, *Dokl. Akad. Nauk. U.S.S.R.*, **104,** 517, 1955.
(18) G. Westerhout, *B.A.N.*, **14,** 215, 1958.
(19) G. Westerhout and J. H. Oort, *B.A.N.*, **11,** 323, 1951.
(20) H. M. Johnson, *Ap. J.*, **118,** 370, 1953.
(21) D. E. Osterbrock, *Ap. J.*, **122,** 235, 1955.
(22) H. A. Lower, *Ap. J.*, **89,** 137, 1939.
(23) T. K. Menon, *Ap. J.*, **127,** 28, 1958; and Doctoral Thesis, Harvard University, Chapter IV, 1956.
(24) J. H. Blythe, *M.N.*, **117,** 652, 1957.
(25) J. G. Bolton, K. C. Westfold, G. J. Stanley and O. B. Slee, *Aust. J. Phys.*, **7,** 96, 1954.
(26) H. C. Ko and J. D. Kraus, Rep. Ohio State University Radio Obs. No. 4, 1955.

IMPROVED MEASUREMENTS OF THE POSITIONS OF 17 INTENSE RADIO STARS

B. Elsmore

(Communicated by M. Ryle)

(Received 1958 July 28)

Summary

Some observations at a wave-length of 1·9 m, which have been aimed at improving the accuracy of the declinations of the sources, are based on the times of transit across two interferometers having inclined axes. The method of using the Cambridge Radio Telescope in this way to form a crossed axis interferometer is described, and the accurate positions of 17 sources are given. The positions derived in the third Cambridge Survey are included for comparison.

1. *Introduction.*—The Cambridge Radio Telescope (**1**) has recently been used at a wave-length of 1·9 m for a new survey of radio stars. A detailed account of this survey, which will be referred to as the third Cambridge Survey (3C survey) is to be published shortly (**2**) but as some preliminary results are available it was thought worth while to check the positions of a number of the intense stars by an independent method. The present paper describes this method and gives the accurate positions of 17 sources.

In the past, determinations of the times of transit have provided measurements of right ascension more accurate than those of declination. The present observations, which are aimed at improving the accuracy of the declinations, are based on measurements of the times of transit across the principal planes of two interferometers having inclined axes (**3**). The method of using the Cambridge radio telescope in this way to form a crossed axis interferometer is described in the next section, and the results and a discussion are given in Section 3.

2. *The methods of observation.*—The declination of each radio star was determined from two observations at a wave-length of 1·9 m, taken on successive days, using first one diagonal pair of aerials of the Cambridge radio telescope and then the other. The pairs of aerials were connected in turn to a phase-switching receiver (**4**) to comprise two separate interferometers with their axes inclined at a small angle (10°5′), as shown in Fig. 1. The difference between the times of transit T_1 and T_2 in Fig. 2 across the two fictitious meridians is a measure of declination; the accuracy of the measurement is greatest for sources near the zenith Z and is least for sources near the horizon.

The reception polar diagram of the individual aerials limits the observation to an interval near the central meridian transit, indicated by T_0 in Figs. 2 and 3, which corresponds to axis O in Fig. 1. The transit T_1 may be derived, however, by subtracting from the measured time t_1 in Fig. 3 (*b*) an integral number N of fringe periods; the number N is derived from a knowledge of the approximate position of the source.

The periodicity of the interference fringes (shown dotted in Fig. 3 (*b*)) depends upon the mean wave-length, which is difficult to measure precisely

when the receiver pass-band is wide and possibly asymmetric, and errors in this measurement become serious when N is large. However, by inserting between one aerial and the receiver an additional cable, whose electrical length may be exactly determined, the fictitious meridian may be moved through a known angle to such a position that N is small for any given source; it then becomes a small circle parallel to the original meridian. In the example shown

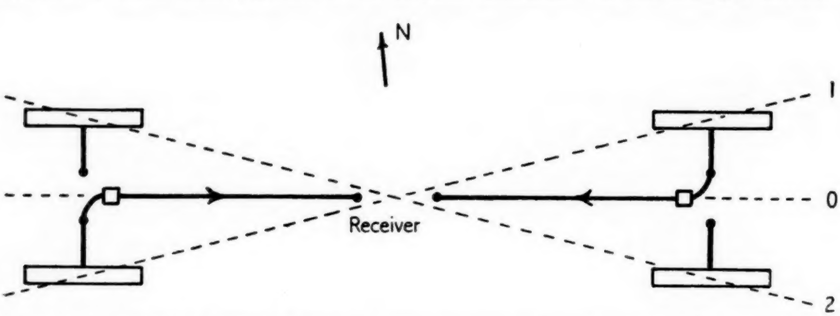

FIG. 1.—*Showing the Cambridge Radio Telescope connected to form two separate interferometers with axes 1 and 2.*

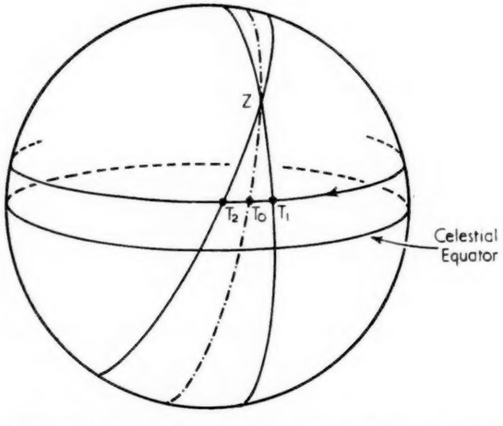

FIG. 2.—*Celestial sphere illustrating the fictitious meridians of a crossed axis interferometer. The times of transit of a star are T_1 and T_2.*

graphically in Fig. 3 (*b*), an additional cable of electrical length three nominal wave-lengths (3 × 188 cm), inserted between the SW aerial and the receiver, will move the collimation plane from T_1 to a measured point near t_1; similarly, in Fig. 3 (*c*), T_2 will move to near t_2 when the additional cable is inserted in the path between the SE aerial and the receiver. In the interval between t_1 and t_2 any small difference between the mean wave-length and the nominal wave-length is now unimportant.

In order to calibrate the system and to ensure that there is no difference in the phase angles introduced by two pre-amplifiers, a c.w. signal at the nominal wave-length of the receiver is passed down two equal cables and into the pre-amplifiers, the outputs of which are connected through equal cables

to the phase-switching receiver as in Fig. 4. An additional cable, whose length is determined by the declination of the source to be observed as described above, is inserted into one path near the receiver and adjustments are made by the addition of further small lengths of cable so that the two paths differ by a predetermined exact number of wave-lengths. The phase angle of the individual aerials is determined from observations of radio stars which have been identified with optical objects and whose positions are accurately known.

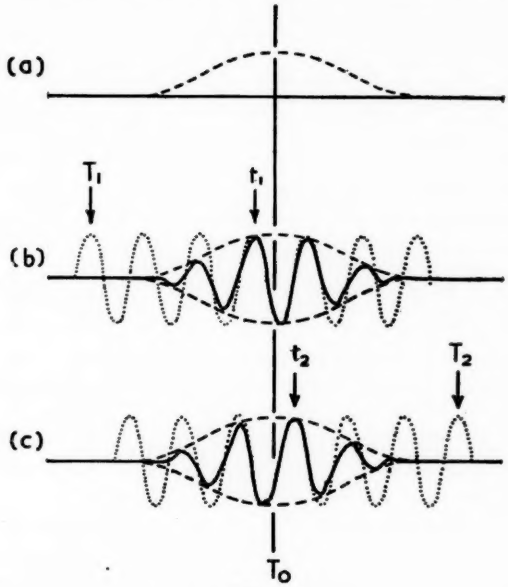

FIG. 3.

(*a*) *The reception polar diagram of the individual aerials.*

(*b*) *The full line indicates the recorder output produced by the transit of a star across the NE/SW interferometer. The dotted line shows the maxima and minima and T_1 is the time of transit across the fictitious meridian.* (*Time increases towards the right.*)

(*c*) *T_2 is the time of transit across the fictitious meridian of the NW/SE interferometer.*

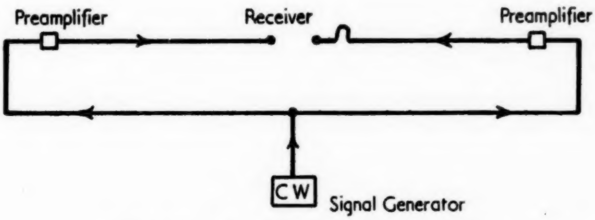

FIG. 4.—*The arrangement used for calibration.*

The times t_1, t_2 may be determined accurately from the times of zero deflection; the output of the receiver is therefore applied to a photographic recording system, designed to operate only near the times of crossovers and to record on 35 mm film moving at a speed of one inch in six seconds. Fig. 5 shows a section of film produced during one of the transits of 2C.34.

The right ascension of each source is derived from the mean of the times of transit across the two skewed axis interferometers.

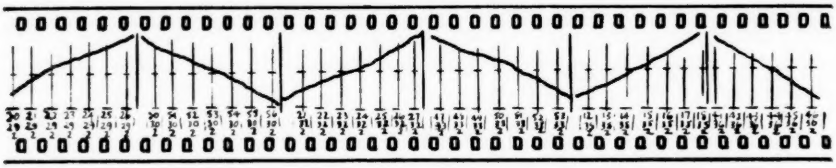

FIG. 5.—*A part of the film produced by the photographic recorder, during one of the transits of 2C.34.*

3. *Results and discussion.*—Errors in position may arise from four causes: (i) instrumental effects; (ii) limitation of reading accuracy (i.e. signal-to-noise effects); (iii) confusion effects due to weak adjacent sources; and (iv) refraction in the terrestrial ionosphere and atmosphere.

(i) *Instrumental effects.*—The present determination of the declination of a source depends upon measurements of the times of transit, in contrast to the method used in the 2C and 3C surveys, which required measurements of the relative amplitudes of the records on successive days. Measurements have shown that the overall phase stability of the aerials, pre-amplifiers, cables and receiver remains constant to within 10°, corresponding to 5 cm of path difference, over periods of several months. The overall gain stability has been found to vary from day to day by up to 15 per cent, particularly in the presence of heavy rain or frost on the aerial feeder system.

The errors in declination caused by such gain variations in the 2C and 3C surveys are likely to be greater than those caused by phase variations in the present method. For intense sources, for which the instrumental effects are more severe than those caused by the confusion effects of weak adjacent sources (see (iii) below), the new method, therefore, has considerable advantages.

The apparent positions of the intense sources in the constellations of Taurus, Virgo, Cygnus and Cassiopeia (I.A.U. Nos. 05N2A, 12N1A, 19N4A and 23N5A respectively) were compared with the corresponding positions of the optical objects and were used to derive the collimation error of the system in declination. This error $3'{\cdot}0$ ($\pm 1'{\cdot}3$) was then used to correct the observed positions of the other sources.

(ii) *Limitation of reading accuracy, and noise fluctuations.*—The probable errors quoted arise mainly from the noise fluctuations and were derived from the scatter of the times of at least eight crossovers, obtained during each individual transit observation, from which the time T across the fictitious meridian was derived. Many of the transit observations were repeated several times.

(iii) *Confusion effects.*—The errors due to the presence of weak sources in the reception pattern can be computed statistically from the spatial distribution of sources. Some indication of the extent of these confusion effects is also obtained from the scatter of the times of crossovers as in (ii) above, and these effects are included in the quoted errors of the less intense sources.

(iv) *Ionospheric refraction.*—The refraction of the radio waves in the terrestrial ionosphere has been investigated by Smith (**3**), who showed that the error in right ascension is a maximum at dawn and dusk, but the error at this wave-length is unlikely to exceed 0′·15 of arc.

The error in declination may be larger but is unlikely to exceed 0′·5 of arc for zenith angles less than 60°.

Since these errors are less than those discussed above no corrections for refraction have been applied.

The positions have been corrected for precession, nutation, and aberration and refer to epoch 1950·0, and are listed with the 2C survey (**5**) numbers.

TABLE I

Number	R.A.	Error	Dec.	Error	Δ R.A.	Approximate flux density	Notes
	h m s	s	° ′	′	s	10^{-26} MKS	
2C 34	00 22 38·3	3	63 53	3	16·2	*110*	IAU 00N6A
	00 22 37	*2*	*63 52*	*2*			(*a*) SN 1572
94	01 06 12·7	1·0	13 02	4·3	3·2	*58*	
	01 06 13	*3·0*	*13 04*	*9*			
379	04 15 00·3	1·5	37 51	2·5	4·9	*60*	
	04 15 05	*2·0*	*37 50*	*4*			
404	04 33 53·5	1·5	29 37	3·0	4·1	*204*	IAU 04N3A
	04 33 55	*4·0*	*29 34*	*3*			
440	05 01 17·4	2·0	38 03	2·8	5·0	*85*	
	05 01 21	*4·0*	*38 03*	*8*			
724	08 10 00·9	1·5	48 23	2·2	7·0	*95*	IAU 08N4A
	08 10 03	*3·0*	*48 22*	*3*			
805	09 17 52·1	2·0	45 53·5	2·0	6·4	*42*	IAU 09N4A
	09 17 54	*2·0*	*45 52*	*2*			(*b*)
855	09 58 56·3	3·0	29 04	2·8	4·1	*30*	(*b*)
	09 58 56	*7·0*	*29 00*	*10·0*			
1175	14 09 32·0	2·0	52 25	3·4	8·4	*74*	IAU 14N5A
	14 09 32	*3·0*	*52 26*	*5·0*			
1185	14 16 41·2	2·0	06 46·5	4·5	3·2	*63*	(*c*)
	14 16 40	*8·0*	*06 46*	*7·0*			
1402	16 26 56·2	1·8	39 39·5	2·0	5·1	*49*	IAU 16N4A
	16 26 54	*5·0*	*39 38*	*3·0*			(*d*) NGC 6166
1432	16 48 42·1	1·5	05 04	6·3	3·1	*300*	IAU 16N0A
	16 48 43	*5·0*	*05 10*	*10·0*			
1473	17 17 59·6	1·8	−00 57	6·8	3·1	*180*	
	17 17 59	*3·0*	*−00 50*	*6·0*			
1569	18 28 16·5	3·0	48 42	2·5	7·0	*70*	
	18 28 12	*3·0*	*48 43*	*3·0*			
1686	20 12 19·8	2·0	23 24	3·6	3·6	*102*	(*b*)
	20 12 17	*2·0*	*23 26*	*5·0*			
1775	21 21 30·7	3·0	24 49·5	4·2	3·8	*62*	(*c*)
	21 21 31	*4·0*	*24 48*	*7*			
1870	22 43 33·9	3·0	39 19·0	2·8	5·1	*50*	
	22 43 30·0	*5·0*	*39 21·0*	*3·0*			

Notes to Table I

(*a*) Supernova of 1572 (**6**).

(*b*) 2C position changed by a R.A. lobe.

(*c*) 2C position changed by a Dec. lobe.

(*d*) IAU designation incorrect. Should be 16N3A.

Mr D. O. Edge has kindly made available some preliminary positions obtained in the 3C survey by the alternative and largely independent method, and these are included in Table I for purposes of comparison; they are given in italics beneath the results of the present observations. His measurements of flux density are also included in column 7 in units 10^{-26} watts m^{-2} $(c/s)^{-1}$.

Since the axis of the instrument is not exactly east–west, the area defining the probable error of a source has the form of a parallelogram, which may be derived for each source by reference to Fig. 6. The inclination of the

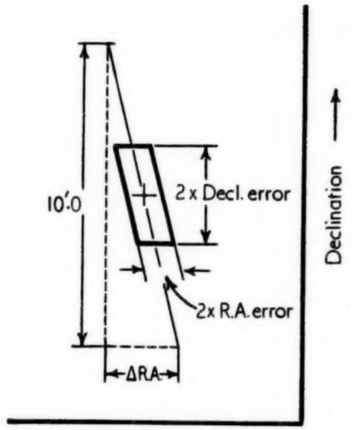

FIG. 6.—*The parallelogram defining the probable errors of the radio sources.*

parallelogram may be derived from the value given in column 6 in the table, Δ R.A. which is the change in R.A. for a change of 10'·0 of arc in declination.

Possible identifications both with optical objects and with radio sources found in recent surveys are indicated in the final column.

Acknowledgments.—The author is indebted to Mr D. O. Edge for generously providing the positions and flux densities from the 3C survey, prior to publication. He also wishes to thank Dr J. R. Shakeshaft for kindly reading and commenting on this paper, and Mr Ryle, without whose help and suggestions these observations could not have been undertaken.

Mullard Radio Astronomy Observatory,
Cavendish Laboratory,
Cambridge:
1958 *July* 8.

References

(1) M. Ryle and A. Hewish, *Mem. R.A.S.*, **67**, 97, 1955.
(2) D. O. Edge, J. R. Shakeshaft, S. Archer, J. E. Baldwin and W. B. McAdam (in preparation).
(3) F. G. Smith, *M.N.*, **112**, 497, 1952.
(4) M. Ryle, *Proc. Roy. Soc.* A, **211**, 351, 1952.
(5) J. R. Shakeshaft, M. Ryle, J. E. Baldwin, B. Elsmore and J. H. Thomson, *Mem. R.A.S.*, **67**, 106, 1955.
(6) J. E. Baldwin and D. O. Edge, *The Observatory*, **77**, 139, 1957.

RADIAL VELOCITIES OF FUNDAMENTAL SOUTHERN STARS

William Buscombe and Pamela M. Morris

(Received 1958 July 3)

Summary

Newly determined radial velocities are given for 12 standard-velocity stars and 63 other bright stars south of the equator. The plates, taken with the three-prism Cassegrain spectrograph of the 30-inch reflector, have a dispersion of 36 A/mm at Hγ. The Stromlo velocities of the standard-velocity stars were found to agree satisfactorily with measurements at other observatories on the Lick system. Velocity residuals for individual spectral lines are discussed.

The stars on the programme have been chosen from the FK3 and N30 position catalogues. At least three spectrograms of each star have been measured. A luminosity class is given on the revised Yerkes system for stars of early type. 29 new constant velocities are announced, as well as 18 whose variability has been detected for the first time. Observations have been resumed on 15 stars previously known to have variable velocity.

Selection of programme stars.—In 1954 June, when repeated tests on I.A.U. standard-velocity stars showed that the performance of the three-prism Cassegrain spectrograph was reliable for velocity determinations, regular observing was commenced on stars from two principal lists. The first included stars of early type in the region of the Scorpio–Centaurus cluster, and the other was planned for observations during the spring and summer, when the cluster cannot be observed. As the practical limiting magnitude is around 7·0 (photographic), stars in the standard catalogues FK3 (1) and N30 (2) were chosen, for which accurate proper motions are available, but reliable radial velocities lacking. From right ascensions 17 through 0 to 8 hours, south of declination $+20^\circ$, about 300 stars brighter than visual magnitude 6·5 were selected, for which either no velocity has been published, or else the velocity remains uncertain, i.e. quality *c*, *d*, or *e* in the *General Catalogue of Stellar Radial Velocities* (3).

Standard velocity stars.—The observing experience of the initial test period showed that for an observatory as far south as Mt Stromlo (latitude -35°) the standard-velocity stars recommended to Commission 30 of the I.A.U. (4) are not sufficient. About 20 additional stars south of declination -30° were provisionally selected from those with velocities of quality *a* in the Radial Velocity Catalogue, and consistent agreement between Lick and Cape observations. The selection was made in such a way that at least one of these stars could be observed at any time of the night. Several of these have been observed on a significant number of nights with the stars of the N30 programme, and the measures are summarized in the first part of Table I.

Observation and measurement.—Details of the observing routine at the telescope, and processing in the dark-room, have been outlined in an earlier communication (5) to the Society. To eliminate the curvature of the spectral lines on the plates, a curved slit has been in use since 1956 August. All the measurements reported in the present paper have been made with Zeiss Abbe

comparators. The emission lines of the iron arc comparison source have been measured so close to the tips adjacent to the star spectrum that corrections for curvature of the lines on the older spectrograms were negligible. 15 to 20 unblended lines from this source are measured on each plate as a precise scale of wavelengths. An interpolation curve is drawn showing the deviations from the standard settings computed by the Cornu formula for the prismatic dispersion. The derived velocities, corrected to the Sun, are listed in Tables I and II. The results are quoted only to the nearest integral kilometre per second, as the decimal fractions are considerably below the limiting accuracy for real significance. The various participants in this programme hope to announce further results from time to time, when sufficient data are available for other groups of stars.

Wavelengths for stellar lines.—Wavelengths for stellar absorption lines (denoted in Table III by the letter P), which Petrie (**6**) recommended after his studies with the single-prism dispersion of 30 A/mm at $H\gamma$, were used as a basis for the reductions. For each line the residuals from the mean plate velocities have been examined. Among A stars in particular, no standards have been selected for which the consistency of the average velocities for all lines on the plate could be verified. The mean velocity residuals for stars of each range of the later spectral types are of the same order as those reported by Wright (**7**) and Evans (**8**). Measurements of a particular line were considered to deviate *significantly* if the algebraic mean residual ΔV_λ of its Doppler velocity from the mean velocity $\bar{V}$ for all lines on a plate, in a group of plates of the same spectral type, exceeds three times the standard error $\sigma_{\Delta V}$ of the mean residual. The wavelengths of lines which consistently give velocities in closer agreement with the simple mean for a plate are listed in the middle column of Table III. While a few of the lines recommended by Petrie give slight systematic deviations from the average plate velocities, some additional lines seem consistently reliable on the Stromlo spectrograms.

TABLE I

Stars with constant velocities

Column

1 Number in Henry Draper Catalogue (*Harvard Annals*, 91–99).

2 Constellation designation. For southern stars lacking a Greek Bayer letter, the Gould number is quoted from Uranometria Argentina (*Cordoba Resultados*, **1**).

3 Visual apparent magnitude, from the revised Harvard Photometry (*H.A.*, **50**).

4 Spectral type, from the Henry Draper Catalogue.

5 Mean radial velocity relative to the Sun, from Mt Stromlo spectrograms, to nearest integral kilometre per second.

6 Probable error of the mean, from deviations of individual plate velocities, in km/sec.

7 Number of plates measured.

8 Revised spectral type on MK system, determined from Mt Stromlo spectrograms by M. L. Woods (*Mem. Commonwealth Obs.*, **3** (12), 1955), A. de Vaucouleurs (*M.N.*, **117**, 449, 1957) or P. M. Morris (unpublished).

9 Mean radial velocity from R. E. Wilson's *General Catalogue of Radial Velocities* (ref. **3**). The lower-case letters denote quality by internal consistency of the published velocity measures from individual plates, as follows:—

a Probable error of mean less than 0·9 km/sec from at least 5 plates
b ,, ,, ,, ,, ,, ,, 2·0 ,, ,, ,, ,, 3 plates
c ,, ,, ,, ,, ,, ,, 5·0 ,, ,, ,, ,, 2 plates
d ,, ,, ,, ,, ,, ,, 10·0 ,, ,, ,, ,, 1 plate
e Large probable errors for single plates of early-type stars.

The succeeding digit indicates the number of plates measured previously at the Lick Observatory (designated by the capital letter L).

TABLE I (*continued*)

Column

10 Notes, including the suspicion of variable velocity when the probable error of the mean velocity, multiplied by $\sqrt{n}$, exceeds the average probable error for the scatter of velocity measures from individual lines on the various plates.

(1) HD	(2) Star	(3) m_V	(4) Sp.	(5) $\bar{V}$ km/s	(6) p.e. ±	(7) n	(8) Sp. Type	(9) GCRV	(10) Notes
4128	β Cet	2·24	K0	+13	0·2	25	G8 III	+13	
20794	82 Eri	4·30	G5	+89	0·2	7	G5 V	+87	
36079	β Lep	2·96	G0	−14	0·5	9	G2 II	−14	
81797	α Hya	2·16	K2	−3	0·4	6	K3 III	−4	
108903	γ^1 Cru	1·61	M2	+22	0·4	14	M3 II	+21	
109379	β Crv	2·84	G5	−8	0·3	5	G5 II	−8	
150798	α TrA	1·88	K2	−3	0·3	14	K2 III	−4	
168454	δ Sgr	2·84	K0	−20	0·2	19	K2 III	−20	
196171	α Ind	3·21	K0	−1	0·6	5	K0 III	−1	
203608	γ Pav	4·30	F8	−30	0·6	3	F5 V	−30	
204867	β Aqr	3·07	G0	+6	0·6	7	G0 Ib	+7	
223647	γ^1 Oct	5·10	G5	+12	0·5	4	G5 III	+14	
4211	λ^2 Scl	5·97	K0	+24	0·6	4			
6192	ω Phe	6·00	K0	+13	0·5	3			
8498	109G Scl	5·82	K5	−16	0·6	3			
9896	12G Hyi	6·12	F2	−19	0·3	3	F2 V		
10042	14G Hyi	6·06	G5	−1	0·7	5			
13940	135G Phe	5·86	K0	+14	1·7	4			Var?
15975	λ^1 For	5·88	K0	+13	0·5	4			
22789	τ For	6·08	A0	+39	1·8	4	A0 V		
24626	ι Eri	5·12	B5	+25	1·0	5	B6 IV	+18*c*7L	
29435	253G Eri	6·29	B8	+15	1·7	5	B9 IV–V		
30422	268G Eri	5·97	A2	+19	1·3	5	A3 III–IV		
34172	ξ Men	5·85	K0	−5	0·6	3			
34868	12G Col	5·75	A0	+18	1·1	5	A0 IV		
40953	κ Men	5·56	B8	+10	2·4	5	B9·5 V		
51557	ι Vol	5·52	B8	+19	1·9	4	B6 IV	+18*c*5L	
183806	63G Tel	5·87	A0	−8	1·7	4	Ap		
188097	76G Pav	5·82	A3	−10	0·9	5	Am		
194215	296G Sgr	5·97	K0	−14	1·3	5			Var?
199623	8G Ind	5·88	F5	−21	0·5	4	F6 V		
200073	43G Mic	5·94	K0	+7	1·5	3			Suspected subdwarf
203949	68G Mic	5·69	K0	−76	1·3	5			
207229	54G Ind	5·65	K0	−6	0·3	3		−1*d*1L	
208741	66G Oct	5·91	F2	+7	1·5	3	F3 III		Var?
216437	ρ Ind	6·14	G0	−3	0·6	4			
219077	23G Tuc	6·24	G0	−26	1·4	3			
219765	τ Oct	5·56	K0	+31	0·9	5			
220096	11G Scl	5·81	G5	+13	1·1	5			
221420	83G Oct	5·78	K0	+26	0·8	3			
222820	36G Tuc	5·66	K5	−13	1·5	3			
223352	δ Scl	4·64	A0	+6	2·1	5	A0 V	+14*d*5L	
224022	27G Phe	6·01	F8	−10	0·5	4	F8 V		
224361	42G Tuc	6·04	A2	−13	2·7	3	A2p		
224834	τ Phe	5·66	K0	+8	0·4	4			

TABLE II

Stars with variable velocity

Column
1 Henry Draper number and constellation designation } As in Table I.
2 Visual magnitude and HD spectral type }
3 Julian date and decimal for time of mid-exposure.
4 Radial velocity relative to the Sun.
5 Internal probable error of deviations from the mean velocity for the plate to velocities for the individual lines.
6 Revised spectral type } As in Table I, cols. 8–9.
7 Mean radial velocity in Catalogue }
8 Notes, including references to earlier publications from other observatories quoting individual plate velocities.

(1) HD Star	(2) m_V Sp	(3) JD 243....	(4) V km/s	(5) p.e. ±	(6) Sp	(7) GCRV	(8) Notes
2884	4·52	5025·072	+33	4·8	B8 V	+10c7L	*Lick Publ.*, **16**.
β′ Tuc	B9	5315·277	+12	3·3			
		6036·276	+36	4·0			
		6094·157	+ 9	6·0			
4293	6·00	4966·211	+ 6	5·0	A7 III	+ 1c5C	*M.N.*, **117**.
70G Phe	A5	4968·229	+26	2·5			Under observation
		5325·262	+62	6·5			for orbit
		5716·175	+26	2·9			
		6035·270	+40	2·0			
		6120·093	−17	2·1			
		6144·016	−40	2·2			
		6150·970	−27	2·7			
		6154·969	−36	2·6			
7312	5·91	4966·244	+52	2·7	A7 III		Under observation
102G Scl	A5	4968·258	+39	1·5			for orbit
		5000·188	− 2	2·3			
		5347·206	+31	1·8			
		5362·164	+20	2·0			
		5745·132	+24	4·3			
		5760·073	−23	5·3			
		5776·022	+13	3·1			
		5812·954	+15	4·2			
		5825·938	−34	3·6			
		6036·295	+ 6	3·5			
		6067·245	− 2	2·9			
		6086·181	+42	3·3			
		6120·117	−21	2·0			
		6125·140	−21	3·1			
		6151·000	+12	2·5			
10800	5·88	5357·203	− 8	1·6			
3G Oct	G0	6151·034	−14	2·3			
		6182·974	+ 6	0·8			
15233	5·47	5001·206	−24	2·2	F2 IIIp	+27c5L	*Lick Publ.*, **16**.
λ Hor	F2	5325·334	−31	3·3			
		5711·249	−34	5·2			

TABLE II (*continued*)

(1) HD Star	(2) m_v Sp	(3) JD 243	(4) V km/s	(5) p.e. ±	(6) Sp	(7) GCRV	(8) Notes
20121	5·92	5414·111	+ 1	1·9	F6 III	+34c4L	*Lick Bull.*, **15**.
71G Eri	F2	6125·173	+ 9	2·0			Visual binary
		6151·067	− 5	3·3			
		6176·010	+ 6	2·9			
		6178·005	+ 4	2·3			
21722	5·96	5357·271	− 2	1·4	F5 IV		
59G Hyi	F2	6115·214	+20	1·3			
		6125·208	+16	1·8			
		6151·116	+14	1·9			
		6183·017	+10	1·2			
21981	6·01	5357·283	−20	3·2	A2 V		
44G Hor	A0	5414·130	−18	4·3			
		5741·231	− 1	3·1			
		5760·186	−17	4·3			
		6094·236	− 5	3·3			
22231	5·60	5385·217	+30	1·9		+40c2L	*Lick Bull.*, **15**.
45G Hor	K0	5742·247	+31	1·1			
		6095·238	+40	1·5			
		6126·218	+44	1·5			
		6148·120	+36	0·9			
		6177·063	+35	2·9			
24706	5·77	5348·317	+ 3	2·2			
55G Hor	K0	5361·254	+ 9	1·0			
		6128·205	0	1·4			
		6154·133	− 7	1·2			
		6156·082	0	1·3			
		6212·969	− 3	0·9			
		6216·010	− 2	2·5			
41843	5·72	5025·269	+28	1·6	A1:V		
74G Col	A0	5800·167	+ 5	1·4			
		6150·219	− 7	3·3			
		6151·206	+ 9	3·3			
		6176·132	− 2	2·7			
46936	5·57	5778·256	+ 7	3·8	B8 V	+42c3L	*Lick Publ.*, **16**.
50G CMa	B9	5809·146	+31	8·6			
		6176·157	+33	7·4			
		6178·134	+28	5·2			
		6262·915	− 5	8·8			
54732	5·98	5062·256	+15	1·0			
28G Car	G5	6176·197	+38	2·5			
		6262·949	+35	2·0			
59635	5·41	5826·171	+29	5·7	B3 III	+26c4L	*Lick Publ.*, **16**.
98G Pup	B8	6176·227	+40	4·3			
		6178·199	+20	4·6			
		6262·976	− 5	4·4			

TABLE II (*continued*)

(1) HD Star	(2) m_v Sp	(3) JD 243	(4) *V* km/s	(5) p.e. ±	(6) Sp	(7) GCRV	(8) Notes
67523	2·88	5585·880	+40·5	0·9		+ 47*a*	*Lick Publ.*, **16**.
ρ Pup	F5	5585·897	+39·2	0·9			*Cape Ann.*, **10** (8).
		5585·928	+42·7	1·1			*Ap. J.*, **124**.
		5585·954	+46·3	0·7			*Observatory*, **77**.
		5585·976	+48·7	1·2			
		5586·001	+42·0	1·0			
		5586·022	+44·3	1·0			
		5778·170	+47·3	1·2			
		5778·185	+41·7	1·7			
		5778·205	+42·5	1·4			
		5778·222	+45·0	1·1			
		5778·244	+47·8	1·6			
		5778·267	+52·5	1·9			
173117	5·76	5612·212	+34	2·0	B5 V		
94G Sgr	B8	5985·171	− 6	6·9			
		5987·173	+48	4·0			
		5997·167	+15	3·6			
175510	5·03	5270·166	+10	4·6	B9 III	− 6*d*5L	*Lick Publ.*, **16**.
λ Tel	B9	5360·919	− 9	6·4			
		5586·274	+18	7·8			
188899	5·05	5265·160	− 2	3·6	A2 IV	− 4*c*8LY	*Lick Publ.*, **16**.
61 Sgr	A0	5293·135	+ 2	3·3			*Yerkes Publ.*, **7**.
		5647·133	+64	6·1			
		6036·084	− 2	2·5			
		6083·967	+12	3·3			
189198	5·80	4967·046	0	6·2	A7 IIIp	− 6*c*4C	*M.N.*, **117**.
259G Sgr	A5	5591·328	+37	3·8			Under observation
		5612·280	+34	4·1			for orbit.
		5646·194	+24	3·2			
		5715·990	+13	5·8			
		5995·202	− 5	2·5			
		6035·118	−23	1·7			
		6038·097	−12	1·6			
		6067·610	+20	2·5			
		6083·987	+15	2·6			
		6085·946	−28	2·5			
		6092·006	+16	2·8			
193571	5·64	5000·937	−16	2·0	A1 V	−17*c*3L	*Lick Bull.*, **15**.
κ′ Sgr	A0	5298·126	+ 1	2·1			
		5734·015	−14	2·4			
		5741·929	−28	2·9			
199443	5·95	4974·029	+ 7	3·2	A5 IIIp		
64G Cap	A3	4999·961	−15	2·5			
		5028·917	−20	3·4			
		5290·199	+24	3·4			
		5293·179	+25	3·9			
		5987·262	+16	3·0			

TABLE II (*continued*)

(1) HD Star	(2) m_v Sp	(3) JD 243....	(4) V km/s	(5) p.e. ±	(6) Sp	(7) GCRV	(8) Notes
203705	5·54	4974·078	+ 7	3·1	A9 III		
18 Aqr	A5	4999·984	+ 4	2·0			
		5024·947	−19	4·2			
		5354·012	+39	3·1			
204960	5·73	5266·275	+16	1·1			
3G Gru	K0	5354·025	− 1	1·2			
		5716·057	+ 6	1·3			
		6035·149	+22	1·2			
207052	5·43	5379·968	−24	2·5	A2 V	+ 1*c*6LY	*Lick Publ.*, **16**.
λ Cap	A0	5742·985	−23	2·8			*Yerkes Publ.*, **7**.
		6036·149	+33	2·9			
		6067·083	− 6	2·7			
211539	5·74	5057·937	+32	3·2			
υ Oct	K0	5348·092	+21	1·8			
		5354·072	+ 5	3·2			
211838	5·36	5025·970	−10	6·1	B8 V	− 9*c*7LY	*Lick Publ.*, **16**.
ρ Aqr	B8	5360·053	0	4·2			*Ap. J.*, **64**.
		6067·101	+30	5·8			
		6086·035	+ 8	6·8			
212132	5·82	4967·128	+43	1·7	F0 IVp		
π^2 Gru	F0	5269·283	+32	2·3			
		5759·967	−14	2·1			
214085	6·11	5711·119	+10	2·8	A4 V		Under observation
51G Gru	A2	5743·025	− 1	2·4			for orbit.
		5771·958	−36	2·1			
		5777·942	−18	3·2			
		6038·149	+52	2·3			
		6067·125	+31	2·8			
		6086·061	−31	2·2			
215789	3·69	4971·133	+11	1·9	A2 V	0*c*3L	*Lick Publ.*, **16**.
ϵ Gru	A2	5321·178	− 3	2·1			
		6036·203	+ 7	2·0			
		6084·071	− 1	3·3			
		6094·076	−23	2·3			
		6115·009	− 6	1·4			
222095	4·86	4970·181	+26	3·5	A2 V	+10*c*5L	*Lick Publ.*, **16**.
11G Phe	A2	5295·297	+51	3·6			Under observation
		5321·228	− 1	1·4			for orbit
		5716·092	+31	2·5			
		5740·050	−32	3·4			
		5987·318	+ 9	2·1			
		6115·043	− 4	4·6			
		6143·938	+ 1	3·8			
		6154·949	− 7	1·5			

TABLE II (*continued*)

(1) HD Star	(2) m_v Sp	(3) JD 243....	(4) V km/s	(5) p.e. ±	(6) Sp	(7) GCRV	(8) Notes
222847	5·26	4967·186	+48	11·5	B8 V	+14*d*6LY	*Lick Publ.*, **16**.
106 Aqr	B8	5269·347	+32	4·8			*Ap. J.*, **64**.
		5361·128	+23	8·1			
		6036·237	+17	4·6			
225132	4·62	5295·347	+33	6·3	A0:IV	−5*d*13LY	*Lick Publ.*, **16**.
2 Cet	B9	5361·152	+33	6·8			*Yerkes Publ.*, **7**.
		6035·255	+33	7·2			
		6115·065	+26	5·3			

TABLE III

Wave-lengths of lines consistently measured

Sp. Type	Velocity Low	Velocity Average		Velocity High
B0–B9	3933·664 P	4009·27	4267·167 P	4069·766 P
	3964·727 P	4026·14 P	4340·468 P	4072·162
	3968·465	4101·737 P	4471·477 P	4075·868
	3970·074 P	4128·051 P	4481·228 P	4116·103
	4130·876 P	4143·759		4387·928 P
A0–F2	3933·684 P	4005·205	4132·060	4215·600 P
	3968·494 P	4030·615 P	4143·686	4250·510 P
	4118·678	4045·796 P	4260·429	4254·348 P
	4202·042	4063·555 P	4307·914 P	4340·526 P
	4325·765	4071·687 P	4404·726 P	4481·293 P
		4077·710	4415·137 P	
		4101·750 P		
F4–G5	4077·710 P	4005·205 P	4143·772	4134·478
	4132·230	4030·673 P	4202·093 P	4191·593
	4282·640 P	4045·827 P	4215·761	4235·913
	4325·777 P	4063·607 P	4260·429 P	
		4071·751 P	4307·914	
		4092·710 P	4340·540 P	
		4101·743 P	4404·745 P	
		4118·702	4415·137	
G8–K5	4005·205 P	4030·673 P	4235·913	4134·478
	4034·494	4045·827 P	4254·330 P	4191·593
	4101·743	4063·607	4260·429 P	4215·761
	4132·230	4071·751 P	4325·777 P	4307·914
	4282·640 P	4077·710 P	4404·745 P	4340·540 P
		4092·512 P	4415·137 P	
		4118·702 P	4427·319 P	
		4143·772	4454·929	
		4202·093 P	4461·793	

TABLE IV

Observers and measurers

Name	Standard Velocity Observed	Standard Velocity Measured	N30 Programme Observed	N30 Programme Measured
W. Buscombe	41	65	142	183
H. Gollnow	68	10	29	13
J. Graham *	1	13	1	22
G. Hagemann	5	87	2	13
W. Heintz †	15	1	35	0
P. Morris	6	17	41	125
A. Przybylski	42	15	63	0
Totals	178		313	

* Sydney University: summer assistant, 1957–58.
† Munich Observatory: guest observer, 1954–55.

Acknowledgments.—In presenting the results of a part of our extensive programme for determining radial velocities, we wish to thank the other observers and assistants for their help and co-operation. The work could never have got under way without the painstaking attention by Dr Gollnow to many details of the final design and operation of the spectrograph, and his collaboration in choosing the observing lists of programme and standard stars. Messrs Banham and Thomas, with their associated craftsmen, have spared no effort in applying their skill to the construction and maintenance of the instrument.

Mount Stromlo Observatory,
Canberra, Australia:
1958 *May* 15.

References

(1) Dritter Fundamentalkatalog des Berliner Astronomischen Jahrbuches: I. Teil (*Veröff Astr. Rechen-Inst. Berlin-Dahlem*, No. 54, 1937); II. Teil (A. Kopff, *Abh. Preuss. Akad. Wiss., Phys.-math., Kl.*, No. 3, 1938).
(2) H. R. Morgan, *Astr. Papers Am. Eph. Naut. Almanac*, **13**, (3), 1952.
(3) R. E. Wilson, Carnegie Institution Publication No. 601, Washington, 1953.
(4) R. F. Sanford, J. H. Moore and J. A. Pearce, *Trans. I.A.U.*, **7**, 311, 1950.
(5) W. Buscombe, *M.N.*, **116**, 262, 1956.
(6) R. M. Petrie, *Pub. D.A.O.*, **9**, 297, 1953, (B stars); *J.R.A.S.C.*, **42**, 213, 1948—Contr. D.A.O. No. 11 (A stars); *J.R.A.S.C.*, **40**, 325, 1946—Contr. D.A.O. No.4 (F–K. stars).
(7) K. O. Wright, *Pub. D.A.O.*, **9**, 167, 1952.
(8) D. S. Evans, *M.N.A.S.S.A.*, **13**, 25, 1954.

SPECTRAL TYPES AND RADIAL VELOCITIES IN THE GALACTIC CLUSTER NGC 3293

M. W. Feast

(Communicated by the Radcliffe Observer)

(Received 1958 May 7)

Summary

112 spectra of 35 stars have been used for the determination of spectral types and 89 of these spectra for the determination of the radial velocities of 26 of the stars. The spectral types taken together with Dr T. E. Houck's photometric measures show the H–R diagram expected for a young cluster. The stars are mainly of early B type with luminosity classes from V to Ib. An Mo Iab star is almost certainly a cluster member. The radial velocities show a dependence on magnitude (Fig. 3) which is large and unexplained. The Ca II interstellar lines are free of the effect, which may be possibly related to the Trumpler effect.

1. *Introduction.*—The study of galactic clusters containing early B type stars is of interest for several reasons. It appears to be generally agreed that such clusters must be quite young and that a study of their Hertzsprung–Russell diagrams is of importance for theories of stellar evolution. In addition, the H–R diagrams are of interest in checking the luminosity scale of the MK system. Again, it would appear rather likely that a considerable number of these clusters are dynamically unstable and will expand eventually, passing through a stage in which they would be identified as stellar associations (cf. (**1**) etc.). A study of the motions of the cluster members is therefore desirable. Finally, a determination of the radial velocities of clusters of early B type stars is of importance for galactic rotation studies.

NGC 3293 is a compact cluster in Carina ($10^{h}\,34{\cdot}5$ $-58^{\circ}\,00$ (1950)) not far from, and perhaps associated with, the η Carinae complex (see for instance the photograph shown in (**2**)). Fig. 1 (Plate 9) is reproduced from a photograph of the region of NGC 3293 taken by Dr A. D. Thackeray at the Newtonian focus of the Radcliffe 74-inch reflector. The cluster is also shown on the charts of the HD extension (**3**) (chart No. 127). A few stars Npr. the main cluster and which may be associated with it are included in the present discussion. Star No. 1, the only O type star in this region, is the centre of an emission nebula (Gum (**4**), No. 30) and the whole cluster is involved in faint nebulosity (c.f. (**2**), Fig. 6). Mrs E. v. P. Smith (**2**) has published polarization measurements of seven stars in the cluster. Miss D. Hoffleit (**5**) and Morgan, Whitford and Code (**6**) have published the spectral types of a few stars in the cluster. Objective prism surveys have revealed 10 OB stars in the cluster (**7**) and one Mo supergiant (**8**). The spectral types and radial velocities of the two brightest stars were included in the first Radcliffe catalogue (**9**) and of No. 1 in the second catalogue (**10**). Some years ago an important, unpublished, photometric study

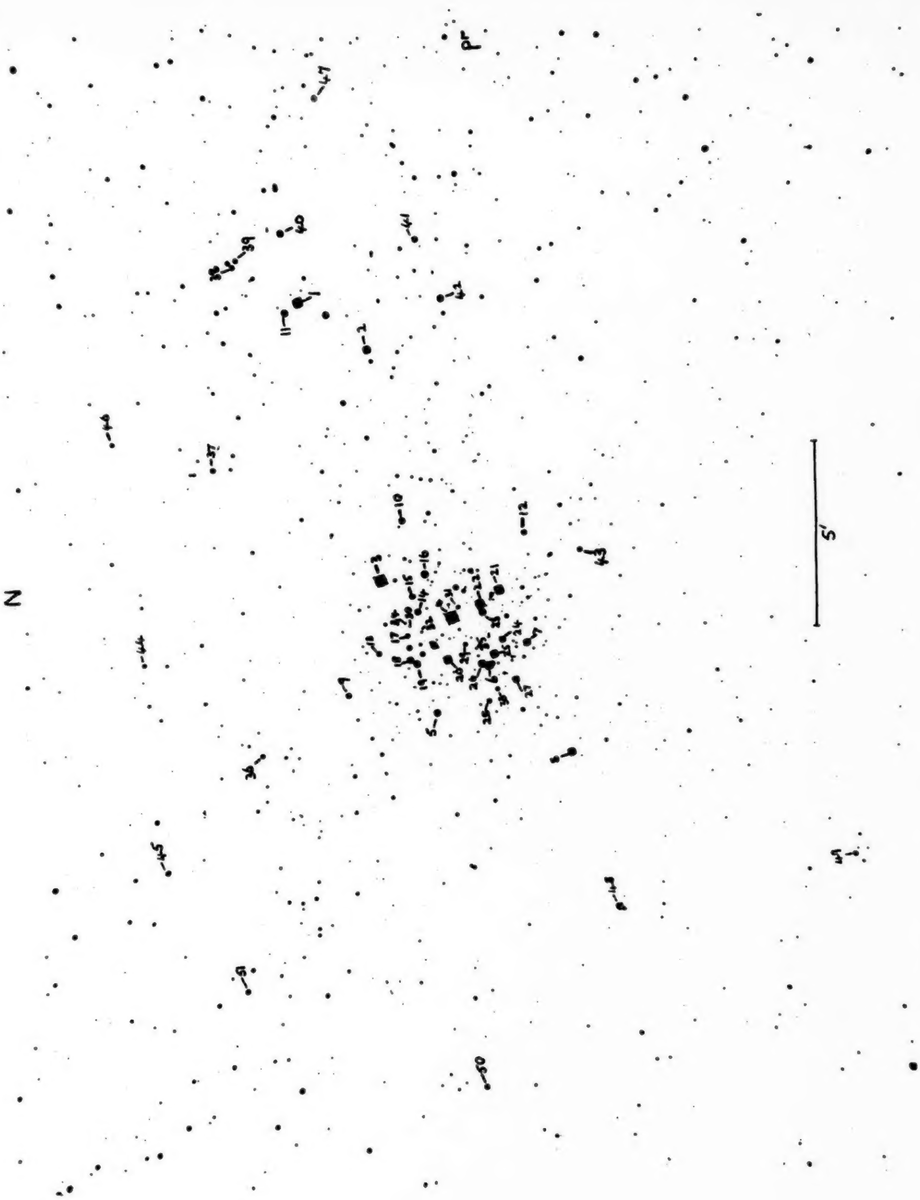

FIG. 1.—*Photograph of the region of NGC 3293 from a 74-inch Radcliffe Newtonian plate taken by Dr A. D. Thackeray.*

of the cluster was made by Dr T. E. Houck at the Cape, Boyden and Radcliffe Observatories. NGC 3293, which is listed as Lacaille 4375 in the Cordoba work (**11**), has been referred to as the II Carina association (**12**) though it is considerably smaller than the well-known O and B associations.

2. *Spectral types.*—The present study of NGC 3293 is based on 112 spectra of 35 stars. The spectra were all obtained with the two-prism spectrograph at the Cassegrain focus of the 74-inch Radcliffe reflector. 86 spectra were obtained with the $f/3{\cdot}7$ camera (49 A/mm at $H\gamma$), 3 with the $f/6$ camera (29 A/mm at $H\gamma$) and 23 with the $f/2$ camera (86 A/mm at $H\gamma$). In estimating the spectral types, all these plates were employed but the radial velocities dealt with later depend only on the spectra taken with the two higher dispersions. The types were estimated in the usual way by comparison with standard stars of the MK system. Though types of the three stars, Nos. 1, 3 and 4, have been published previously (**9**) (**10**), the types given here (which differ very slightly from those given earlier) are independent re-determinations. The 35 stars studied include the 31 stars for which Dr Houck has made photometric measurements.

The results are given in Table I. The HD, HDE or CPD number is given where possible and the stars are identified in Fig. 1. The types of Hoffleit (**5**), Morgan, Whitford and Code (**6**) and the HD types are included where available for comparison. The fragmentary overlap with Hoffleit and with Morgan, Whitford and Code may be regarded as satisfactory. Columns 7 and 8 contain data kindly supplied in advance of publication by Dr Houck. The visual magnitudes, m_V, should be close to the Johnson V magnitude system. The colours $(B-V)$ were converted from Dr Houck's instrumental system using a relation supplied by him. Using the intrinsic colours of the O and B type stars given by Hiltner (**13**), the colour excesses and absorption corrections were determined (a ratio of total to selective absorption of 3·0 being adopted) and the magnitude corrected for absorption, m_0, found. The absorption corrections range from $0^m{\cdot}57$ to $1^m{\cdot}38$ and an assumption of uniform reddening over the whole cluster would have resulted in a very poorly defined sequence in the HR diagram. Column 9 of Table I gives the values of m_0, and column 10 the distance moduli of the individual stars using the calibration of the MK system given by Johnson and Hiltner (**14**).

Star No. 21 is that previously listed as an M0 supergiant by Blanco and Münch (**8**). The slit spectra now obtained confirm and refine this classification. The intrinsic colour of an M0 Iab star was taken from Johnson and Hiltner (**14**). The distance moduli of the B stars and of No. 21 agree sufficiently well to confirm the membership of the star in the cluster. The radial velocity results of the next section also support this result. Stars 1, 2 and 11 in the Npr. "flare" do not have significantly different distance moduli from the cluster stars and were included with them in deducing the mean modulus. It cannot be claimed with any certainty that these stars do belong to the cluster though a "flare" of this kind would not be unique (cf. NGC 2169 (**15**)). However the mean distance modulus of the cluster is not appreciably affected by including or omitting these stars. A mean modulus of 12·08 is found from 31 stars. A standard error, due to scatter of the individual moduli, of $\pm 0^m{\cdot}1$ is found. This, of course, does not include the uncertainty due to systematic errors in the calibration of the MK system, etc. This distance modulus corresponds to a distance of 2·6 kpc with an "internal" standard error of about $\pm 0{\cdot}1$ kpc.

TABLE I

Spectral types and photometric data

Star	HD HDE or CPD No.	Radcliffe MK type	Hoffleit type (5)	M.W.C. type (6)	HD type	m_V	$B-V$	m_0	m_0-M
1	91824	O7	O7		Oe5	8·15	−0·05	7·34	12·4
2	91850	B1 III	B1 IV:		B2	9·12	+0·14	7·92	12·3
3	91943	B0·5 Ib	B0·5 I	B0·5 Ib	B0	6·72	+0·06	5·70	11·5
4	91969	B0 I(b ?)	B0 Ia	B0 Ib	B0	6·52	+0·01	5·59	11·8
5	92024	B1 III			B	9·06	−0·04	8·40	12·8
6	92007	B0·5 III	B0 II		B	8·22	+0·07	7·59	12·5
7	91983	B1 III	B1 III		B	8·59	+0·04	7·69	12·1
8	92044	B0·5 III	B0·5 II		B0	8·27	+0·15	6·98	11·7
9	303065	B2 V			B8	9·99	−0·02	9·33	11·3
10	303067	B1 V			B5	9·56	+0·04	8·66	11·8
11	303068	B1 V			B	10·02	−0·01	9·27	12·4
12	303075	B1 V			B8	10·03	+0·05	9·10	12·2
13	−57° 3522	B2 V				10·18	−0·03	9·55	11·6
14	−57° 3507	B1 V		B0·5 V		9·28	−0·04	8·62	11·7
15	−57° 3504	B1 V				10·01	+0·01	9·20	12·3
16	−57° 3500	B1 III		B0·5 V		8·74	−0·02	8·02	12·4
17	−57° 3514	B2–3 V:							
18	−57° 3524	B1 V				9·30	−0·07	8·73	11·8
19	−57° 3524	B1 III				9·10	+0·18	7·72	12·1
20	−57° 3523	B1 III				8·03	+0·02	7·19	11·6
21	−57° 3502	M0 Iab(b ?)				7·31	+2·06	6·17	11·5
22	−57° 3506	B1 II		B1 II		7·62	+0·07	6·63	11·5
23	−57° 3506	B1 III				9·21	+0·03	8·34	12·7
24	−57° 3517	B1 III				9·22	+0·03	8·35	12·8
25	−57° 3521	B1 III				8·15	+0·06	7·19	11·6
26	−57° 3526	B1 III				9·28	−0·04	8·62	13·0
27	−57° 3527	B0·5 III				8·95	+0·05	7·96	12·7
28	−57° 3531	B1 V				10·25	+0·04	9·35	12·4
29	−57° 3518	B2 V				10·67	+0·02	9·89	11·9
30		B5 V::							
31		B2 V				11·55	0·00	10·83	12·8
32		B8,Ve				12·97	+0·23	12·01	11·5
33	−57° 3528	B2 V				10·65	+0·04	9·81	11·8
34		B8 V							
35		B6–8 V:							

Note.—The following pairs of stars have the same CPD numbers : 6 and 26, 18 and 19, 22 and 23.

The HR diagram for NGC 3293 is shown in Fig. 2. The luminosity class assigned to each star is indicated in this figure and it will be seen that the correlation of luminosity class and m_0 (or M) is satisfactory. The scatter in m_0 at a given type for each luminosity class is no greater than that found in other works of this kind (e.g. h and χ Per (**16**)). It is not clear whether this scatter could be reduced by refining the process of spectral typing or whether most of it is inherent in the method of spectroscopic parallaxes. There appears to be

no tendency within the accuracy of the results, for different subgroups (of type and luminosity class) to give systematically different distance moduli. That is, there appears to be no significant deviations from the Johnson and Hiltner (**14**) calibration of the MK system. It should be pointed out that we have not taken into account the fact that a good proportion of the stars are probably binaries (see Section 3). This will, of course, affect the magnitudes to some extent. However, the stars known to be variable in velocity do not appear to differ systematically in the HR diagram from the other stars.

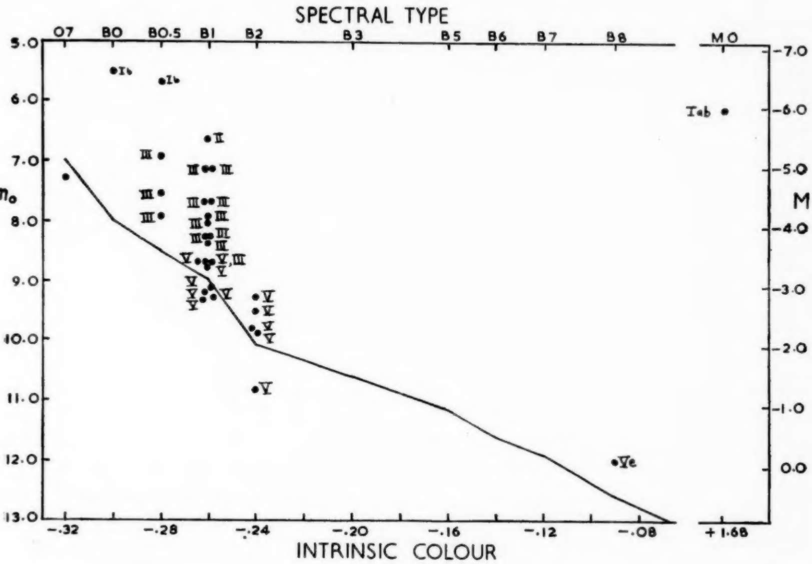

FIG. 2.—*Hertzsprung–Russell diagram for NGC* 3293. *The absolute magnitude* (*M*) *scale depends on a distance modulus of* 12·1. *The luminosity classes of the stars are shown. The line is the 'zero age' main sequence of Johnson and Hiltner* (**14**).

The sequence defined by the B stars in the HR diagram is like that found in other groups of similar stars, e.g. the Orion region (**17**) and h and χ Per (**16**). Its interpretation as evolution away from the main sequence for the more massive stars is well-known. The one M type supergiant found is similar in type to the M stars found in h and χ Per and similarly fits into the present theories of stellar evolution.

The O7 star (No. 1) in the "flare" does not follow the general trend but probably lies on or near the main sequence. This fact, however, cannot be used as evidence against its membership in the cluster. In fact O type stars which deviate from the general sequence in this way are found in several clusters and associations, e.g. Orion Nebula (**17**), h and χ Per (**16**) and I Gem (**18**).

It is unfortunate that magnitudes and colours are not available for four faint stars in Table I, as these would have strengthened the lower part of the HR diagram. Extension of the photometry to fainter stars is clearly desirable in view of the possibility of finding deviations from the main sequence, e.g. (**19**).

However, accurate spectral types for many fainter stars might present some difficulties, as the faintest stars in the present programme reach about $13^{m}(m_V)$. If we adopt a distance of 2·6 kpc and a radius of about 4·5 minutes of arc, then we obtain a linear radius of 3·5 pc, a fairly average value for an open cluster. For convenience, a number of stars in the field of Fig. 1, which have not been included in the present work but for which HD or HDE types are available, are collected together in Table II. Few, if any, are likely to be cluster members.

TABLE II

Field stars (probably non-members)

No.	HD or HDE	Type
36	303066	A2
37	303069	B8
38	303070	A
39	303071	A
40	303072	G5
41	303073	B8
42	303074	A0
43	303076	K5
44	303061	B
45	303062	B8
46	303060	A0
47	302981	A0
48	92121	A3
49	303077	F0
50	303064	B3
51	303063	A0

3. *The radial velocities of the stars.*—The radial velocity data are collected in Table III. In the case of star No. 3 the first six observations, and in the case of star No. 4 the first five observations are taken from (**9**) whilst in the case of No. 1 the first four observations are taken from (**10**). The observing and reduction procedures employed were those previously described (**9, 10**). It is noted that, since all calculations were originally carried out to the nearest 0·1 km/sec and only rounded off in compiling Table III, the quoted means do not always agree exactly with the means of the tabulated velocities. Of the 26 O and B stars in the programme, 9, or one star in three, give evidence of being binaries, either from showing variable velocities or doubling of lines. It is possible that one or two of these stars might, on further examination, turn out to have sensibly constant velocities. However, since we detect binaries only when their orbits are suitably inclined to the plane of the sky, we may in any case conclude that NGC 3293 is rich in binaries.

The mean velocity of the cluster is $-14{\cdot}1 \pm 1{\cdot}8$(s.e.) km/sec. This was determined from those B stars for which two or more spectra were available and which were not classified as variable velocity stars. The three stars in the flare (Nos. 1, 2 and 11) were omitted from the mean, which therefore depends on 15 B stars. It will be seen that this mean agrees very well with the M0 supergiant (-12 ± 1 (s.e.) km/sec) supporting the latter's cluster membership. The velocity of the M0 star was determined using the wave-lengths recommended for the late type stars by the Victoria workers (**20**). Though these wave-lengths were not tested for stars later than K8, their use for an M0 star will not have introduced any appreciable errors.

TABLE III

Radial velocities in NGC 3293

No. 1 O7

			Star km/sec	Ca II km/sec
1952	IV	3·801	+27 (8)	+ 7 (1)
	IV	5·750	−22 (4)	+ 7 (1)
	IV	6·792	+ 7 (4)	
	V	15·715	−22 (7)	+ 5 (1)
1957	IV	20·867	−36 (8)	+ 1 (1)
	IV	23·794	−45 (8)	+ 8 (2)
	VI	9·783	−14 (6)	+ 7 (2)
			−15:	**+ 6**

Variable velocity. Range 72.

No. 2. B1 III

			Star km/sec	Ca II km/sec
1957	IV	20·897	−16 (7)	− 2 (1)
	IV	23·817	− 4 (5)	0 (2)
	VI	12·742	− 7 (5)	+11 (2)
			− 9	**+ 3**

No. 3. B0·5 Ib

			Star km/sec	Ca II km/sec
1952	IV	9·829	0 (8)	+11 (1)
	IV	16·838	−21 (15)	0 (1)
	V	2·827	− 6 (14)	+ 4 (1)
1953	I	19·069	− 9 (8)	+ 1 (2)
	I	24·029	− 7 (18)	− 3 (1)
	IV	9·850	− 2 (14)	+ 3 (1)
1958	III	3·125	− 7 (12)	+ 7 (1)
	III	8·824	− 3 (10)	+ 1 (1)
			− 7	**+ 3**

No. 4. B0 I(b ?)

			Star km/sec	Ca II km/sec
1953	I	22·071	− 1 (11)	+ 7 (1)
	I	27·056	+ 4 (17)	− 4 (1)
	I	31·051	0 (15)	− 1 (1)
	III	28·843	0 (10)	+ 1 (2)
	V	24·750	− 4 (10)	+ 6 (2)
1958	III	3·139	− 5 (11)	+ 9 (1)
	III	8·831	− 8 (8)	+ 1 (1)
			− 2	**+ 3**

No. 5. B1 III

			Star km/sec	Ca II km/sec
1956	IV	18·788	+18 (8)	− 3 (1)
1957	IV	23·856	−33 (8)	− 2 (2)
	VI	12·781	−34 (10)	+14 (2)
			−16:	**+ 3**

Variable velocity. Range 52.

No. 6. B0·5 III

			Star km/sec	Ca II km/sec
1956	IV	11·774	−25 (7)	+ 3 (2)
1957	IV	13·843	− 9 (6)	− 1 (2)
	VI	9·730	−28 (5)	+10 (1)
			−20	**+ 4**

Lines rather poor.

No. 7. B1 III

			Star km/sec	Ca II km/sec
1956	IV	11·798	−36 (8)	+ 4 (1)
1957	IV	13·828	+48 (9)	− 1 (2)
	VI	9·802	−18 (9)	−11:(1)
			− 2:	**− 1**

Variable velocity. Range 84.

No. 8. B0·5 III

			Star km/sec	Ca II km/sec
1956	IV	11·820	−15 (15)	+ 4 (1)
1957	IV	13·753	−12 (15)	− 3 (1)
	VI	9·768	−11 (9)	−17 (1)
			−12	**− 5**

No. 9. B2 V

			Star km/sec	Ca II km/sec
1957	IV	20·979	+ 4 (8)	+16 (2)
1958	III	2·872	+ 5: (6)	0 (1)
	III	9·097	−24 (9)	+10 (1)
			− 5	**+ 9**

Probably variable velocity. Range 29.
Spectra show some signs of line doubling.

No. 10. B1 V

			Star km/sec	Ca II km/sec
1957	III	22·791	+ 6 (7)	+ 1 (2)
	IV	23·894	−20 (8)	− 5 (1)
1958	III	9·002	−18 (9)	− 2 (1)
			−10	**− 2**

No. 11. B1 V

			Star km/sec	Ca II km/sec
1957	IV	23·772	− 7 (10)	− 2 (1)

No. 12. B1 V

			Star km/sec	Ca II km/sec
1957	IV	22·940	−56: (3)	− 5 (2)

Lines broad and indications of doubling.

No. 13. B2 V

			Star km/sec	Ca II km/sec
1957	IV	22·975	− 6 (10)	− 2 (1)
1958	III	2·947	0 (8)	+ 5 (1)
			− 2	**+ 2**

No. 14. B1 V

			Star km/sec	Ca II km/sec
1957	III	22·814	−16 (6)	+12 (1)
	V	28·771	−28 (9)	+ 5 (2)
	VI	9·689	− 4 (8)	+12 (1)
	VI	12·822	− 9 (7)	+20:(1)
			−14	**+11**

TABLE III (*continued*)

No. 15. B1 V:

		Star km/sec	Ca II km/sec
1957 IV	23·701	−10: (5)	+ 1 (2)
1958 III	3·054	:	− 9 (1)
			− 4

Lines scatter widely and there are indications of a binary nature. No satisfactory mean can be determined for the second spectrum.

No. 16. B1 III

		Star km/sec	Ca II km/sec
1956 IV	18·814	−26 (13)	+ 1 (1)
1957 IV	7·909	−17 (17)	− 1 (1)
VI	9·829	−27 (12)	
		−23	**0**

No. 18. B1 V

		Star km/sec	Ca II km/sec
1957 IV	7·815	− 4 (11)	+ 1 (2)
V	28·808	−23 (11)	+ 4 (1)
VI	15·731	−22 (7)	− 6 (1)
		−16	**0**

No. 19. B1 III

		Star km/sec	Ca II km/sec
1957 IV	7·850	−18 (5)	+ 2 (2)
V	28·849	−19 (4)	+ 2 (2)
VI	15·688	−25 (6)	+ 6 (1)
		−21	**+ 3**

Lines poor.

No. 20. B1 III

		Star km/sec	Ca II km/sec
1956 IV	18·762	−20 (9)	− 9 (1)
1957 IV	20·701	−28 (9)	+ 1 (1)
VI	9·716	−20 (11)	− 6 (1)
		−23	**− 5**

No. 21. M0 Iab(b ?)

		Star km/sec	Ca II km/sec
1956 IV	11·840	−14 (6)	
1957 II	7·905	−14 (7)	
IV	20·938	−11 (13)	
VI	9·862	−10 (5)	
		−12	

No. 22. B1 II

		Star km/sec	Ca II km/sec
1956 IV	18·769	−11 (15)	− 5 (2)
1957 IV	23·838	− 8 (17)	0 (2)
VI	9·756	−14 (11)	
		−11	**− 2**

No. 23. B1 III

		Star km/sec	Ca II km/sec
1957 IV	20·837	− 1 (11)	− 9 (1)
V	28·694	+19 (12)	+ 2 (1)
VI	15·775	−10 (9)	− 4 (1)
		+ 3:	**− 4**

Possibly variable velocity. Range 29.

No. 24. B1 III

		Star km/sec	Ca II km/sec
1957 IV	7·880	− 5 (6)	− 1 (1)
V	28·732	−14 (8)	+ 2 (1)
VI	15·821	−18 (5)	
		−12	**0**

No. 25. B1 III

		Star km/sec	Ca II km/sec
1956 IV	18·754	−22 (6)	− 4 (1)
1957 IV	20·792	−14 (7)	− 2 (2)
VI	9·744	−24 (5)	− 1 (1)
		−20	**− 2**

Lines rather diffuse.

No. 26. B1 III

		Star km/sec	Ca II km/sec
1956 IV	18·838	+ 2 (6)	+ 3 (2)
1957 IV	20·808	−32 (5)	+ 4 (2)
VI	12·674	−18 (7)	+ 2 (1)
		−16:	**+ 3**

Lines rather poor. Probably variable velocity. Range 34. Possible indications of line doubling.

No. 27. B0·5 III

		Star km/sec	Ca II km/sec
1956 IV	18·862	−24 (10)	−19 (1)
1957 IV	13·737	− 3 (11)	− 1 (2)
VI	12·706	−18 (12)	+ 5 (1)
		−15	**− 5**

No. 28. B1 V

		Star km/sec	Ca II km/sec
1957 IV	23·735	−13: (3)	+ 4 (2)
1958 III	8·860	:	+ 1 (1)
			+ 2

Individual measures scatter too widely for a meaningful mean in the second spectrum. There are indications of line doubling. Probably a binary.

Explanation of Table III

The observations are listed chronologically under each star. The time of each observation (U.T.) is given followed by the derived stellar and interstellar velocities (reduced to the Sun). The figures in brackets are the numbers of lines contributing to each velocity. The adopted means are given in heavy type followed by brief comments on variability etc.

An analysis of the velocities of the 15 B stars defined as above, shows the mean square deviation from the mean to be $\sigma_0^2 = 46{\cdot}6\,(\text{km/sec})^2$ whilst the inter-agreement of the individual determinations of the velocities of these 15 stars yields a mean square observational error of $\sigma_e^2 = 15{\cdot}4\,(\text{km/sec})^2$. The difference between these two quantities is large and if interpreted as a velocity dispersion in the cluster (or an expansion of the cluster) yields a true mean square deviation $\sigma^2 = 31{\cdot}2\,(\text{km/sec})^2$; $\sigma = 5{\cdot}6$ km/sec. However, it is necessary to investigate whether effects in the stars themselves can give rise to line shifts which might be misinterpreted as Doppler shifts due to space motion. That there may well be some effect of this kind is seen if the measured radial velocities are plotted against the values of m_0 (Fig. 3*a*). It is clear that the bright and

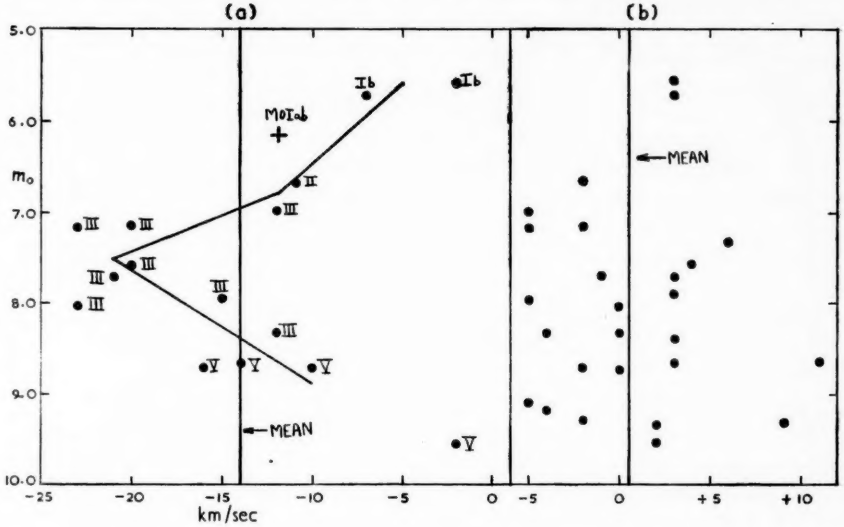

FIG. 3.—*Relation of radial velocity to m_0 for (a) stars with constant velocities, (b) Ca II interstellar lines.*

faint stars give more positive velocities than those of intermediate brightness. It will be clear that the scatter of the points about the line which has been sketched in is no greater than that to be expected from the observational error estimated above ($\sigma_e = 3{\cdot}9$ km/sec). For comparison, in Fig. 3*b* are plotted the velocities determined from the interstellar Ca II lines. The absence of any magnitude dependence in these velocities is evidence against the effect of Fig. 3*a* being due to observational causes such as guiding errors etc. If the stellar velocities are plotted against m_V rather than m_0 the effect is still present though there is some slight indication that there is more scatter in that case.

One of the most conspicuous features of Fig. 3 is that the velocities of two supergiants (No. 3 and No. 4) are considerably positive with respect to the giants. Now these two velocities depend mainly on the measures previously published (**9**). Whilst the general observational procedure and methods of reduction were the same in that case as in the present work, there were two changes: (1) in the present programme Kodak 103aO plates were used for all

the stars as against the finer grained Ilford SBS or I.S.R. plates used in (**9**); and (2) in the case of most of the stars on the present programme a spectrum width of 0·42 mm was used as compared with a width of 0·20 mm for the earlier programme (cf. (**10**)). Though it would appear extremely unlikely that either of these changes could have introduced any systematic velocity errors of the magnitude shown in Fig. 3, it was felt necessary to check the point. The last two results in the cases of stars No. 3 and No. 4 in Table III were taken under conditions identical with the rest of the programme (103aO plates, 0·42 mm spectrum width). It will be clear from Table III that if these velocities had alone been used essentially the same results would have been obtained. In one case the velocity of the star would be increased and in the other decreased.

It is natural to enquire whether erroneous wave-lengths of some of the spectrum lines could produce a spurious effect of this kind. It will at once be obvious that since all the observed B stars in the cluster have approximately the same spectral types (an extreme range of B2 to B0 with most stars B0·5 or B1) any effect on wave-lengths is almost certainly due to luminosity effects. Since it seems that luminosity effects in the B stars vary monotonically from the dwarfs to the supergiants it is obviously difficult to explain Fig. 3*a* in this way. The adopted wave-lengths have been discussed previously (**10**); in particular, certain corrections to the I.A.U. wave-lengths of He 4026, 4471 were applied following the work of Petrie (**21**) and Radcliffe investigations. The corrections were

(1) He 4026	Luminosity classes I–II	:	no correction
	Luminosity classes III–V	:	apply correction +4 km/sec
(2) He 4471	Luminosity classes I–IV	:	no correction
	Luminosity class V	:	apply correction +10 km/sec.

The +10 km/sec correction to 4471 for the dwarfs is the most important of the two corrections and if it had not been applied to these stars they would be plotted with smaller (more negative) velocities in Fig. 3. However, so far as the effect we are dealing with is concerned, such changes are negligible. For the four dwarfs plotted (Nos. 10, 13, 14 and 18) the effect of this correction on the means is 1·2, 1·1, 1·4 and 1·0 km/sec respectively. This example, furthermore, makes clear that in order to explain Fig. 3 as due to erroneous wave-lengths very large shifts of a few lines, or shifts of the order of 10 km/sec for a considerable number of the lines, would be necessary. Neither alternative appears at all likely.

To investigate further whether the effect could be traced to erroneous wave-lengths, or alternatively to a deviation of lines due to certain elements only, the velocities derived from individual lines were investigated. The results are summarized in Fig. 4. The stars were arranged in four groups:

(1) Stars No. 3 and No. 4:	mean $m_0 = 5{\cdot}6$
(2) Stars No. 8 and No. 22:	mean $m_0 = 6{\cdot}8$
(3) Stars Nos. 20, 25, 6, 19 and 16:	mean $m_0 = 7{\cdot}5$
(4) Stars Nos. 27, 24, 14, 10 and 18:	mean $m_0 = 8{\cdot}5$.

Star No. 13 which is shown plotted in Fig. 3*a* ($m_0 = 9{\cdot}55$) is omitted in Fig. 4 as it is of rather too different a magnitude and velocity to be included in the last group and single stars are of too low weight to be plotted separately.

In Fig. 4 the dependence of velocity on m_0 is shown for the H lines, He I lines, a group of lines of Si, C and O and also the Ca II interstellar lines for these same 14 stars. The numbers in the diagram are proportional to the weights of each point and the horizontal lines indicate the magnitude of the standard errors. Both H and He I reproduce the effect shown by the mean velocities. In the case of the Si, O and C group, which is of lower weight than H and He, the three brighter groups of stars show the effect though the fainter group fails to show the increase in velocity shown by the mean curve. However, the standard errors of the quantities involved indicate that there is no significant deviation from the mean curve. As in the case of Fig. 3 *b*, where more measurements are plotted the interstellar Ca II results of Fig. 4 do not show any significant dependence on m_0.

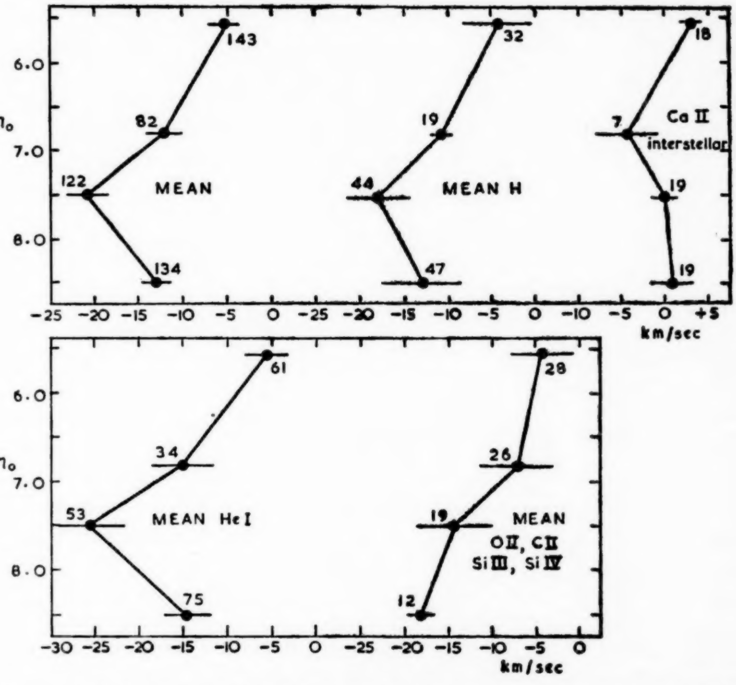

FIG. 4.—*Relation between radial velocity and m_0 for stars arranged in groups and for lines of different elements. The numbers are proportional to the weights and the lengths of the horizontal lines to the standard errors.*

The dependence of the velocities on magnitude clearly rules out a discussion of the internal motions of the cluster. No convincing explanation of the phenomenon can be suggested and it is most desirable to confirm the effect in other clusters. The published data on velocities in open clusters containing stars of similar spectral type to NGC 3293 do not appear sufficient to carry out further tests. It is, however, of some interest to note that in the Pleiades a similar effect may perhaps be present (cf. Smith and Struve (**22**) Fig. 1), though, of course, the spectral types and luminosities of the stars are quite different in

NGC 3293. Further work would probably be necessary to decide conclusively whether the effect is definitely present in the Pleiades.

The positive displacement of the supergiants with respect to the giants in NGC 3293 is reminiscent of the " Trumpler " effect (**23**): the positive velocities exhibited by some O type stars in galactic clusters with respect to the B type members. The interpretation of this effect as a gravitational red-shift has been much discussed on account of the exceptionally large masses that this implies for the O type stars involved. It is desirable to extend the work on the clusters showing the Trumpler effect to fainter magnitudes to determine whether the fainter cluster stars also show positive residuals. It will be recalled that the trapezium stars of Orion show a positive velocity with respect to the nebulosity (**24**). Mass motion in the stellar atmospheres of course remains a possibility but it is not at all clear why it should result in a magnitude dependence of the form of Fig. 3*a*.

It is of some interest to calculate the velocities which NGC 3293 and the clusters showing the Trumpler effect are expected to have due to galactic rotation. Using the standard value of the solar motion and the Camm linear approximation without the K term and adopting $A=17{\cdot}5$ km/sec/kpc, $R_0=8{\cdot}9$ kpc, $l_0=327^\circ{\cdot}7$ (**25**), we obtain the results given in Table IV. For

TABLE IV

Observed velocities and velocities calculated from galactic rotation constants for NGC 3293, the Orion region and clusters showing Trumpler effect

Cluster NGC	Distance (pc)	V_C (calculated) km/sec	V_B (**23**) km/sec	V_O (**23**) km/sec	V_C-V_B	V_C-V_O
2244	1660 (**26**)	+39	+35 (6)	+44 (3)	+ 4	−5
2264	870 (**26**)	+25	+19 (11)	+33 (1)	+ 6	−8
2353	760 (**23**)	+30	+20 (5)	+35 (1)	+10	−5
2362	1450 (**26**)	+43	+34 (7)	+43 (1)	+ 9	0
6871	1340 (**23**)	− 8	−21 (3)	−11 (2)	+13	+3
7380	1840 (**23**)	−36	−43 (4)	−40 (1)	+ 7	+4
				Mean	+ **8**	−**2**
Orion	400 (**26**)	+22	Trapezium stars (**24**) = +32 km/sec Nebula (**24**) = +18 km/sec			
3293 stars	2600	+ 1	Measured stellar velocities : −23 to −2 km/sec			
gas	1300 ?	+ 4	Measured Ca II velocities : +0·5 km/sec			

the Trumpler clusters (**23**) V_B and V_O are the mean velocities for the B stars and the O stars respectively; the difference (V_O-V_B) is therefore the value of the Trumpler effect. The number of stars used in each mean is given in brackets. In the case of NGC 3293 the predicted velocity is more positive than that of any of the stars measured, though the difference from the supergiants and faint dwarfs is relatively small. The results of Table IV show that so far as galactic rotation alone is concerned the O stars of the Trumpler clusters have as much claim to represent the true cluster velocity as the B stars. A similar situation exists in the Orion Nebula where again the predicted velocity falls between that of the trapezium stars and that of the gaseous nebula.

In concluding this section it should be remarked that the velocities of the three stars in the " flare " of the cluster do not materially add to the discussion already given of their possible cluster membership.

4. *The Ca II interstellar velocities.*—Listed in Table III are the velocities of the interstellar Ca II lines. Generally only K was measured but in some cases H was resolved from He and could also be measured. The results yield a mean value of $+0{\cdot}5 \pm 0{\cdot}8$ (s.e.) km/sec. For a comparison with the stellar results we find $\sigma_0{}^2 = 18{\cdot}2\,(\mathrm{km/sec})^2$ $\sigma_e{}^2 = 9{\cdot}5\,(\mathrm{km/sec})^2$ and therefore $\sigma^2 = 8{\cdot}7\,(\mathrm{km/sec})^2$ $\sigma = 2{\cdot}9$ km/sec. Whilst there is no dependence of the velocity on the magnitude of the star in which it is found there is some indication of a dependence on the star's position. This is shown in Fig. 5*a* where the velocities are plotted in the

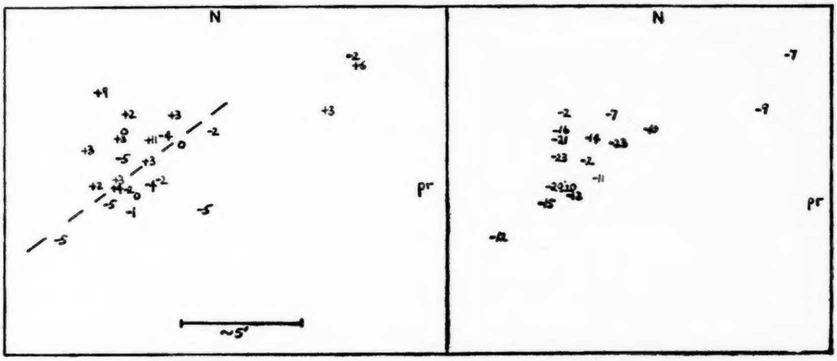

(a) CaII (b) Stars

FIG. 5.—*Radial velocities for (a) interstellar Ca II, (b) stars plotted on the plane of the sky (cf. Fig. 1).*

positions of the stars in the sky. On the other hand, there does not appear to be any noticeable relation between the stellar velocity and the star's position (Fig. 5*b*). The line in Fig. 5*a* which roughly divides the more positive from the more negative velocities (omitting the three stars in the flare) is approximately parallel to the galactic equator. It might appear likely that any Ca II absorption from gas associated with NGC 3293 contributes only a fraction of the total line absorption observed since the velocities given by the stars and gas are quite different and, further, the difference in the velocities is of the wrong sign to be interpreted as an expanding cloud of gas about the cluster, as has been found in the case of some groups of B type stars (**27**). On the other hand, the mean Ca II velocity agrees better with the velocity predicted from galactic rotation for 2·6 kpc than for 1·3 kpc (Table IV). However, the difference is relatively small and does not allow us to fix the mean distance of the Ca II absorption with any accuracy. A gradual change of Ca II velocity with position in the sky is not surprising, and the effects of differential galactic rotation of clouds at different distances, together with the known velocity dispersion amongst individual clouds, will be sufficient to account for the value of σ found above.

Table V summarizes some of the results found in this work.

TABLE V

Some data on NGC 3293

Distance modulus $(m_0 - M)$	=	12·08
Distance	=	2·6 kpc
Approximate diameter	=	3·5 pc
Mean velocity	=	$-14{\cdot}1 \pm 1{\cdot}8$ (s.e.) km/sec
Mean Ca II interstellar velocity	=	$+0{\cdot}5 + 0{\cdot}8$ (s.e.) km/sec.

Acknowledgments.—I am deeply indebted to Dr A. D. Thackeray not only for some very helpful discussions and suggestions, but also for carrying out duplicate measurements of some of the spectra. I should like to thank Dr A. J. Wesselink for his helpful advice on various matters connected with the work. Dr T. E. Houck most kindly placed his unpublished photometric measures at my disposal; their importance to the investigation can hardly be over-estimated.

Radcliffe Observatory,
Pretoria :
1958 *April.*

References

(1) S. van den Bergh, *Ap. J.*, **125**, 445, 1957.
(2) E. van P. Smith, *Ap. J.*, **124**, 43, 1956.
(3) A. J. Cannon and M. W. Mayall, *Harvard Annals*, **112**, 147, 1949.
(4) C. S. Gum, *Mem. R.A.S.*, **67**, 155, 1955.
(5) D. Hoffleit, *Ap. J.*, **124**, 61, 1956.
(6) W. W. Morgan, A. E. Whitford and A. D. Code, *Ap. J.*, Sup. **2**, 41, 1955.
(7) L. Münch and W. W. Morgan, *Tonantzintla y Tacubaya Bol.*, No. 8, p. 19, 1953.
(8) V. M. Blanco and L. Münch, *Tonantzintla y Tacubaya Bol.*, No. 12, p. 17, 1955.
(9) M. W. Feast, A. D. Thackeray and A. J. Wesselink, *Mem. R.A.S.*, **67**, 51, 1955.
(10) M. W. Feast, A. D. Thackeray and A. J. Wesselink, *Mem. R.A.S.*, **68**, 1, 1957.
(11) B. A. Gould, *Cordoba Resultados*, **19**, 183, 1897.
(12) Washburn Observatory Annual Report, *A.J.*, **60**, 312, 1955.
(13) W. A. Hiltner, *Ap. J.*, Sup. **2**, 389, 1956.
(14) M. L. Johnson and W. A. Hiltner, *Ap. J.*, **123**, 267, 1956.
(15) T. Cuffey and S. W. McCuskey, *Ap. J.*, **123**, 59, 1956.
(16) H. L. Johnson and W. W. Morgan, *Ap. J.*, **122**, 429, 1955.
(17) S. Sharpless, *Ap. J.*, **116**, 251, 1952.
(18) D. Crawford, D. N. Limber, E. Mendoza, D. Schulte, H. Steinman and T. Swihart, *Ap. J.*, **121**, 24, 1955.
(19) M. F. Walker, *Ap. J.*, Sup. **2**, 365, 1956.
(20) J. K. McDonald, *J. R.A.S. Canada*, **XLII**, 220, 1948.
(21) R. M. Petrie, *Pub. D.A.O. Victoria*, **9**, 297, 1953.
(22) B. Smith and O. Struve, *Ap. J.*, **100**, 360, 1944.
(23) R. J. Trumpler, *P.A.S.P.*, **47**, 249, 1935.
(24) O. Struve and J. Titus, *Ap. J.*, **99**, 84, 1944.
(25) M. W. Feast and A. D. Thackeray, *M.N.*, **118**, 125, 1958.
(26) H. L. Johnson, *Ap. J.*, **126**, 121, 1957.
(27) G. Münch, *Ap. J.*, **125**, 42, 1957.

ON APPARENT LUMINOSITY IN GENERAL RELATIVITY

V. Joseph

(Communicated by F. A. E. Pirani)

(Received 1958 July 4)

Summary

A formula for apparent luminosity, valid in an arbitrary space-time, is derived from the conservation equations of the electromagnetic stress-energy tensor for a null field, by the use of optical coordinates and tetrads.

---

1. *Introduction.*—One of the major contributions of relativity theory to modern physical thought is the notion of *field*, the most important example of which is the radiation field. The electromagnetic radiation field is described by a skew-symmetric tensor $F_{\mu\nu}$ satisfying Maxwell's equations

$$\frac{\partial F_{\mu\nu}}{\partial x^\sigma} + \frac{\partial F_{\nu\sigma}}{\partial x^\mu} + \frac{\partial F_{\sigma\mu}}{\partial x^\nu} = 0, \qquad F^{\mu\nu}{}_{;\nu} = 0, \tag{1.1}$$

while the electromechanical properties of the field are expressed by the electromagnetic stress-energy tensor $E^{\mu\nu}$

$$E^{\mu\nu} = -g^{\nu\beta}F_{\beta\alpha}F^{\mu\alpha} + \tfrac{1}{4}g^{\mu\nu}F^{\alpha\beta}F_{\alpha\beta}, \tag{1.2}$$

which satisfies the conservation laws

$$E^{\mu\nu}{}_{;\nu} = 0. \tag{1.3}$$

From (1.1) we can derive (1) a "wave" equation in general relativity, for the propagation of the field quantities $F_{\mu\nu}$:

$$g^{\alpha\beta}F_{\mu\nu;\,\alpha\beta} = 2R_{\mu\nu\alpha\epsilon}F^{\epsilon\alpha} - R_\mu{}^\epsilon F_{\epsilon\nu} + R_\nu{}^\epsilon F_{\epsilon\mu}, \tag{1.4}$$

the symbols having their usual meanings.

In flat space-time (1.4) reduces to the ordinary wave equation, showing that the field quantities are propagated with fundamental velocity. In a non-flat space-time the solution of (1.4), subject to specified boundary conditions, presents a formidable problem (2), except in some simple cases (3). In view of this difficulty there have been various attempts to obtain particular solutions of the electromechanical equations (1.3) rather than the field equations (1.1). It has been shown (4) that a test particle (corpuscle) arising, through certain limiting processes, from the stress-energy tensor $E^{\mu\nu}$, moves along a null geodesic. This result is in accordance with the principle of relativistic geometrical optics, usually expressed in the variational form:

$$ds = 0, \qquad \delta\int ds = 0. \tag{1.5}$$

From quantum theory we are familiar with the idea of a photon as a particle whose relative energy is $h\nu$ and whose 4-momentum is a null vector. In general relativity the formula for the Doppler shift of a radiating star can be derived either (*a*) from geometrical optics, using the quantum hypothesis for corpuscles

moving along null geodesics or (*b*) from kinematical wave optics based on the properties of null 3-surfaces in space-time. Kermack, McCrea and Whittaker (**5**) have shown that the two viewpoints (*a*) and (*b*) lead to the same formula. They have thereby established the internal consistency of the particle and wave descriptions of the electromagnetic radiation field in general relativity theory in so far as the formula for Doppler shift is concerned.

In the present paper it is shown that the particle and wave descriptions of the radiation field lead to identical results also for the apparent luminosity of a radiating star. A general expression for apparent luminosity was first obtained by Walker (**6**) using geometrical optics, although particular cases of this expression had been given earlier by Milne (**7**) and Tolman (**8**). Here Walker's general formula is derived from the conservation laws of the electromagnetic stress-energy tensor for a null field, without employing the language of geometrical optics. This approach to the problem of luminosity seems the more natural one in a field theory.

The result established here is exact and invariant. It has been found convenient to use the physically significant system of coordinates known as optical coordinates (**9**) but the results are independent of this choice. The tetrad formulation is used to describe in an invariant way the local experience of the observers concerned.

2. *Optical coordinates and tetrads.*—We begin with an arbitrary space-time with metric

$$ds^2 = g_{\mu\nu}\, dx^\mu\, dx^\nu \tag{2.1}$$

of signature $(1, -1, -1, -1)$.

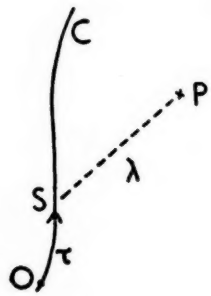

FIG. 1.

Let C be the world line of a star in space-time (2.1). Consider a set of four unit orthogonal vectors $\lambda_{(\alpha)}{}^\mu$ at O, $\lambda_{(0)}{}^\mu$ being time-like and tangent to C, and $\lambda_{(a)}{}^\mu$ being space-like. (Latin letters $a, b, \ldots$ range and sum over 1, 2, 3.) A tetrad field along C can be generated by Fermi-propagation of the vectors $\lambda_{(a)}{}^\mu$, thus

$$(\delta_\nu{}^\mu - \lambda^\mu \lambda_\nu)\frac{\delta \lambda_{(a)}{}^\nu}{\delta \tau} = 0 \tag{2.2}$$

where λ^μ is the unit tangent vector to C and τ is the arc-distance as measured from O.

Physically, the tetrad $\lambda_{(\alpha)}{}^{\mu}$ at any event on C is interpreted as the local Minkowskian frame of an observer whose 4-velocity is $\lambda_{(0)}{}^{\mu}$ and who uses local cartesian axes $\lambda_{(a)}{}^{\mu}$ (**10**).

The coordinates x^{μ} of an event P on the forward null geodesics through any point S on C can be written in the form:

$$x^{\mu} = f^{\mu}(l^1, l^2, l^3, \tau, \lambda) \tag{2.3}$$

where l^1, l^2, l^3 are the direction cosines of the null geodesic SP at S with respect to the cartesian axes $\lambda_{(a)}{}^{\mu}$, that is:

$$l^a = -\frac{p_{\mu}\lambda_{(a)}{}^{\mu}}{p_{\mu}\lambda_{(0)}{}^{\mu}} \tag{2.4}$$

p^{μ} being any null vector tangent to SP at S, τ is the proper time as measured by a clock moving along the world line C, and λ is the projected distance of the null geodesic SP with respect to the 4-velocity $\lambda_{(0)}{}^{\mu}$ of the star at S, that is

$$\lambda = \int_S^P \lambda_{(0)\mu}\, dx^{\mu} \tag{2.5}$$

the integrand at any M point on SP being obtained by parallel propagation of $\lambda_{(0)}{}^{\mu}$ along the curve SP to M; if $\lambda_{(0)}{}^{\mu}$ is the vector at M on SP, then its value at a neighbouring point N on SP is given by

$$[\lambda_{(0)}{}^{\mu}]_M = [\lambda_{(0)}{}^{\mu}]_N - \Gamma_{\alpha\beta}{}^{\mu}\lambda_{(0)}{}^{\alpha}\, dx^{\beta}$$

where dx^{β} is the infinitesimal displacement vector MN and the $\Gamma_{\alpha\beta}{}^{\mu}$ are Christoffel symbols.

Since $l^a l^a = 1$ by (2.4), the equations (2.3) define a transformation of coordinates from the system x^{μ} to "optical coordinates" (**7**) λ, τ, α, β (α, β being any two independent functions of l^a) in a domain D of space-time where the forward null geodesics through points on C do not intersect one another. Let the metric of space-time in the new optical coordinate system be

$$ds^2 = h_{\mu\nu}\, dy^{\mu}\, dy^{\nu}, \tag{2.6}$$

where $y^0 = \lambda$, $y^1 = \tau$, $y^2 = \alpha$ and $y^3 = \beta$.

It is shown in Appendix I that

$$h_{0\mu} = 0 \quad (\mu \neq 1) \qquad \text{and} \qquad h_{01} = 1 \text{ in } D. \tag{2.7}$$

That is, the metric (2.6) can be written in the form

$$ds^2 = 2\, dy^0\, dy^1 + h_{ij}\, dy^i\, dy^j \qquad (i, j = 1, 2, 3). \tag{2.8}$$

It should be realized that the optical coordinates λ, τ, α, β are observable quantities with direct physical significance in the sense that an operational procedure can be specified for measuring them. They are constructed in an invariant manner depending only on the choice of world line C, and not on any pre-existing coordinate system in space-time. τ, α, β can be realized by the single observer moving along the world line C, while λ can be evaluated with the cooperation of a set of observers stationed along the null line SP at relative rest with respect to the observer with world line C.

The concept of relative velocity of two separated observers may be generalized conveniently to general relativity in the following way.

Let $\lambda_{(\alpha)}{}^{\mu}$, $\eta_{(\alpha)}{}^{\mu}$ be the coordinate tetrads of two observers S, P whose world lines are C and C' (Fig. 2); the backward cone of null geodesics at an event P on C' intersects C in S. Consider a time-like 4-vector $\lambda_{(0)}{}^{\mu}$ at P which is obtained

by parallel propagation of $\lambda_{(0)}{}^{\mu}$ from S along the null geodesic SP. Then the scalar v given by

$$v^2 = 1 - \{\lambda_{(0)}{}^{\mu}\eta_{(0)\mu}\}^{-2}, \tag{2.9}$$

evaluated at P, is the magnitude of the velocity of the observer S relative to the observer P. The direction cosines l_a of the velocity are

$$l_a = -\lambda_{(0)}{}^{\mu}\eta_{(a)\mu}\{\lambda_{(0)}{}^{\mu}\eta_{(b)\mu}\lambda_{(0)}{}^{\nu}\eta_{(b)\nu}\}^{1/2}. \tag{2.10}$$

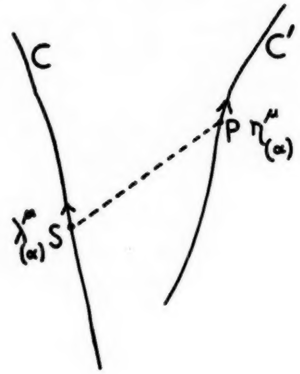

FIG. 2.

The concept of "relative rest", due to Kermack, McCrea and Whittaker (5) is a special case of the concept of relative velocity (2.9) of two separated observers. S is said to be at rest relative to P if his velocity relative to P is zero.

3. *Propagation of null field.*—In relativity theory there are two physically distinguishable electromagnetic radiation fields: (i) null-field and (ii) non-null field (11, 12). We shall consider the propagation of null fields in general relativity. The stress-energy tensor $E^{\mu\nu}$ for a null field can be written in the form

$$E^{\mu\nu} = Un^{\mu}n^{\nu}, \tag{3.1}$$

where n^{μ} is a null vector and U a scalar function. It is readily seen that the sum of two null fields is in general not a null field.

L. Mariot (13) has shown that n^{μ} generates a null geodesic in space-time. In optical coordinates (2.6) n^{μ} may be taken as

$$n^{\mu} = [1, 0, 0, 0], \tag{3.2}$$

since SP (Fig. 1) is a null geodesic.

The conservation equations (1.3) for $E^{\mu\nu}$ read:

$$(-h)^{-1/2}\frac{\partial}{\partial y^{\nu}}\{(-h)^{1/2}E^{\mu\nu}\} + \left\{\begin{matrix}\mu \\ \sigma\nu\end{matrix}\right\}E^{\sigma\nu} = 0. \tag{3.3}$$

For a null field with stress-energy tensor $E^{\mu\nu}$ given by (3.1), equations (3.3) reduce to the single equation

$$\frac{\partial}{\partial\lambda}\{(-h)^{1/2}U\} = 0,$$

whence

$$U = \frac{A}{(-h)^{1/2}}, \tag{3.4}$$

where A is an arbitrary function of τ, α and β only. From (2.8)

$$\det(h_{\mu\nu}) = -\det(h_{pq}) \text{ where } p, q = 2, 3$$

that is

$$h = |h_{\mu\nu}| = -|h_{pq}|.$$

Therefore $$(-h)^{1/2} = |h_{pq}|^{1/2}.$$

Hence $$U = \frac{A}{|h_{pq}|^{1/2}}. \tag{3.5}$$

The intensity of radiation as measured by an observer P (Fig. 2) moving along the world line C', is given by the scalar I,

$$I = E^{\mu\nu}\eta_{(0)\mu}\eta_{(0)\nu} = Un^\mu n^\nu \eta_{(0)\mu}\eta_{(0)\nu}, \qquad I = U[\eta_{(0)0}]^2. \tag{3.6}$$

We can express $\eta_{(0)0}$ in terms of two observable quantities with respect to the observer P: (i) the velocity v of S relative to P and (ii) the angle θ between the direction of the ray PS and the direction of the relative velocity v.

The direction ratios of the null line PS with respect to the tetrad $\eta_{(\alpha)}{}^\mu$ are:

$$n_\mu \eta_{(a)}{}^\mu \tag{3.7}$$

and the direction ratios of the relative velocity of S with respect to $\eta_{(\alpha)}{}^\mu$ are

$$-\lambda_{(0)}{}^\mu \eta_{(a)\mu}. \tag{3.8}$$

Thus the angle θ between these two directions is given by

$$\cos\theta = -n_\mu \eta_{(a)}{}^\mu \lambda_{(0)}{}^\rho \eta_{(a)\rho}[n_\sigma \eta_{(b)}{}^\sigma n_\tau \eta_{(b)}{}^\tau \lambda_{(0)\pi}\eta_{(c)}{}^\pi \lambda_{(0)\nu}\eta_{(c)}{}^\nu]^{-1/2}. \tag{3.9}$$

This expression may easily be rewritten in terms of v and $\eta_{(0)0}$ only (Appendix II). On solving the resulting equation (A 2.7) for $\eta_{(0)0}$ one obtains

$$\eta_{(0)0} = (1 - v^2)(1 + v\cos\theta)^{-1}. \tag{3.10}$$

The expression (3.6) for the intensity of radiation becomes

$$I = \frac{A}{|h_{pq}|^{1/2}} \frac{1 - v^2}{(1 + v\cos\theta)^2}. \tag{3.11}$$

Thus we have established a formula for the apparent luminosity (intensity of radiation) of a radiating body S in terms of observable quantities λ, τ, α, β, v and θ. The parameter A depends on the radiating body only.

This result has been found without the introduction of geometrical optics or entities like photons and the relation $E = h\nu$.

We shall now show that this result agrees with that obtained by Walker **(6)** from geometrical optics.

The cross-sectional area V of a thin pencil of null geodesics issuing from the radiating body at S (Fig. 2) and meeting the instantaneous space of P is, for the metric (2.8), given by

$$V = |h_{pq}|^{1/2}\, d\alpha\, d\beta. \tag{3.12}$$

Let p^μ be the momentum of 4-vector of a photon whose world line is SP; then the Doppler shift D is

$$D = \frac{\text{frequency of photon relative to } \lambda_{(\alpha)}{}^\mu}{\text{frequency of photon relative to } \eta_{(\alpha)}{}^\mu},$$
$$= \frac{\text{energy of photon relative to } \lambda_{(\alpha)}{}^\mu}{\text{energy of photon relative to } \eta_{(\alpha)}{}^\mu},$$

by the quantum hypothesis.

Therefore

$$D = \frac{p^\mu \lambda_{(0)\mu}}{p^\mu \eta_{(0)\mu}}.$$

But

$$p^\mu = h\nu[1, 0, 0, 0],$$

and

$$\lambda_{(0)\mu} = [1, 1, 0, 0] \text{ at } S,$$

where ν is the frequency of the photon relative to $\lambda_{(0)\mu}$. Hence

$$D = [\eta_{(0)0}]^{-2}. \tag{3.13}$$

From (3.5) and (3.6), we obtain

$$I = B/V\, D^{-2}$$

by (3.12) and (3.13). This is, in fact, result (1) in Walker's paper (**6**), B depending on the source only.

The derivation of I as presented here confirms the validity of the corpuscular description of the radiation field in the case of apparent luminosity.

4. *Application to special theory.*—We shall illustrate the use of the formula (3.11) in the special relativity case when the world line of the radiating star is a geodesic in Minkowskian space-time. With the world line C of the star as base line, the space-time metric can be written in optical coordinates as

$$ds^2 = d\tau^2 + 2\, d\tau\, d\lambda - \lambda^2(d\alpha^2 + \sin^2\alpha\, d\beta^2). \tag{4.1}$$

The intensity of radiation as measured by an observer P (Fig. 2) is given by (3.14) as

$$I = \frac{A}{\lambda^2 \sin^2\alpha} \frac{1 - v^2}{(1 + v\cos\theta)^2} = \frac{\epsilon}{\lambda^2} \frac{1 - v^2}{(1 + v\cos\theta)^2}, \tag{4.2}$$

where ϵ depends on the source only, and λ is the projected distance of the null geodesic SP with respect to the 4-velocity of the radiating star. In order to relate I to the observer's notion of distance, it is convenient to give the result in terms of the projected distance μ of SP with respect to the 4-velocity of the observer P. Thus

$$\mu = \int_S^P \eta_{(0)\mu}\, dy^\mu = \int_S^P \eta_{(0)\mu} \frac{dy^\mu}{d\lambda}\, d\lambda = \eta_{(0)\mu} \frac{dy^\mu}{d\lambda} \int_S^P d\lambda,$$

i.e.

$$\mu = \lambda\eta_{(0)0} = \lambda(1 - v^2)^{1/2}(1 + v\cos\theta)^{-1}. \tag{4.3}$$

Therefore (4.2) reads

$$I = \epsilon\mu^{-2}(1 - v^2)^2(1 + v\cos\theta)^{-4}.$$

Putting $v = \tanh u$ we obtain

$$I = \epsilon\mu^{-2}(\cosh u + \cos\theta \sinh u)^{-4}. \tag{4.4}$$

This result agrees with that obtained by Robertson (**14**). However, Robertson's treatment of the subject involved the use of a particular coordinate system (rectangular cartesian) in extended regions of space-time, the formulation apparently being non-invariant.

Acknowledgments.—This work was carried out under a programme supported in part by Wright A.D.C., A.R.D.C., U.S.A.F., through its European office. The author is grateful to the University of Ceylon for a maintenance grant.

King's College, London,
Strand, W.C.2:
1958 *June* 3.

Appendix I

Form of metric in optical coordinates.—We now derive equation (2.7)

$$h_{0\mu}=0 \quad (\mu\neq 1), \qquad h_{01}=1$$

for the metric in optical coordinates (2.6)

$$ds^2=h_{\mu\nu}\,dy^\mu\,dy^\nu.$$

The proof is similar to that given in Temple's paper (9).

Since the equation of C is given by $\lambda=0$ we have, for a displacement along C,

$$h_{ij}\,dy^i\,dy^j=d\tau^2 \quad \text{if} \quad \lambda=0 \qquad [i,j=1,2,3].$$

That is

$$\left.\begin{array}{c} h_{11}=1 \\ h_{pq}=0, \qquad h_{p1}=0 \end{array}\right\} \text{ if } \lambda=0 \tag{A 1.1}$$

where p, q assume the values 2, 3.

For a displacement along any null geodesic at S, $\tau=$ const.,

$$h_{\mu\nu}\,dy^\mu\,dy^\nu=h_{00}\,d\lambda^2.$$

That is

$$h_{p0}=0 \quad \text{if} \quad \lambda=0. \tag{A 1.2}$$

The equations of the null geodesics from S, namely $y^j=$ const., $y^0=\lambda$, must satisfy the differential equations

$$\frac{d^2y^\mu}{d\lambda^2}+\Gamma_{\alpha\beta}{}^\mu\frac{dy^\alpha}{d\lambda}\frac{dy^\beta}{d\lambda}=0 \tag{A 1.3}$$

and

$$h_{\mu\nu}\,dy^\mu\,dy^\nu=0.$$

The parameter λ has been chosen in virtue of (2.5). It follows that

$$\Gamma_{00}{}^\mu=0 \qquad \text{and} \qquad h_{00}=0 \text{ in } D. \tag{A 1.4}$$

That is,

$$2\frac{\partial h_{\mu 0}}{\partial\lambda}-\frac{\partial h_{00}}{\partial y^\nu}\equiv 2\Gamma_{nn,\mu}=0.$$

Therefore by (A 1.4) we have

$$\frac{\partial h_{\mu 0}}{\partial\lambda}=0 \quad \text{in} \quad D.$$

$$\left.\begin{array}{ll} \text{Hence} & h_{10} \text{ is independent of } \lambda \\ \text{and} & h_{p0}=0 \quad \text{by} \quad (\text{A } 1.2) \end{array}\right\}. \tag{A 1.5}$$

By definition of λ (2.5)

$$\lambda=\int_S^P \lambda_{(0)\mu}\,dy^\mu=\int_S^P \lambda_{(0)}{}^\mu h_{\mu\nu}\frac{dy^\nu}{d\lambda}\,d\lambda=k\int_S^P d\lambda$$

since $k=\lambda_{(0)}{}^\mu h_{\mu\nu}(dy^\nu/d\lambda)$ is constant along SP in virtue of

$$\frac{\delta\lambda_{(0)}{}^\mu}{\delta\lambda}=0 \qquad \text{and} \qquad \frac{\delta}{\delta\lambda}\left(\frac{dy^\nu}{d\lambda}\right)=0.$$

Thus

$$\lambda_{(0)}{}^\mu h_{\mu 0}=1 \text{ along } SP.$$

At S,

$$\lambda_{(0)}{}^\mu=\delta_1{}^\mu \text{ by (A 1.1)},$$

and so:

$$h_{10}=1 \text{ at } S.$$

Hence by (A 1.5)

$$h_{10} = 1 \text{ in } D. \tag{A 1.6}$$

Relations (2.7) follow from (A 1.4), (A 1.5) and (A 1.6).

Appendix II

We shall derive the relation

$$\cos\theta = \frac{1 - \eta_{(0)0}(1 - v^2)^{-1/2}}{\eta_{(0)0}\{(1 - v^2)^{-1} - 1\}^{1/2}}.$$

Introducing the notation

$$\eta_\mu{}^{(\alpha)} = \epsilon^{\alpha\beta}\eta_{(\beta)\mu}, \tag{A 2.1}$$

where

$$\epsilon^{\alpha\beta} = \operatorname{diag}\{1, -1, -1, -1\},$$

we can write (3.9) in the convenient form

$$\cos\theta = n_\mu \eta_{(a)}{}^\mu \lambda_{(0)}{}^\rho \eta_\rho{}^{(a)}[\{-n_\sigma \eta_{(b)}{}^\sigma n^\tau \eta_\tau{}^{(b)}\}\{-\lambda_{(0)\pi}\eta_{(c)}{}^\pi \lambda_{(0)}{}^\nu \eta_\nu{}^{(c)}\}]^{-1/2}. \tag{A 2.2}$$

Now

$$n_\mu \eta_{(a)}{}^\mu \lambda_{(0)}{}^\rho \eta_\rho{}^{(a)} = n_\mu \eta_{(a)}{}^\mu \eta_\rho{}^{(a)} \lambda_{(0)}{}^\rho = n_\mu \eta_{(\alpha)}{}^\mu \eta_\rho{}^{(\alpha)} \lambda_{(0)}{}^\rho - n_\mu \eta_{(0)}{}^\mu \eta_\rho{}^{(0)} \lambda_{(0)}{}^\rho.$$

But

$$\eta_{(\alpha)}{}^\mu \eta_\rho{}^{(\alpha)} = \delta_\rho{}^\mu, \tag{A 2.3}$$

and so

$$n_\mu \eta_{(a)}{}^\mu \lambda_{(0)}{}^\rho \eta_\rho{}^{(a)} = n_\rho \lambda_{(0)}{}^\rho - \{n_\mu \eta_{(0)}{}^\mu\}\{\eta_\rho{}^{(0)} \lambda_{(0)}{}^\rho\}.$$

Also

$$n_\sigma \eta_{(b)}{}^\sigma n^\tau \eta_\tau{}^{(b)} = n_\sigma \eta_{(b)}{}^\sigma \eta_\tau{}^{(b)} n^\tau = n_\sigma \eta_{(\alpha)}{}^\sigma \eta_\tau{}^{(\alpha)} n^\tau - n_\sigma \eta_{(0)}{}^\sigma \eta_\tau{}^{(0)} n^\tau = n_\sigma n^\sigma - [n_\mu \eta_{(0)}{}^\mu]^2. \tag{A 2.3}$$

Therefore

$$n_\sigma \eta_{(b)}{}^\sigma n^\tau \eta_\tau{}^{(b)} = -[n_\sigma \eta_{(0)}{}^\sigma]^2,$$

since n^μ is null. Similarly

$$\lambda_{(0)\pi}\eta_{(c)}{}^\pi \lambda_{(0)}{}^\nu \eta_\nu{}^{(c)} = \lambda_{(0)}{}^\rho \lambda_{(0)\rho} - [\lambda_{(0)}{}^\rho \eta_\rho{}^{(0)}]^2 = 1 - [\lambda_{(0)}{}^\rho \eta_\rho{}^{(0)}]^2.$$

Thus

$$\cos\theta = [n_\rho \lambda_{(0)}{}^\rho - (n_\mu \eta_{(0)}{}^\mu)(\eta_{(0)\rho}\lambda_{(0)}{}^\rho)][(\lambda_{(0)}{}^\rho \eta_\rho{}^{(0)})^2 - 1]^{-1/2}(n_\sigma \eta_{(0)}{}^\sigma)^{-1}. \tag{A 2.4}$$

From (2.9) we have

$$\eta_{(0)}{}^\rho \lambda_{(0)\rho} = (1 - v^2)^{-1/2}. \tag{A 2.5}$$

Since $\lambda_{(0)}{}^\rho$ is propagated parallel with SP and $\delta n^\rho/\delta\lambda = 0$, $n_\rho \lambda_{(0)}{}^\rho$ is constant along SP. Therefore

$$[n_\rho \lambda_{(0)}{}^\rho]_P = [n_\rho \lambda_{(0)}{}^\rho]_S = 1, \tag{A 2.6}$$

since $h_{11} = 1$ at S by (A 1.1).

Substituting (A 2.5) and (A 2.6) in (A 2.4), we obtain

$$\cos\theta = [1 - (\eta_{(0)}{}^\mu n_\mu)(1 - v^2)^{-1/2}][(1 - v^2)^{-1} - 1]^{-1/2}(n^\mu \eta_{(0)\mu})^{-1},$$

that is,

$$\cos\theta = \frac{1 - \eta_{(0)0}(1 - v^2)^{-1/2}}{\eta_{(0)0}\{(1 - v^2)^{-1} - 1\}^{1/2}} \tag{A 2.7}$$

by (3.2).

References

(1) Eddington, A. S., *Mathematical Theory of Relativity*, C.U.P., p. 175.
(2) Lichnerowicz, A., *Théories Relativistes de la Gravitation et de l'Électromagnétisme*, Masson, Paris (1955) Chapter II.
(3) Ueno, Y., *Prog. Theor. Phys.*, **12,** 461, 1954.
(4) Robertson, H. P., *Proc. Edin. Math. Soc.* (2), **5,** 63, 1936.
(5) Kermack, W. O., McCrea, W. H. and Whittaker, E. T., *Proc. Roy. Soc. Edin.*, **53,** 31, 1933.
(6) Walker, A. G., *M.N.*, **94,** 159, 1933.
(7) Milne, E. A., *Zs. f. Astrophys.*, **6,** 90, 1933.
(8) Tolman, R. C., *Proc. Nat. Acad. Sci.*, **16,** 511, 1930.
(9) Temple, G., *Proc. Roy. Soc.* A, **168,** 122, 1938.
(10) Pirani, F. A. E., *Acta Physica Polonica*, **15,** 389, 1956.
(11) Ruse, H. S., *Proc. Lond. Math. Soc.* (2), **41,** 302, 1936.
(12) Synge, J. L., *Relativity, the Special Theory*, North-Holland Publishing Co., Amsterdam (1956), Chapter IX.
(13) Mariot, M. Louis, *Comptes Rendus Acad. Sci.*, **238,** 2055, 1954.
(14) Robertson, H. P., *Zs. f. Astrophys.*, **15,** 69, 1937.

РЕЗЮМЕ ДОКЛАДОВ, В ПЕРЕВОДЕ НА РУССКИЙ ЯЗЫК

РАССЕЯНИЕ РАДИОВОЛН В СОЛНЕЧНОЙ КОРОНЕ

А. Хьюиш

Из наблюдений радиоизлучения Крабовидной туманности в июне, когда она находится на небольшом угловом расстоянии от Солнца, следует, что излучение подвергается значительному рассеянию при прохождении через солнечную корону. В данной статье описываются ежегодные измерения за период с 1952 по 1958 гг. Были получены следующие новые результаты:

(1) измерения на длине волн в 7,9 м указывают на наличие рефракционных эффектов, сверх рассеяния, которые могут дать сведения о средней электронной плотности в короне;

(2) распространение измерений на более короткую длину волн в 1,9 м позволило более точно определить большое рассеяние на расстоянии наибольшего приближения;

(3) наблюдалось отчетливое изменение в течение цикла солнечных пятен в районе короны на расстоянии $8R_{\odot}$; и

(4) рассеяние анизотропно. Этот результат подтверждает прежнее заключение, что рассеяние производится нитевидными неправильностями, выравненными в магнитном поле и указывает на то, что направление поля приблизительно радиально на расстоянии в $15 \div 20R_{\odot}$.

ИЗМЕРЕНИЕ ПРОФИЛЯ ХРЕБТА СКЛАДКИ НА ЛУННОЙ ПОВЕРХНОСТИ

Гильберт Фильдер

Хребет складки на лунной поверхности измерялся методом, состоящим из измерений меняющейся длины тени, бросаемой на него соседней горой. Вероятные ошибки местонахождения точек ± 330 м в плоскости поверхности и только ± 14 м в направлении перпендикулярном поверхности. По профилю хребта складки видно, что он не может считаться гребнем волны затвердевшей лавы.

УСКОРЕННЫЙ МЕТОД ОБНАРУЖЕНИЯ НЕПТУНА

Р. А. Литтльтон

Описан математический принцип метода обнаружения Нептуна, нуждающегося в значительно меньшем численном вычислении. Время гелиоцентрического соединения может быть найдено исключительно разбором расхождений долготы Урана. Одни эти сведения дают возможность предвидеть долготу, согласно закону Бода, с точностью в пределах 15°. Найдя расстояние на круговой орбите, наиболее согласующейся с наблюдениями, можно предсказать эту долготу с точностью сравнимой с точностью достигнутой Ле Веррье. Указывается как, благодаря подходящему комбинированию условных уравнений, число неизвестных может быть доведено до трех (по сравнению с восьмью в первоначальных методах) для любого расчетного среднего расстояния. Тот же процесс устраняет некоторые неудобные особенности, которые иначе возникли бы для орбиты близь резонанса 2:1.

ЗВЕЗДНЫЕ ГРУППЫ. III. ДВИЖЕНИЯ В ПРОСТРАНСТВЕ НЕСКОЛЬКИХ ЗВЕЗД-КАРЛИКОВ ГЛАВНОЙ ПОСЛЕДОВАТЕЛЬНОСТИ

Олинь Эгген

При помощи звездных величин и цветов, полученных фотоэлектрическим способом, определены фотометрические параллаксы для 359 звезд с известными лучевыми скоростями и собственными движениями, являющихся карликами главной последовательности по спектроскопической классификации обсерваторий Маунт Вильсона или Еркеса. Эти параллаксы применяются для вычисления движений звезд в пространстве по векторам **U**, **V** и **W**. Звезды подразделяются согласно величине движения по W (перпендикулярного к плоскости Галактики), а также по их движению, построенному в плоскости U, V в рисунках 2 до 5. Из этих диаграмм выводится, что распределение движения в пространстве не случайно, по крайней мере для малых величин W.

УРОВНИ ЭНЕРГИИ И ВЕРОЯТНОСТИ ПЕРЕХОДА ДЛЯ FE IV

Р. Г. Гарстанг

Расчитаны квантовомеханические параметры конфигурации $3d^5$ спектра Fe IV и вычислены уровни энергии этой конфигурации. Вычислены вероятности перехода для излучения магнитных диполей и электрических квадруполей для переходов между уровнями конфигурации $3d^5$. Разыскиваются линии [Fe IV] на спектре RR Tel и предлагаются некоторые отождествления.

ФОТОЭЛЕКТРИЧЕСКАЯ КРИВАЯ БЛЕСКА RT СОЗВЕЗДИЯ СКУЛЬПТОРА

Г. Г. Силье и Е. М. Линдсей

Получены, используя 150 см' овый рефлектор Рокфеллера Бойденской обсерватории, фотоэлектрические кривые блеска затменной переменной RT Скульптора, голубого и желтого цвета. Оба максимума не равны и не являются плоским гребнем какого-либо вида. В течение последних 60 лет период этой звезды слегка уменьшался и, принимая это уменьшение за линейное, находим следующее выражение кривой блеска, наиболее согласующееся с наблюдениями:

$$\text{Min.} = \text{JD } 2423736^{d} \cdot 51145 + (0^{d} \cdot 51156702 - 1 \cdot 0568 \times 10^{-10} E)E.$$

РАДИОИЗЛУЧЕНИЕ ИЗ ОБЛАСТИ ОРИОНА

Х. Ришбет

Произведена разведка области Ориона на двух длинах волн при помощи радиотелескопов в Сидней. Радиоизлучение из ярких туманностей в этой области повидимому термического происхождения; но слабый растянутый источник в той же области может излучать не термическим образом и может быть связан с широкой темной туманностью. Сравниваются, при помощи простой модели, радио и оптические наблюдения туманности Ориона M42.

ТОЧНЫЕ ПОЛОЖЕНИЯ 17 СИЛЬНЫХ РАДИОЗВЕЗД

Б. Эльсмор

Даются несколько наблюдений на длине волн в 1,9 м, имеющих целью улучшение точности склонений источников, основаных на периодах прохождения перед двумя интерферометрами с наклонными осями. Описывается такое применение кэмбриджского радиотелескопа, образующего интерферометр со скрещивающимися осями и даются точные положения 17-ти источников. Для сравнения приведены положения, определенные третьей кэмбриджской съёмкой.

ЛУЧЕВЫЕ СКОРОСТИ ФУНДАМЕНТАЛЬНЫХ ЮЖНЫХ ЗВЕЗД

Вильям Баскомб и Памела М. Моррис

Даются вновь определенные лучевые скорости 12-ти звезд с нормальными скоростями, а также 63-х ярких звезд, находящихся южнее экватора. Дисперсия снимков, полученных при помощи трехпризматического спектрографа Касгрэйна, 36 А/мм при $H\gamma$. Скорости, найденные обсерваторией Стромло, для звезд нормальной скорости оказались удовлетворяющими измерениям в других обсерваториях системы Лика. Разбираются остаточные скоростидля индивидуальных спектральных линий.

Для исследования были выбраны звезды из позиционных каталогов FK3 и N30. Измерялись по крайней мере три спектрограммы для каждой звезды. Приведен класс светимости по пересмотренной системе Еркес для звезд раннего типа. Даются 29 новых постоянных скоростей, а также 18 скоростей, переменность которых обнаружена впервые. Возобновлены наблюдения над 15 звездами, скорости которых заведомо переменны.

СПЕКТРАЛЬНЫЕ ТИПЫ И ЛУЧЕВЫЕ СКОРОСТИ В ГАЛАКТИЧЕСКОМ СКОПЛЕНИИ NGC 3293

М. В. Фист

112 спектров 35-ти звезд послужили для определения их спектральных типов и 89 тех же спектров—для определения лучевых скоростей 26-ти из этих звезд. Эти спектральные типы, совместно с фотометрическими измерениями д-ра Т. Э. Хоука, приводят к диаграмме Герцшпрунга-Ресселя, чего следовало ожидать для молодого скопления. Звезды принадлежат, большей частью, к раннему типу В с классами светимости от V до Ib. Звезду Mo, Iab можно с уверенностью включить в скопление. Обнаружена большая и необъяснимая зависимость лучевых скоростей от звездной величины (рис. 3). Это явление не влияет на междузвездные линии Ca II и возможно связано с эффектом Трамплера.

О ВИДИМОЙ СВЕТИМОСТИ В ОБЩЕЙ ТЕОРИИ ОТНОСИТЕЛЬНОСТИ

В. Джозеф

Из уравнений сохранения тензора электромагнитной энергии-напряжения для нулевого поля, при помощи оптических координат и тетрадов, выводится формула для видимой светимости, применимая в произвольном пространстве-времени.